LIFE PREDICTION OF POWER LINE DAMPER

Kalombo Remy Badibanga

(Student No: 210556681)

Submitted in fulfilment of the academic requirements for the degree of Master of Science in Mechanical Engineering

School of Engineering
College of Agriculture, Engineering and Science
University of KwaZulu-Natal
Supervisor: Dr Richard Loubser
Durban, South Africa
December, 2012

DECLARATION

I, Kalombo Remy Badibanga declare that

1. The research reported in this dissertation, except where otherwise indicated, is my original research.

2. This dissertation has not been submitted for any degree or examination at any other university.

3. This dissertation does not contain other persons' data, pictures, graphs or other information, unless specifically acknowledged as being sourced from other persons.

4. This dissertation does not contain other persons' writing, unless specifically acknowledged as being sourced from other researchers. Where other written sources have been quoted, then:

   a. Their words have been re-written but the general information attributed to them has been referenced;
   b. Where their exact words have been used, then their writing has been placed in italics and inside quotation marks, and referenced.

5. This dissertation does not contain text, graphics or tables copied and pasted from the Internet, unless specifically acknowledged, and the source being detailed in the dissertation and in the References sections.

Signed: …….. Date: ……..

Kalombo R. Badibanga (Candidate)

As the candidate's Supervisor I agree/do not agree to the submission of this dissertation.

Signed: …….. Date: ……..

Dr Richard Loubser (Supervisor)

ACKNOWLEDGEMENTS

Glory and Praise to Jehovah, the Almighty God who allowed me to achieve this research work.

I express my sincerest gratitude to Dr Richard Loubser for his dedicated supervision and his priceless assistance throughout this study. I gratefully acknowledge Mr Pravesh Moodley, for his laboratory and administration support during my study. My gratitude goes to Prof Alex Araujo,Prof Aida Fadel, Prof Jorge Ferreira, Dr Freddie Inambao, Mr Logan Pillay, Mr Thabani Nene, Mrs Leena Rajpal, Mrs Charlain King, Mr Ojo Evans, Mr Joseph Kapuku, and UnB staffs for their encouragements and supports.

I would like to thank Eskom, PFISTERER, THRIP, who funded this research through the VRTC. Without the funding, this research would not have been possible.

Further, I would like to take this opportunity to thank my Mum and Dad who taught me to never give up. Also, I want to thank all my brothers, sisters, nieces, nephews and cousins.

Special thanks to Rachel Kalunga who deserves a medal for her patience and support. I will forever be thankful to all my friends for the moral support provided.

Lastly, I would like to thank all those who have contributed, either directly or indirectly to the preparation, research and compilation of this project report.

ABSTRACT

Power line function is to transfer electrical power. Power lines represent a major component in the transport process of electricity and they are subjected to various types of failures. Causes of failure include wind-induced oscillations or Aeolian vibrations. Wind causes transmission line conductors to undergo oscillatory motions which cause failure. To mitigate oscillations of line conductors, Stockbridge dampers are used. It has been observed that dampers are subjected to the same undesirable and destructive effects from vibrations as the conductors they are meant to protect. In the case of a damper, the cyclic bending as well as the friction between its wire cables are caused by vibrations leading to failure.

The mathematical model describing the bending stress of the symmetrical Stockbridge damper's messenger cable near the clamped end is analyzed. The reliability of the mathematical model is assessed using experimental data obtained from the forced response test conducted at the VRTC laboratory at the University of KwaZulu-Natal, Durban. Data from the experiment has been compared with the MatLab model established by the researcher.

Due to friction between the wires of the messenger cable, variation of temperature is observed in the messenger cable during operation. Change of temperature of the messenger cable was investigated, as a function of time, at constant velocity and constant displacement. Experimental data were generated during dynamic characteristic tests on Stockbridge dampers and thereafter the prediction of the variation temperature was undertaken.

There are various mechanical characteristics of a damper that can be affected with time. To reach the aim of this study, three types of vibration test were conducted on the Stockbridge damper: the fatigue test, the forced vibrations test and the free vibrations test. Tests were conducted on a shaker machine with new and used Stockbridge dampers to determine the remaining life of those dampers by looking at their different mechanical properties. The frequency domain and time spectrum were used to display the results. The fatigue test investigated one of the commonest types of Stockbridge damper failure, namely, loss of the small mass because of sustained high frequency resonance. Ultimately, data correlated well and two mathematical models were developed: one for predicting damage in the life of a Stockbridge damper (based on the highest resonance frequency of the damper), and one for predicting the temperature of the messenger cable.

TABLE OF CONTENTS

LIST OF FIGURES

LIST OF TABLES

CHAPTER 1

INTRODUCTION

1.1 Statement of the problem

Cables or conductors are widely used in various engineering constructions such as bridges, overhead transmission lines, guyed masts, and other structures where large tension are involve. Being able to withstand large tensions is an amazing conductor property which is why conductors or cables are used as overhead transmission lines. Overhead transmission lines are very exposed to the forces of the wind, causing them to vibrate. The types of vibrations are Aeolian, gallop or wake induced, depending on the intensity of the wind. The ultimate result of power line vibration is fatigue failure.

The largest investment component of the power transmission is conductor so they need to be protected against wind induced vibration. Stockbridge dampers are used to mitigate oscillations of line conductors, but they are subjected to the same undesirable and destructive effects of vibrations as the conductors they are meant to protect. The cyclic bending and the friction between its cables caused by vibration can lead to failure.

1.2 Aims and Objectives

Mechanical components and structures have mechanical proprieties which are a function of their lifetime and performance. The mechanical proprieties and behaviours of Stockbridge dampers such as resonance frequencies and displacement or acceleration of the mass weight are a function of the damper life. The changing of the dampers' characteristics are a function of its life which is the numbers of years or cycles for dampers to get to failure.

The aim of this research was to identify or derive a model that relates the performance characteristics of Stockbridge dampers to their useful life time. Mechanical proprieties were collected on new as well used dampers in order to develop the background knowledge required to interpret the characteristic curves of dampers according to their life time, and to explain the different modes of failure affecting dampers (e.g. the loss of mass weight of dampers after some period of work time).

Hence the project is devoted focused at:

- the modeling of Stockbridge damper's damage according to its mode of failure,
- the prediction of remaining life of Stockbridge damper.
- the modal analysis of Stockbridge damper
- the simulation of dynamic behavior of Stockbridge damper

1.3 Research publication

The following publications have been produced in this project with respect to the research conducted:

- Badibanga, K. R., Loubser, R. and Moodley, P. 2012. Bending stress of Stockbridge damper messenger cable: Experimental data and modelling. Paper presented at 18th World Conference on Non Destructive Testing, WCNDT, April 2012.
- Badibanga, K. R., Loubser, R. and Moodley, P. 2012. Temperature variation of messenger cable during the variation of Stockbridge damper. Paper presented at 8th South African Conference on Computational and Applied Mechanics, SACAM, September 2012.

1.4 Brief chapter overviews

The explanation of each chapter is briefly given below in order to provide an overview of the whole dissertation.

The background and the introduction of the study is presented in Chapter 1, as well as the aims of the project.

Chapter 2 describes power line motion and associated mechanical vibrations. Some devices to mitigate power line vibration are presented.

Chapter 3 presents a review of the literature related to this project, particularly in relation to the Stockbridge damper and the engineering issues of mechanical damage and remaining life.

Chapter 4 presents the equipment and materials used in this project and describes the standard tests for Aeolian vibration and the methodologies used in this project.

Chapter 5 presents the experiments which tested the Stockbridge damper, and the results of those tests.

Chapter 6 presents the conclusions from the study, and proposes possible future work.

CHAPTER 2

POWER LINE MOTION

2.1 Introduction

The function of power lines is to transfer electric power. Power lines and other flexible structure are subjected to the static and dynamic forces from wind, rain, snow and earthquakes. Static and dynamic forces cause power lines to move on the tower. Wind has a forceful impact on power line motion because it can produce a large deflection. This chapter presents an overview of power line motion.

2.2 Shedding phenomenon

Structures exposed to a fluid stream are subject to force. Because of eddy or vortex shedding, this force acts perpendicular to the fluid stream. The non-dimensional number to describe the shedding phenomenon is known as the Strouhal number, S, and is related to excitation frequency by the relation:

$$S = \frac{f_s D}{V} \tag{2.1}$$

Where,

f_s : Frequency of excitation in Hertz [Hz],

D : Dimension of structure project on the normal plan to the fluid direction in meter [m],

V : Velocity of the fluid flow [m/s].

For power line vibration, the Strouhal number is in the range of 0.185 up to 0.22 (Chan, 2006). To derive the large range of wind induced frequency, the IEEE 664 standard (2007) for the Strouhal number is $S = 0.185$. Therefore, the vibration frequency of power lines in the range of wind induced vibration is determined by the following equation:

$$f = 0.185 \frac{V_w}{D_c} \tag{2.2}$$

With:

f : Frequency [Hz],

V_w : The wind velocity [m/s],

D_c : Diameter of conductor [m].

2.3 Classification of overhead power line motion

Power lines vibrate in different ways depending on the weather condition which could be the rain, the temperature or the wind. The cyclic motion of power lines or conductors are briefly developed below. The comparison between them according to the frequency range and amplitude of vibration is given in Table 2.1 which shows a comparison of the cyclic power line motion according to the damage duration. The different mechanics of vibration amplitude, vibration frequency, energy transfer, and motion patterns distinguish the types of cyclic power line motions. There are three types of cyclic vibration:

- Aeolian vibration;
- galloping conductor;
- wake induced vibration.

2.3.1 The Aeolian vibration

It has been observed from the early 1920's that power lines vibrate because of wind. Aeolian vibration is the vibration of power lines caused by wind velocity in the range of 1m/s to 7m/s (Chan, 2006), and is characterized by high frequency and low amplitude. When the wind blows the general shedding vortices from the conductors are the main cause of the Aeolian vibration. Air changes course at leeward of the conductor depending on the wind speed, the dimension of conductor as well as on the roughness. The conductor is pushed upward as vortex sheds from the bottom of the conductor and vice versa. Figure 2.1 shows the aeolian vibration which has been induced by vortex shedding. Regular formation of vortex leads to

pressure differences which cause an alternative force. This quick repetition of vortex causes the vertical vibration of the conductor. The conductor resonates when the shedding frequency is close to the natural frequency. This phenomenon leads the conductor to significant vibration (Caetano, 2007).

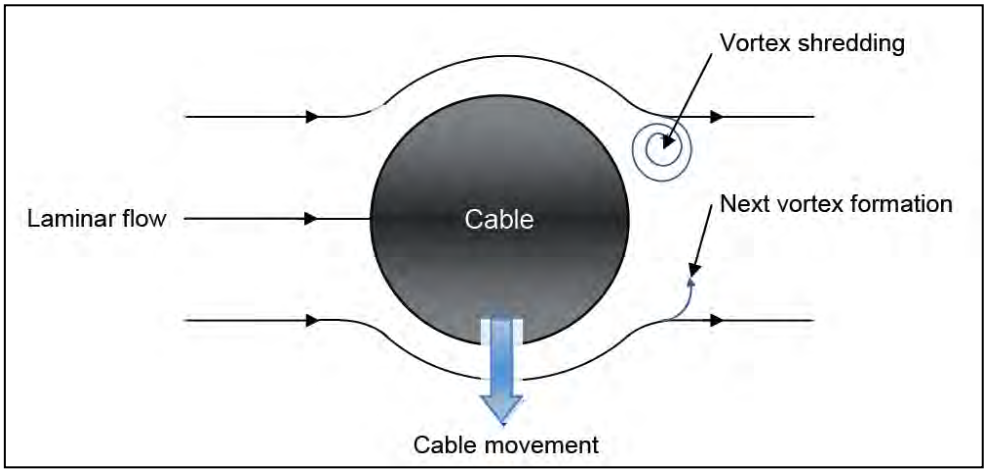

Figure 2.1: Aeolian vibration which is induced by shedding vortex (Elkin, 2010)

2.3.2 The galloping of power line

The primarily vertical motion of power lines with a low frequency and high amplitude is called galloping. The galloping phenomenon occurs at the freezing temperature point of the air which creates ice on the power line when the wind blows. When the wind acts upon the asymmetrical iced surface of the power lines, the amplitude of vibration can approach or exceed even the sag of the power line for the span involved. The power transmitted to the power line by the wind in this manner is greater than that from Aeolian vibrations. Therefore, the galloping is the most dangerous phenomenon for power lines. It can break not only the conductor but also the hardware on the transmission line (e.g. insulator pins, dampers, suspension hardware).

2.3.3 The wake induced vibration

The moderate-to-strong crosswinds which arise from shedding produce cyclic bending of power lines. This phenomenon is called wake induced vibration and is peculiar to bundled power lines. It is an aerodynamic instability problem which arises in one conductor due to moderate and strong wind. For this type of vibration, several types of power line motions are compressed. It has been observed that wake induced vibrations occur mainly on dry bar

conductors, but do also appear on power lines when it is rainy or when they are iced. Figure 2.2 shows two types of power line motion (Doucy et al., 1979).

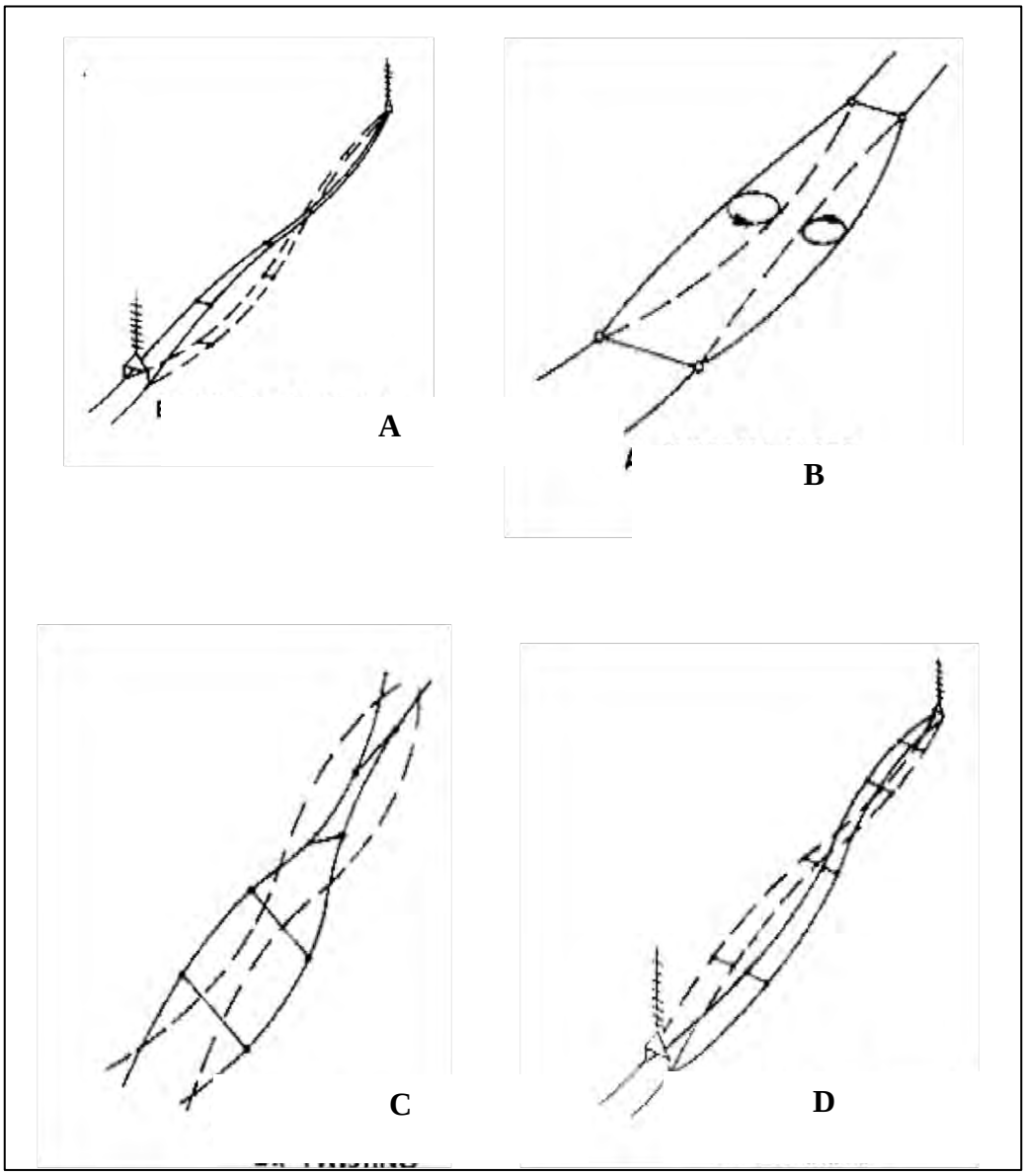

Figure 2.2: Two types of power lines vibration motion_ (A) and (B) are galloping and, (C) and (D) are wake induced vibration

2.4 Comparison of different power line motion

A brief comparison of the three types of power line motion is given in Table 2.1 and in Table 2.2 (Doucy et al., 1979; Chan, 2006).

Table 2.1 shows a comparison regarding the range frequency as well the amplitude of vibration as a function of the diameter of the conductor power line. The weather condition especially the wind velocity is also given in the same table.

Table 2.1: Comparison of different type of cyclic power line motion according to the frequency, the amplitude vibration and the wind velocity

	Aeolian Vibration	Galloping Vibration	Wake induced vibration
Type of power line effected	All	All	All
Approx. amplitude range Function of conductor diameter	0.01 to 1 D_c D_c is conductor diameter	5 to 300 D_c D_c is conductor diameter	0.5 to 80 D_c D_c is conductor diameter
Approx. range of frequency	3 to 150Hz	0.08 to 3Hz	0.15 to 10Hz
Velocity of wind	1 to 7 m/s	7 to 18 m/s	4 to 18 m/s

The comparison regarding to the damage of conductor power line is given in the Table 2.2. The damage life in number of years is given. The Table 2.2 describes also the type of conductors affected by the damage mode, also the main cause of damage.

Table 2.2: Comparison of different type of cyclic power line motion according to factors

Factor Damage	Aeolian Vibration	Galloping Vibration	Wake induced vibration
Approx. time required for severe damage to develop	3 months to 20+ years	1 to 20 hours	1month to 8+ years
Damage's direct cause	Cyclic bending cause metal fatigue	High dynamic load	Conductor clashing, Wear in hardware
Power line component affected by damage	Shield wire strands, conductor	Structure, insulators, conductor, all hardware	Suspension hardware, conductors strands, damper

2.5 Mitigate the power line vibrations

Vibrations are undesirable phenomena as they generate fatigue cycles which accumulate and lead to material failure after some months or years. Aeolian vibration, which is the focus of this project, generally occurs when wind speed is in the range of 1 to 7 m/s (Chan, 2006). To minimize the risk of damaging lines and to protect the latter against fatigue failure due to vibration, dampers are used. Various types of dampers including spiral dampers, Bretelle dampers, Festoon dampers, and Stockbridge dampers are presented below.

2.5.1 Spiral dampers

The spiral damper (Figure 2.3) is usually used on small conductors in order to dissipate the high frequency and small vibration amplitudes of conductor (Chan, 2006). Made in one piece of polyvinyl chloride (PVC) material and spiral shaped, it is divided into two parts: the gripping and the damping sections (Chan, 2006). During its operation, the energy is dissipated when the conductor slaps down and up between opposite sides of the preformed helix . This damper is also called spiral impact damper.

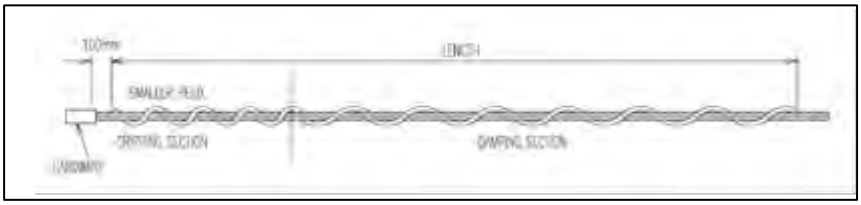

Figure 2.3: Spiral dampers (Chan, 2006)

2.5.2 Bretelle dampers

Bretelle dampers (Figure 2.4) seem to be economically attractive. However, there are numerous factors to be considered in their use. Maintenance of conductor-to-steel clearances can result in higher tower cost and the indoor laboratory investigations could be difficult to conduct because of its configuration. Widely used in France, they present some defiance in function, and difficulty in troubleshooting and maintenance. Originally used as a safety component, they have been adopted as damping devices. Bretelle dampers are made of a scrap of conductor with the same diameter as the line (Chan, 2006) and acts like the jumper or bridge at a tension tower.

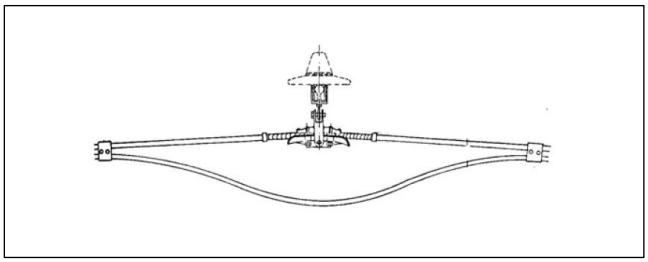

Figure 2.4: Bretelle damper (Chan, 2006)

2.5.3 Festoon dampers

Similar to Bretelle dampers in that they also use scrap conductor, Festoon dampers are more expensive than the former. Festoon dampers (Figure 2.5) have been used on numerous spans, especially in the cold countries such as Norway where it is preferred to avoid the damage of conductors by galloping and Aeolian vibration (Chan, 2006).

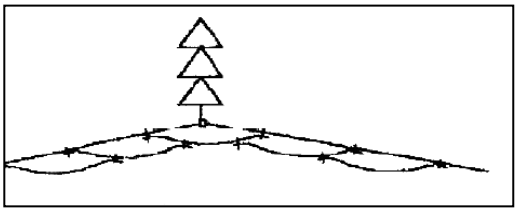

Figure 2.5: Festoon damper (Chan, 2006)

2.5.4 Stockbridge damper

The Stockbridge damper was patented by G. H. Stockbridge in 1920 as a device which is mounted on the conductor to mitigate mechanical vibrations. The original type of Stockbridge damper is shown in Figure 2.6. Low cost and maintenance free are the main advantage of this type of damper. Also, it does not need any additional support to be fixed onto the conductor line.

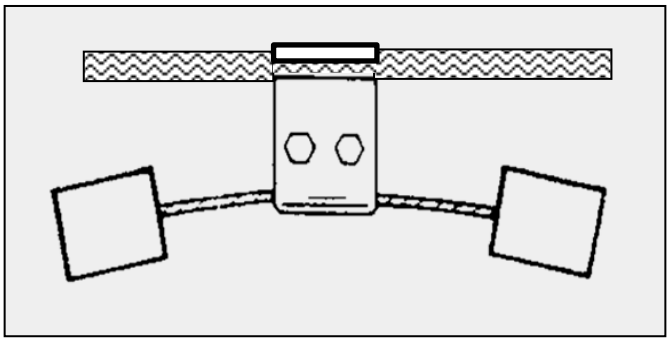

Figure 2.6: The original type of Stockbridge damper

The original Stockbridge damper has undergone many transformations and developments. First of all, in 1932 Monroe and Templin enhanced the damper with two degrees of freedom. This damper has been designed in such way that the moment of inertia and the shape of mass take advantage of the second mode of vibration in the frequency range of its function like a cantilever beam. Figure 7 shows the Monroe and Templin damper as well its parts. The two damper masses are equal and rigidly attached at the end of a stranded wire cable (messenger cable). In turn, the messenger cable is clamped in the damper clamp which is fixed on the conductor. Because of its symmetry it is called a symmetrical damper.

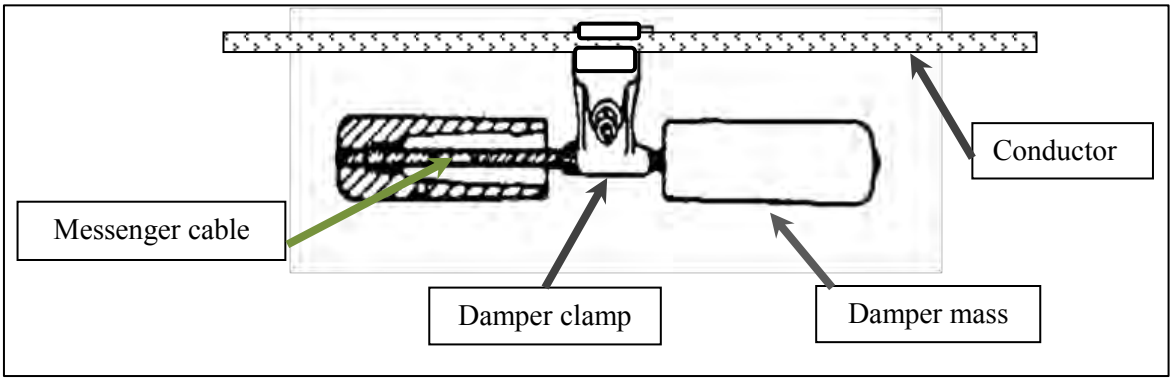

Figure 2.7: Monroe and Templin damper and its parts

After some years, the Monroe and Templin damper was refined again. In 1968, Claren and Diana designed a damper which has two unequal damper masses attached to two unequal lengths of messenger cable (Figure 8). Because of the asymmetrical location of the dampers, the Claren and Diana damper is called an asymmetrical damper, and is very common worldwide.

Figure 2.8: Claren and Diana damper

Basically, the two damper masses are equal and rigidly attached at the end of stranded wire cable (messenger cable). In turn, the messenger cable is clamped in the damper clamp which is fixed on the conductor. According to its symmetrical form, thus it called symmetrical damper (Figure 2.9a). Claren and Diana damper is called asymmetrical damper (Figure 2.9b). The two types of damper are usually named by asymmetrical (Claren and Diana damper) and symmetrical damper (Monroe and Templin), and in addition, they add the name Stockbridge damper. Figure 2.9 shows the sketch of two types of Stockbridge damper according to the design.

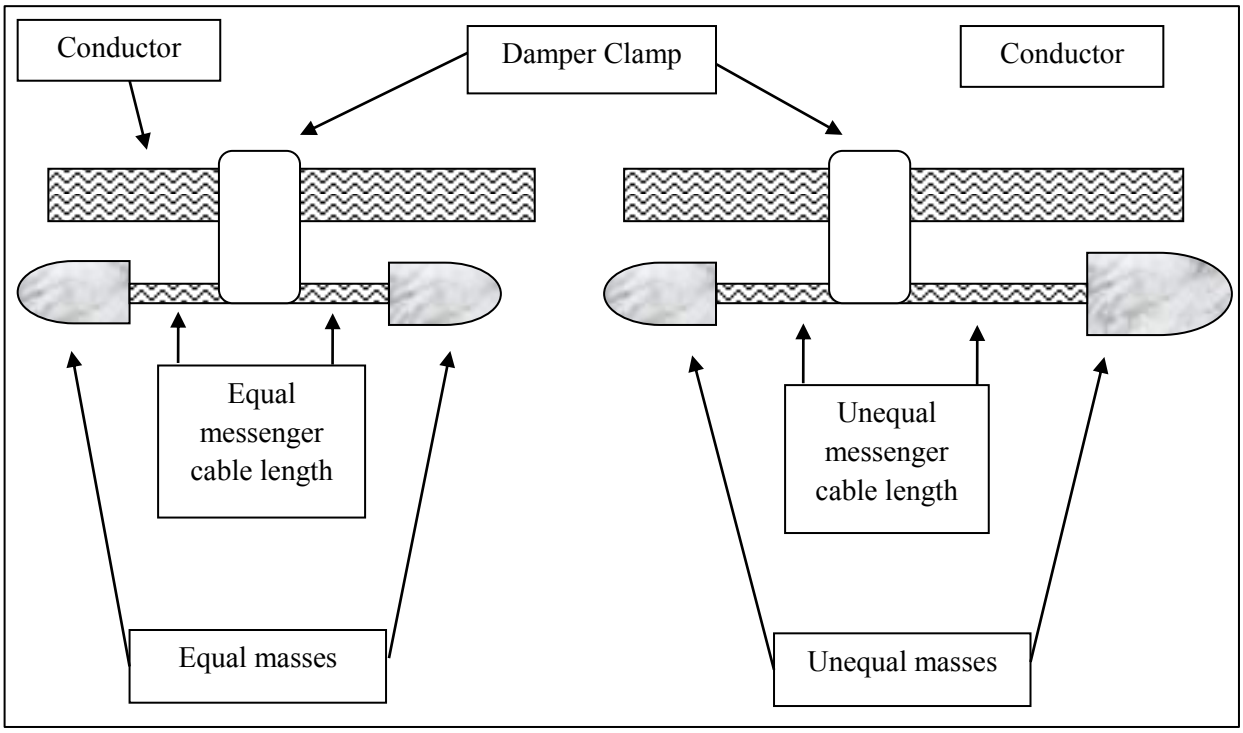

Figure 2.9 ; sketch of (a) Symmetrical Stockbridge damper (Monroe and Templin damper)
(b) Asymmetrical Stockbridge damper (Claren and Diana damper)

2.5.5 Haro damper

The asymmetrical damper was modified by Lauri Haro and Tapani Seppa in 1970. They redesigned the Stockbridge damper with three masses and two damper clamps (Figure 10). The third mass allows for damping of the third mode of vibration. Known as a Haro damper, this damper provides the best vibration damping, although the mounting process requires more care. The messenger cable is 1 meter long and can get bent and damaged, especially during transportation.

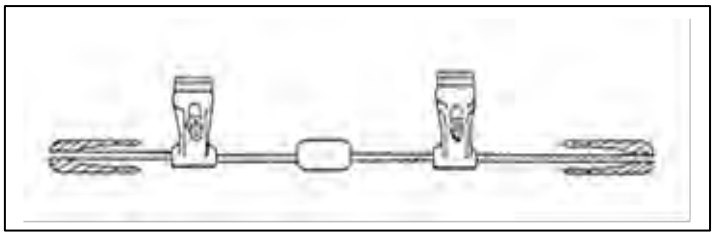

Figure 2.10: Haro damper (Chan, 2006)

2.5.6 Dogbone Damper

The Dogbone damper has been developed in such a way that at a high resonance frequency it reacts with a torsional vibration mode (Figure 11). The torsional vibration mode has been achieved by using damper masses whose the center of gravity is offset in relation to the messenger cable axes. It is called a torsional Stockbridge damper, but they are few on the market.

Figure 2.11: Dogbone damper

CHAPTER 3

LITERATURE REVIEW

3.1 Engineering vibration

Vibration occurrence is of interest to civil engineers, medical physicists and geophysics. The reduction of undesirable effect of vibration becomes a first concern of architects, design engineers, mechanical engineers, and civil engineers. One of the aims of acoustics and mechanical engineers is the design and construction of machines which involve vibration. However, some engineering applications need the vibration effect in their function. Nowadays, the concept of mechanical vibration is the most evident phenomenon in mechanical engineering. This section reports briefly on theories of vibration applied in the field of mechanical engineering (Hussey, 1983; Inman, 1996; Tse et al., 1979; Rao, 1990).

3.1.1 Analysis of mechanical vibration

In mechanical vibration, the mass-spring-damper model can be used to understand the response of a vibrating system. Figure 3.1 shows the vibrating system which is constituted by the mass, the damper, the spring, and the excitation.

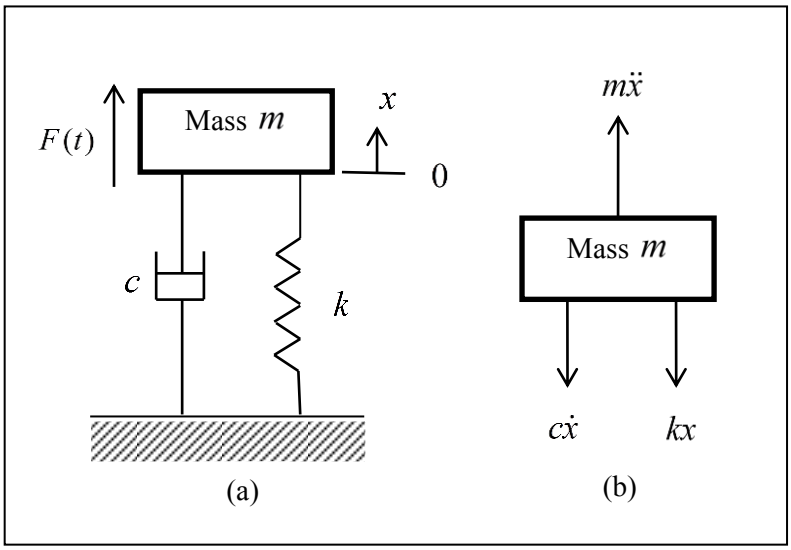

Figure 3.1: (a) Elements constituting the vibratory system and (b) Free body diagram of the system.

The physical vibration is described by the mass m, the damper element c and the spring k. Assuming it is a rigid body, mass can gain or lose energy according to the velocity change of the body. According to Newton's law, the force applied on a mass is a product of the mass and its acceleration. The spring k is assumed to be linear, without mass but possessing elasticity. When the spring is deformed in extension or compression, spring force exists. The linear spring obeys Hooke's law. The damper element c (Figure 3.1) is also assumed to be a solid mass and does not have elasticity. When there is a relative velocity between the two ends, a damping force exists. This force is proportional to velocity in the case of linear damping. The different equations of motion are established by using Newton's law. For the free diagram body shown in Figure 3.1 the system's equation of motion is given as:

$$m\ddot{x} + c\dot{x} + kx = F(t) \tag{3.1}$$

Where m : the mass.

c : the damping coefficient

k : the stiffnes

$F(t)$: the excitation force

Equation 3.1 from Figure 3.1 system has one independent variable to determine the position of the system. Therefore, it is a system of one degree of freedom. Rao (1990) defines the degree of freedom as the number of independent variables required to determine any position and orientation of the vibratory system at any instant time.

3.1.2 Classification of mechanical vibration

The classification of mechanical vibration can be made using the system shown in Figure 3.1. Some of the important classifications are presented in paragraph below.

3.1.2.1 Free vibration

A free vibration occurs when, after an initial disturbance, the system is left to vibrate on its own. The equation of motion for free vibration from Figure 3.1 is:

$$m\ddot{x} + c\dot{x} + kx = 0 \tag{3.2}$$

If during the vibration, the energy is dissipated or lost in the friction or other resistance, the vibration is known as damped vibration (Equation 3.2). On the other hand, if no energy is dissipated or lost, the vibration is called undamped vibration. Figure 3.2 shows the response of free vibration and the level of damping of the system shown in Figure 3.2, in terms of displacement as a function of time.

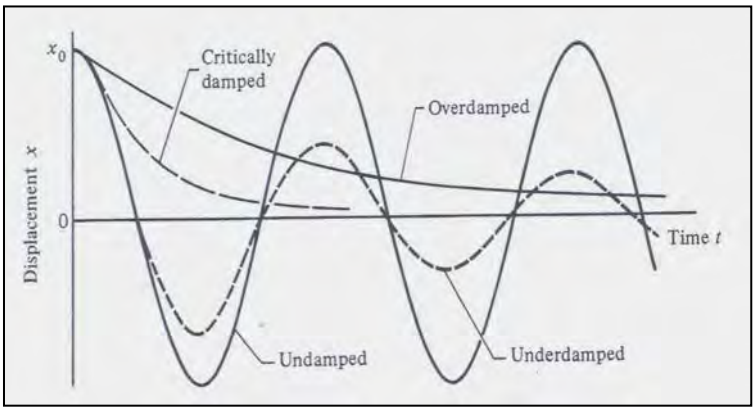

Figure 3.2: Free vibration response of system shown in Figure 3.1 (Tse et al., 1979).

The equation of motion for undamped vibration from Figure 3.1 is given as:

$$m\ddot{x} + kx = 0 \tag{3.3}$$

3.1.2.2 Forced vibration

The forced vibration of a system is the one which occurs when the system is subjected to an external force. In the most cases, the type of force is a repeating force. This kind of vibration happens in many machines such as turbines and diesel engines. Equation 3.1 shows the equation of motion for a forced vibration system. One of the results of a forced vibration is the resonance frequency at which the system undergoes dangerous oscillation. Failures of structures such as turbines, buildings, airplane wings, and bridge have been associated with the occurrence of resonance frequency.

3.1.2.3 Deterministic and random vibration

A deterministic vibration is the result of a vibration where the excitation value (moment or force) is known. The force or moment acting on the system is called deterministic. In the other case where the excitation for vibration is unknown and cannot be predicted the vibration is known as a nondeterministic vibration or random vibration. Figure 3.3 shows a

graph of force excitation for a deterministic vibration and a random vibration as a function of time.

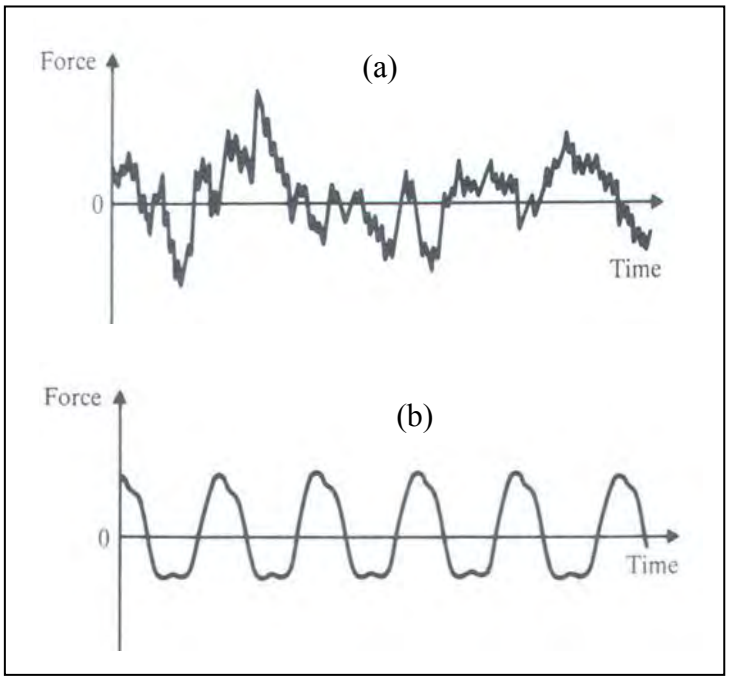

Figure 3.3: (a) Example graph of a random excitation (b) Example graph of a deterministic excitation (Rao, 1990).

3.2 Mechanical behavior of Stockbridge Damper

This part presents some of the research work available on the Stockbridge damper. After much investigation, it is evident that there are few publications on the Stockbridge damper.

Tompkins et al. (1956) established the electrical analogy of the symmetrical Stockbridge damper. After representing schematically the Stockbridge damper on the shaker with the dashpot, spring and mass, the authors made the electrical analogical schematic where the dashpot, spring and mass are analogue to the capacitor, inductor, and resistor (Figure 3.4). At the end of this process they determined the mechanical characteristics of the damper.

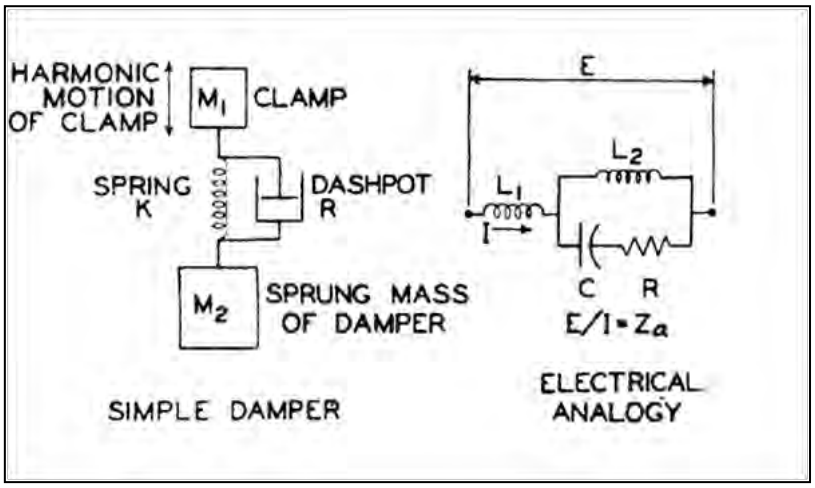

Figure 3.4: Mechanical representation of a Stockbridge damper and its electrical analogy (Tompkins et al., 1956).

The response of a Stockbridge damper according to its harmonic excitation has been analyzed by Claren and Diana (1969). They considered the Stockbridge damper as a system with two degrees of freedom which are the rotation θ_a and the translation x_a. By assuming that the damper's messenger cable is uniform and ideally elastic without any damping, the equation for free vibration is the following:

$$-M\ddot{x}_a + GM\ddot{\theta}_a - k_{xx}x_a + k_{x\theta}\theta_a = 0 \tag{3.4}$$

$$-J_a\theta_a + GM\ddot{x}_a - k_{\theta\theta}\theta_a + k_{\theta a}x_a = 0 \tag{3.5}$$

Considering the damper as a beam with one end fixed and with a mass located at the other end, Claren and Diana (1969) determined the two resonance frequencies (Equation 3.6) as a function of the damper's parameters as follows:

$$\varpi_{1,2}^2 = 2k\frac{(1/3)L^2M + J_a - LGM \mp \sqrt{[(1/3)L^2M + J_a - LGM]^2 - (1/3)L^2(MJ_a - G^2M^2}}{MJ_a - M^2G^2} \tag{3.6}$$

More details about Equations 3.4 and 3.5 will be developed in the following chapter.

The theoretical analysis of Stockbridge damper dynamics has been published by Wagner et al. (1973). Considering the Stockbridge damper has a system with two degrees of freedom,

forces and moment which react on the damper during its vibration have been calculated. In addition, the dynamic stress of Stockbridge damper has been calculated to predict the life of a symmetrical Stockbridge damper. Wagner et al. (1973) developed a fatigue test of the symmetrical Stockbridge damper by exciting the damper at constant displacement (2mm peak to peak) at it highest resonance frequency. Failure of the damper occurs around 160000 cycles and the authors observed that resonance frequency and the dynamic reactance dropped with the number of cycles elapsed (Figure 3.5).

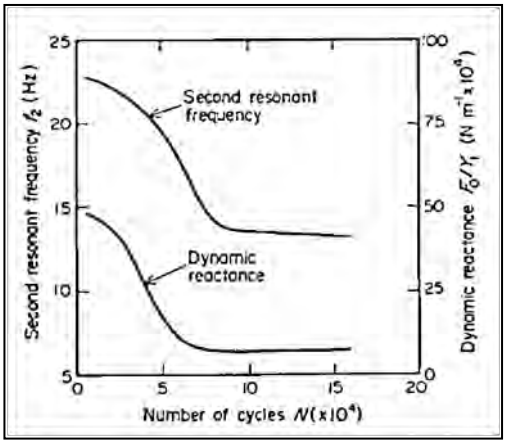

Figure 3.5: Drop of dynamic reactance and resonance frequency of a Stockbridge damper s a function of number of cycles (Wagner et al., 1973).

The optimization of characteristics of a Stockbridge damper mounted on a conductor has been presented by Markiewicz (1995). Markiewicz (1995) demonstrated how the Stockbridge damper can mitigate more power line vibration by changing its position on the line. To achieve the optimization, two dynamic models have been computed, the simplified model and the general model (Figure 3.6). The flexure of the cable is disregarded because the tensile force s and the mass per unity length m are sufficient to describe the behaviour of cable. In the simplified model, the insulator is described by the length l and moment of inertia by J_0. Concerning the general model, the insulator is represented by n taut cable ($q_1, q_2, ..., q_n$) with infinite length connected in series. A is the end point of insulator and B the arbitrary point where the Stockbridge damper is placed.

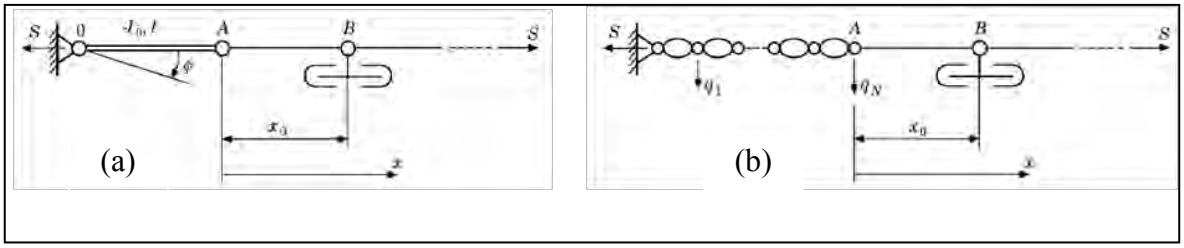

Figure 3.6: Dynamic models of the dead end of span. (a) Simplified model. (b) General model (Markiewicz, 1995).

The result travelling $u(x,t)$ wave is given by the following equation:

$$u(x.t) = U\sin k(x+ct) + V\sin k(x-ct) + W\cos k(x-ct) \tag{3.7}$$

Where the first term represents the incident vibration, the second and the third are the reflected vibrations. Markiewicz determined the dampening which could absorb all vibration from incoming waves. In other words, determine the power dissipation of a damper so that amplitudes of vibration V and W are equal to zero.

Richardson (1996) provided a calculation to determine if dampers are needed or not. Calculations of the energy input by the wind to the conductor and the energy lost from the conductor were also determined. By vibrating the conductor at constant velocity, Richardson found that the energy lost from the conductor and the wind energy are not the same (Figure 3.7) (Richardson, 1996). It has been observed that around a critical point Cr both energies are equal. Before the critical point Cr, the energy lost is less than the wind energy and it is the inverse after the critical point Cr. According to Richardson (1996), before the critical point the damper is needed. By means of this interpolation Richardson (1996) determined if a damper is needed or not. If the energy gap between wind energy entering the conductor system and the energy leaving the system is large, then a damper is required in order to damp that energy gap. The energy gap represents the energy shortfall and must be supplied by the damper. At the end, a good agreement has been found between field tests and Richardson's (1996) calculations. The exact optimal point of damper location on the conductor was not determined in that study.

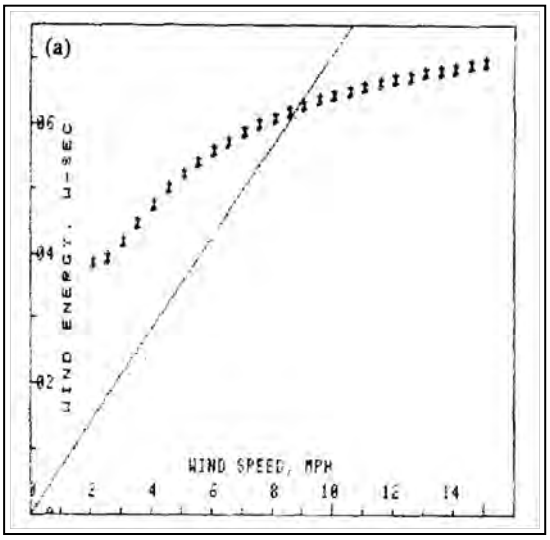

Figure 3.7: Energy lost (straight line) and wind energy (computed points) versus wind speed (Richardson, 1996).

The analysis of the Aeolian vibration of a conductor with a damper has been studied by Vecchiarelli et al. (2000). To investigate the steady-state form of conductor Aeolian vibration, the bending amplitude of the conductor as a function of the vibration frequency, and the function of damper location, the authors performed two numeric analyses.

Lara-Lopez and Colin-Venegas (2001) investigated the endurance of Stockbridge dampers. By knowing the vibration parameters, they presented a method to calculate the life of symmetrical Stockbridge dampers. The authors also presented a dynamic analysis of Stockbridge dampers. For this, they determined the behaviour of a symmetrical damper when it vibrates at first resonance with constant displacement peak to peak. Bending stress near the end clamp σ_i and near the attached point σ_j on the messenger cable are given:

$$\sigma_i = \frac{(PL + M_b)d}{2I_a} \tag{3.8}$$

$$\sigma_j = \frac{M_b d}{2I_a} \tag{3.9}$$

Where P is the shear force, M_b is the bending moment, d and I_a are respectively the diameter and the moment of inertia of messenger cable.

Two calculations methods of the life of Stockbridge damper have also been presented. The first is based on the classical theory and the second is based on cycles calculated by the strain life approach. The classical life is given by the following equation:

$$N = [0.004762(\frac{q}{f})\frac{D_{\max}}{S_u}]^{-\frac{1}{0.157}} \tag{3.10}$$

Where N is the number of cycles to failure

q is the select number $q = \frac{25.4}{2}$ from the experiment done by Lara-Lopez and Colin-Venegas (2001)

f is the first resonance frequency of the damper

$D_{\max}$ is the function value which give the maximum bending stress of the messenger cable.

S_u is the ultimate strength of the messenger cable

The other mathematical expression used by Lara-Lopez and Colin-Venegas to determine Stockbridge damper life is given by the equation below:

$$\frac{\Delta\varepsilon}{2}(N) = \frac{\sigma_f^{'}}{E}(2N)^b + \varepsilon_f^{'}(2N)^c \tag{3.11}$$

Where $\Delta\varepsilon$, $\sigma_f^{'}$, N, E, b, $\varepsilon_f^{'}$ and c are respectively the strain and strain amplitude, number of cycles to failure, the Young's modulus of the messenger cable, fatigue ductility coefficient, and fatigue ductility exponent.

The life of symmetrical damper was calculated by vibrating the damper at constant displacement peak to peak. The constant displacement was varied from 5.98 to 7.26mm. No experiment was conducted by Lara-Lopez and Colin-Venegas to the point of damper failure. The authors found that damper life is very sensitive to the amplitude of variation.

Some years later, Sauter and Hagedorn (2002) developed a massing model for a damper messenger cable (Figure 3.8).

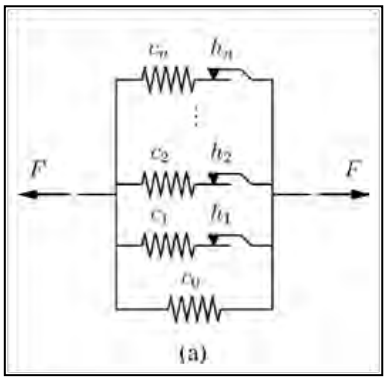

Figure 3.8: Massing model for concentrated element (Sauter and Hagedorn, 2002)

Using the massing model, Sauter and Hagedorn (2002) established an equation of the damper messenger cable motion. Their model is a one-dimensional continuum where the messenger cable wires are not individually modelled. Expecting the messenger cable propriety to change near the clamp, they described it at each position (distributed model or local model). The bending moment $H(s,t)$ as part of the hysteresis and the bending stiffness $EI(s,t)$ of the Jenkin element have been used in the model. $EI(s)$, $c(s)$ and $H(s)$ are numerically determined by data from experiment as a function of the position s.

Diana et al. (2003) evaluated the effectiveness of the Stockbridge damper. In Part I they presented a comparison between testing on a span and testing on a shaker. Part II presented the influence of impedance on the energy dissipated. The forced exerted between the damper on the span and the cable was determined. Figure 3.9 shows the modified damper used to determine the force between the damper and the cable.

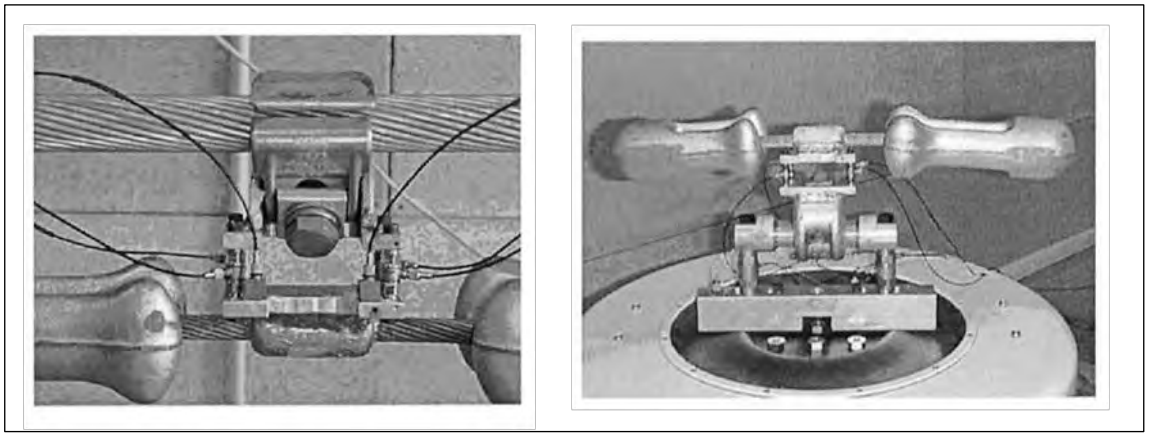

Figure 3.9: Modified damper to determine the force exerted between the damper and the cable (Diana et al., 2003).

Dian et al. evaluated damper impedance in Part II. Based on the test of the damper on the shaker and on the 6 d.o.f of the damper, Diana et al. (2003) made an investigation to determine the single matrix 2x2 for the asymmetrical damper.

The approach of optimizing parameters of the Stockbridge damper has been proposed by Navarro-Canales et al. (2008). Taking into account dynamic behavior, damper parameters have been calculated for the maximum attenuation of Aeolian vibration. In addition, the parameters of Stockbridge damper have been determined for a minimum cost of a symmetrical Stockbridge damper. Among parameters, the mass of weight m and the length of messenger cable L are more important variables than the centre of gravity G and the moment of inertia J for the interval considered (Navarro-Canales et al. 2008). Efficiency of the Stockbridge damper as a function of the messenger cable length L and the mass of weight has also been determined (Figure 3.10).

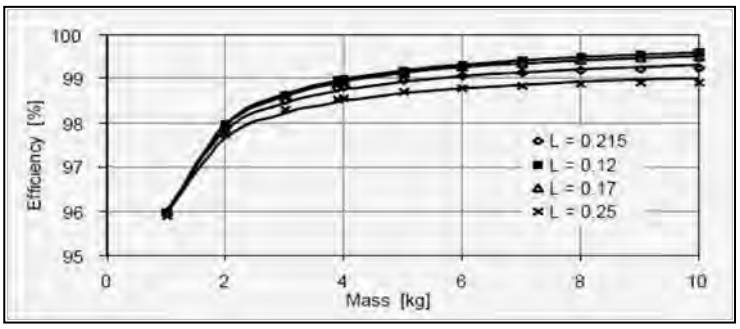

Figure 3.10: The efficiency on the damping side vs mass for different lengths of the messenger cable at constant G and J (Navarro-Canales et al., 2008).

3.3 Damage in mechanical engineering

3.3.1 Introduction

The more-or-less random fluctuations of load subject most structures or machine parts to deformation or failure. The repeated variation in load magnitudes has an important effect on the behaviour of materials. By considering what happens to a structure or machine's parts during its history, it can be observed that the parts undergo damage which increases progressively to the point of failure. During each stress cycle, samples are progressively damaged and the damage accumulates (Newmark, 1950). Therefore, the accumulation of damage is expected in the life of machine parts or structures and requires damage detection strategies.

3.3.2 Structural damage detection

Structural damage can be defined as the reduction of its function and performance. Structure and mechanical component damage are elicited by environmental loading such as force, torque, wind, rain. They are accumulating damage which can be detected by the changing of properties. Any change of physical properties of components or structures will be reflected in its mechanical properties. Therefore, the resonance frequency change of a component during its vibration can be used as a factor to detect its degree of deterioration.

The damage detection by use of frequency was first reported by Adams et al. (1978). Their experiment was conducted on two rectangular aluminium bars, one damaged and the other undamaged. The frequency measured on the damaged bar and the undamaged bar were

calculated and compared. The result was that the damage was located accurately on the bar, by means of frequency.

The modal frequency method has been used by Ju and Mimovich (1988) to diagnose damage in structure. Based on the analytical theory of the loaded spring, they used the modal frequency to detect experimentally the damage in the structures. By using the beam experimentally, the accuracy is around 4% for the damage, and 1% for the location of length.

Salawu (1997) reviewed the damage of structures by using the change of resonance frequency. The effect of structural damage on the natural frequency was first presented, followed by methods to detect and to locate the damage. Finally, Salawu (1997) presented factors that must be considered in damage detection of structures by using the change of resonance frequency.

The change of frequency has been applied in the statistical damage identification of structure by Yong and Hao (2002). The authors developed an algorithm which takes in account the random noise effect from the vibration data as well as from the finite element model.

A technique based on few frequency response functions has been proposed by Hwang and Kim (2004). From their model, it was assumed that the finite element model was adjusted to be closer to the experimental test. The verification of their proposed model was tested on a cantilever beam and on a helicopter rotor.

To overcome the difficulty of noise compatibility with the problem of coordination, Huynh et al. (2005) proposed a technique to detect and locate the damage. Damage detection was obtained from the finite element model applied to a plate structure and a space truss structure.

Damage detection methods based on the changes of natural frequency have been summarized by Yan et al. (2007). The change of frequency has also been used to establish a fatigue model for spot-welded joints (Wang et al., 2008). Using this model, fatigue damage has been established and a good correlation has been proved with the experiment data.

To localize multiple damages in structures, Guo and Li (2008) presented a Bayesian fusion theory. This method of localizing multiple damages is based on using frequency and strain data. The fusion is made of two theories which are the modal strain energy dissipation theory and the frequency change damage detection theory. To illustrate the performance of the

fusion theory, a numerical example was made on a truss structure. Guo and Li demonstrated that the frequency damage change theory, damage detection theory and the strain energy dissipation theory can be used separately to detect and locate damage when there is single damage, but for multiple damages, the Bayesian fusion methods must be applied.

The change of resonance frequency has been used in structural health monitoring by White et al. (2009) for detecting the damage of debonding in composite bonded patches. For that, White et al. (2009) examined scrap repair and checked the health of the repair of the original repair and found that damage could be detected in both cases by using the change of resonance frequency.

Damage detection in bridges has been investigated by Medda and DeBrunner (2009). They vibrated a beam and the vibration signal before and after damage was compared. At the end, technique of damage detection on the bridge was established by using the wavelet packets. This allowed the decomposition of vibration signal in phase also. It was found that damage detection in a bridge depends on the frequency, phase, and the space in the damage direction.

Bo and Wei (2009) used the frequency perturbation of structure to detect damage and establish a new method. The simulation was of a span truss with single and multiple damages analyzed. Their results that the method decreases test error especially for structures with multiple elements damage. The reduction of calculation time, efficiency and raising precision are the main advantages of the method.

A frequency tracking technique was used by Fitzgerald et al. (2010) to develop an algorithm for damage detection of wind turbine blades. The effectiveness of the algorithm was tested by numerical simulation. By using the frequency, it was possible to detect the simulated damage on the blades.

Zishou et al. (2010) provided a new method of damage detection and location based on frequency response and wavelet packet. They investigated a beam where they took the resonance frequency before and after damage. Numerical simulation was made on two continuous beams and it was found that damage could be identified easily and exactly located.

Liu et al. (2011) published the dynamic characteristics of tower structures. Dynamic tests were conducted on a tower and the finite element model established. After analyzing the same type of damage at seven different locations, Liu et al. (2011) found the tower presented

different frequencies. The results indicate that dynamic tests for the detection of damage can be successful.

3.3.3 Cumulative fatigue damage

The cumulative fatigue damage approach is used in the prediction of remaining life of structures and components subject to load cycles.

Over the years a lot of cumulative damage rules have been developed. Fatemi and Yang (1998) classified damage analysis into five groups according to the physical basis:

- the damage curve approach;
- the endurance limit-based approach;
- the S-N curve approach;
- two damage approach;
- the crack growth based approach.

The first concept was suggested by Palmgren (as cited by Fatemi and Yang, 1998). Palmgren's concept is known as the Miner rule:

$$D = \sum_{i=1}^{p} r_i = \sum_{i=1}^{p} \left(n_i / N_{ri} \right) \tag{3.12}$$

Where D is the cumulative damage, r_i represents the cycle ratio, n_i the applied cycles an N_{ri} the total number of cycles to failure.

This concept is a numerical summation of the cycles ratios, in such a way that failure occurs when $D = 1$. Figure 3.11 shows the types of loading charge and the application of the Miner rule.

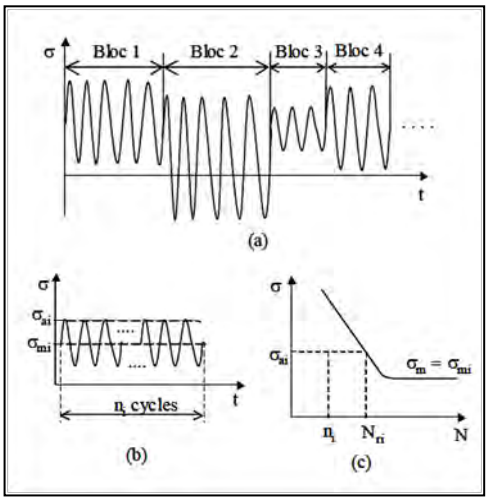

Figure 3.11: Types of loading charge. (a) Sequence composed of several blocks of solicitation. (b) Cycles' number n_i of i^{th} bloc. (c) stress amplitude function of cycles' number (S-N curve) theories (Fatemi and Yang, 1998).

The Miner damage rule is the most used approach because of its facility of application. It does not require any parameter determination. The knowledge of materials' S-N curve is the only necessity.

However, Equation 3.12 does not take into account former solicitation on the sample. In addition to that, it is well known that damage evolution is not linear. Therefore the use of additional rules is necessary. The first nonlinear damage theory represented by Equation 3.13 and depicted in Figure 3.12 was established by Marco and Starkey (1954):

$$D = \sum r_i^{x_i} \tag{3.13}$$

Where x_1 is the quantity which depends on the number of cycles.

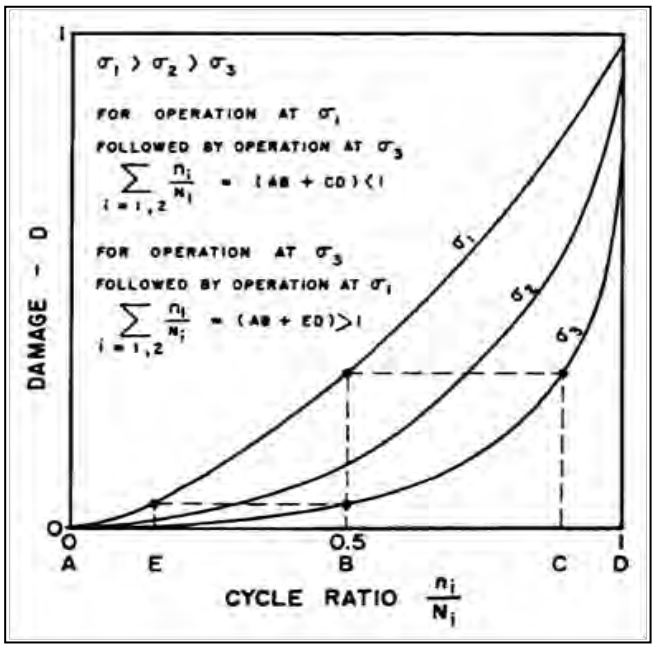

Figure 3.12: Marco-Starkey's plotting of D vs r (Fatemi and Yang, 1998).

According to Ngargueudedjim (2003) and Fatemi and Yang's (1998) classification of damage rules, the endurance limit-based approach (Henry model, Gatts model, Bui Quoc et al. model) could be suitable for analyzing Stockbridge dampers.

3.3.4 Damage models for Stockbridge dampers

After further investigation, Kommers (1945) and Bennett (1946) were the first to suggest the use of endurance strength as a damage measure. However, the correlation between endurance strength and the life of component was not proposed by these researchers. This was made by Henry (1955).

The two hypotheses which guided Henry (1955) in his research are:

The S-N curve (Wohler's curve) could be plotted in the range of stress less than the endurance limit by using Equation 3.14:

$$N_r = \frac{K}{\sigma - \sigma_D} \tag{3.14}$$

Where N_r is the number of cycles

K is the empirical coefficient of material

σ is the stress amplitude

σ_D In the endurance limit of material

For a new component, Equation 3.14 becomes:

$$\sigma = \frac{K_0}{\sigma - \sigma_{D0}} \tag{3.15}$$

With K_0 is the empirical coefficient of material for the new component, σ_{D0} the endurance of the new material.

Equation 3.15 is applied with Weibull's condition $\sigma_{D0} < \sigma < 1.5\sigma_{D0}$ (Ngargueudedjim, 2003).

The endurance limit of material σ is function of the damage of the component and its changing variation is a function of K.

The non-linear damage model was established as a function of endurance limits by Henry (1955):

$$D = \frac{\sigma_{D0} - \sigma_D}{\sigma_D} \tag{3.16}$$

In the same way Henry (1955) established the equation:

$$\sigma_D = \frac{\sigma(1-r)}{\gamma - 1} \tag{3.17}$$

With $r = \frac{n}{N}$ the ratio of the number of cycles

$$\gamma = \frac{\sigma}{\sigma_{D0}} \tag{3.18}$$

Therefore, according to Henry (1955), the damage expression after n_i cycles with the stress amplitude becomes:

$$D_i = \frac{r_i(\gamma_i - 1)}{\gamma_i - r_i} \tag{3.19}$$

Henry's (1955) damage model does not have any parameter to be determined and includes the history of the component. It is applicable to stress less than the endurance limit of material.

Some years later, Gatts (1961) developed a damage model for stress higher than the endurance limit. This damage model had been used with the model of Henry, Shanley and Valluri by Bui-Quoc to make his model (Fatemi and Yang, 1998).

Bui-Quoc et al. (1971) developed two model versions (stress and strain version) based on the endurance limit change. The main hypothesis of this model is that the strength and endurance limit of materials decrease with growing cracks. By using the integration of differential equations and the dimensionless stress ratio, Bui-Quoc (1971) established the stress version of model damage:

$$D = \frac{1-\gamma}{1-\gamma_{ec}} = \frac{r}{r + (1-r)\dfrac{\gamma - \left(\gamma / \gamma_u\right)^m}{\gamma - 1}} \tag{3.20}$$

where $\gamma_{ce} = \dfrac{\sigma_{ce}}{\sigma_{D0}}$ is the critical endurance ratio, $\gamma_u = \dfrac{\sigma_u}{\sigma_{Do}}$ is the ultimate endurance ratio and m is the constant which depends on the material. The strain version was derived from the stress version by replacing the stress parameter by the strain parameter. Therefore, the strains version of model is:

$$D = \frac{r}{r + (1-r)\dfrac{\lambda - \left(\lambda / \lambda_u\right)^m}{\lambda - 1}} \tag{3.21}$$

Figure 3.13 shows the comparison between equation 3.20 (The hybrid theory) and Miner theory (The linear theory) as well as Henry theory.

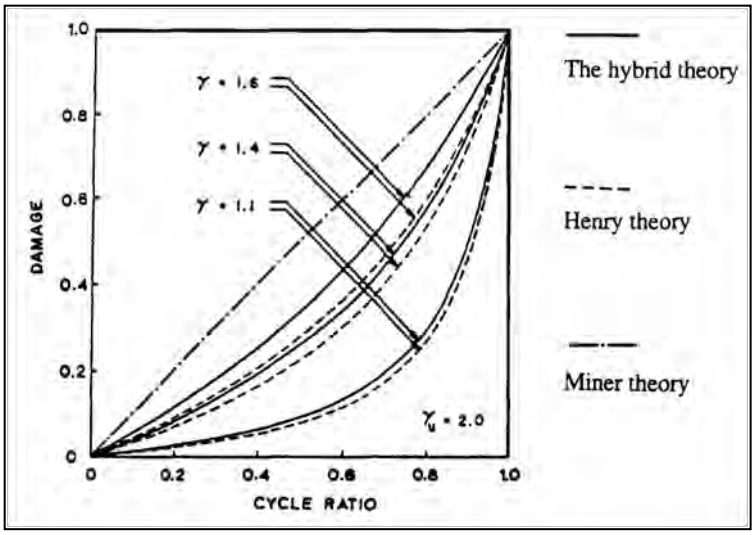

Figure 3.13: Comparison between hybrid, Henry and Miner damage theories (Fatemi and Yang, 1998).

3.4 Remaining life assessment

3.4.1 Introduction

The remaining useful life is the time left for a component or a structure to get to the point of failure or damage. Si et al. (2011) define remaining life as being the length of time from the current time to the end of useful time. The determination of remaining life is important in the process of planning of maintenance, especially in engineering (Jardine et al., 1999; Mazhar et al., 2007). To investigate and to assess the performance of structures or components, proprieties must be evaluated. The investigation of proprieties is a power tool in engineering to assess performance service and to estimate the remaining life of components or structures. Proprieties obtained from plant operational data or from laboratory experiment can be analyzed to determine remaining life. It is well known that remaining life is random, therefore statistical approaches are necessary.

3.4.2 Remaining life

The determination of remaining life of a component is important in the health assessment, management and maintenance of equipment. Therefore, researchers have found the evaluation of life assessment to be of great interest. The life assessment of components is classified as a key ingredient in engineering planning. The following paragraphs present some research conducted on the estimation of life and remaining life.

The estimation of the remaining useful life of conductor has been researched by Havard et al. (1992). The curves of progressive degradation were established and thereafter the remaining useful life established by correlation. The device invented by Central Electricity Generating Board (CEGB) staff was modified and used by Havard et al. (1992) to test the loss of galvanizing on the conductor in situ. The conductor's life was estimated based on zinc loss, tension testing and torsional ductility testing and the correlation established for each case as a function of elapsed years.

Jiqun and Shoutai (2000) presented a method to determinate the remaining life of XLPE used cable. Cable used for 10 years was tested by cutting it into many sections which were then divided into two groups. Each group was tested and the remaining life determined by using linear regression analysis and Weibull's distribution.

The remaining life of 12Cr1MoV steel has been presented by Zhao et al. (2004) by using the Z-parameter method. Their work was based on the Larson-Miller parameter of steel which was transformed in the family of curves with parameter K parallel to the main curve. The correlation of normal distribution was used to establish the relationship between the degree of deterioration and parameter Z.

Mukhopadhyay et al. (1999) presented the remaining life estimation of an economiser boiler which had been in service for a certain time. They established the remaining life of the economiser tube based on stress evaluation and thickness after investigating some mechanical proprieties.

To assess the end of life of a used product, the remaining life estimation has been investigated by Mazhar and Kaebernick (2007). In this study, the neural networks analysis was used as well as the multiple regression method which is the traditional method. They determined the remaining life as the difference between the total life and the actual life.

The life assessment of remaining life for steel tubes (thermal power plant tubes) has been studied by Ray et al. (2007). These tubes had been in the service for some years at optimal levels. The remaining life was determined after an investigation of tensile, hardness and dimensional measurements.

The estimation of remaining life has been a problem for research for a quite long time. A new approach to determining remaining life by using the sequential law has been developed by Siriwardane et al. (2008) especially for railway bridges. Their approach is based on the

sequential law and stress histories. Results obtained of fatigue lives were compared to Miner's rule.

By using the cumulative damage hypothesis, Yeo et al. (2008) developed a fatigue model for asphalt. An accelerated test was conducted on asphalt and the results correlated with those obtained from the laboratory. Stress and the Young modulus were measured and the model developed. The remaining life of the asphalt was determined based on the model established.

The Weibull distribution has been used by Sivapragash et al. (2008) to predict the life as well the remaining life of magnesium alloy. The construction of curves for maximum stress and cycles to failure were made for ZE41A magnesium alloy and thereafter the fatigue life was predicted.

Yan and Guo (2009) improved the Markov model to predict remaining life. To avoid the uncertainty during the remaining life estimation, they used a Fuzzy C_Means model algorithm. To test the accuracy of the model, the unbalance rotor (Bently-RK4) was used.

The life or the remaining life of electronic component devices has been study by Zhang et al. (2009) based on the back propagation of artificial neural networks. The new model was presented after using the accelerated degradation test to reduce the testing time as well as the cost.

Li et al. (2009) calculated the remaining life of underground pipelines calculated using mechanically-based probabilistic methods. In addition, the cumulative distribution function of remaining life has been established. At the end, a methodology was presented which takes into account the random effect of corrosion in the pipe.

Gillen and Celina (2001) presented an approach to predict the remaining life of polymers. After outlining the polymer components, the authors concluded that polymer degradation is a result of the superposition of time and temperature. The remaining life prediction was possible after predicting linearly the life time at an accelerated temperature.

3.4.3 Approach for remaining life

Data collection is the first operation to undertake in remaining life prediction. Si et al. (2011) categorized the data collected into two types:

- The event data (past recorded failure data);
- The condition monitoring data (data which have a direct influence on the determination of the remaining life such as the degradation signal, the environment, the performance).

The second type of data is suitable for the prediction of damper's remaining life. Wang and Christer (2000) classified these data into two classes which are direct and indirect condition monitoring data. Direct monitoring data are those which describe directly the life or the remaining life of structure. This class contains for instance data from crack size and wear. On the other hand, there are indirect monitoring data which only partially or indirectly indicate the state of system. The data from vibration or analysis of oil for prediction of remaining life are part of this class.

According to Wang and Christer (2000), indirect condition monitoring data is suitable for investigating the remaining life of Stockbridge dampers. Figure 4 gives the taxonomy of the remaining life based on the statistical approach which could be used for dampers.

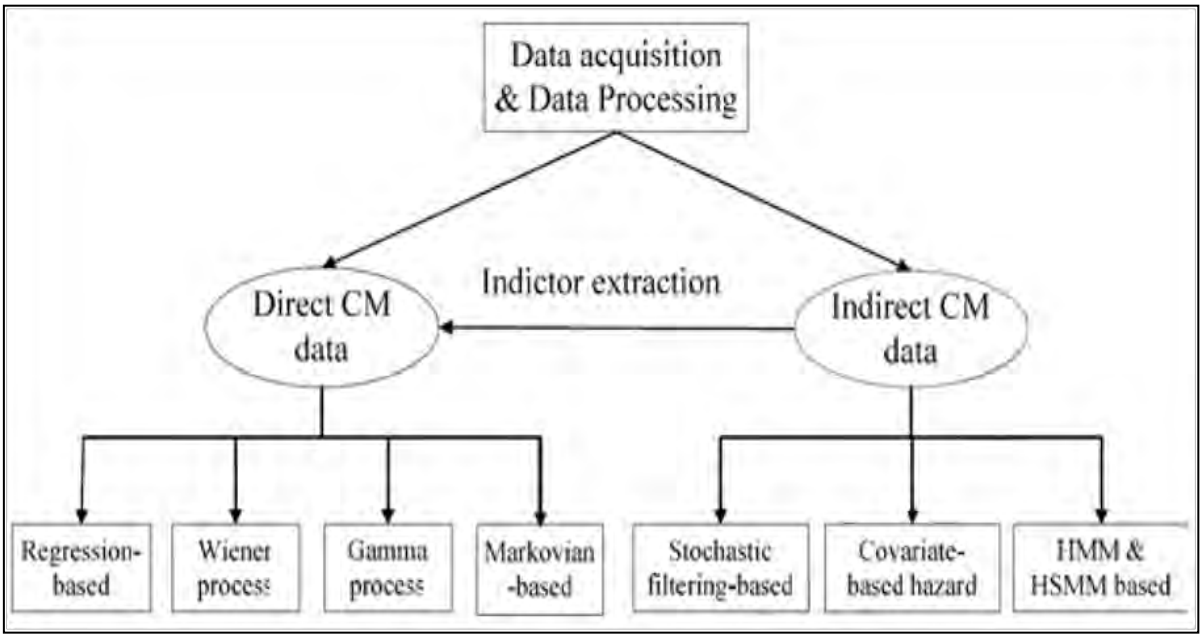

Figure 3.14: Taxonomy of statistical data driven approaches for remaining life (Si et al., 2011).

In order to use the direct condition monitoring data, it is necessary to focus on its extraction. By using signal processing techniques such as Wavelet or Fourier transform, it is possible to extract or compute data from the indirect to the direct condition monitoring data. That

process is called feature extraction. Regression, the Markov model, the Wiener or the gamma process can be used. The Wavelet transformation was used by Qiu et al. (2006) for feature extraction to predict the rolling element bearing. But they did not focus on remaining life. The feature extraction has been used by Gasperin et al. (2011) to predict the remaining useful life. A review of the feature extraction has been made by Jardine et al. (2006).

Life time or remaining life estimation in academic spheres as well as in industry rely on the regression-based method (Li and Nilkitsarama 2009; Meeker and Escobar 1998). The Wiener process has been used by Tseng et al. (2003) and Liao and Elsayed (2006) to determine the lifetime of electrical light. The same process was used by Wang et al. (2000) to determine the remaining life of three water pumps. The gamma process is used for degradation processes which are monotonic and evolving only in one direction such as cracks growing. The crack growing method will not be used in this work. Thus, it is not discussed in this section.

CHAPTER 4

MATERIAL AND METHODS

4.1 Auxiliary Equipment

Tests were carried out at the Vibration Research and Testing Centre (VRTC) at the University of Kwazulu-Natal, Durban, South Africa. VRTC provides an indoor facility laboratory and is mainly focused on testing and researching Aeolian vibration and related mechanical vibration with the guideline provided in IEEE (Institute of Electrical and Electronics Engineers) and IEC (International Electrotechnical Commission)standards. The vibration test system has the essential components shown in Figure 4.1. In this paragraph some of the equipment used in this project is presented.

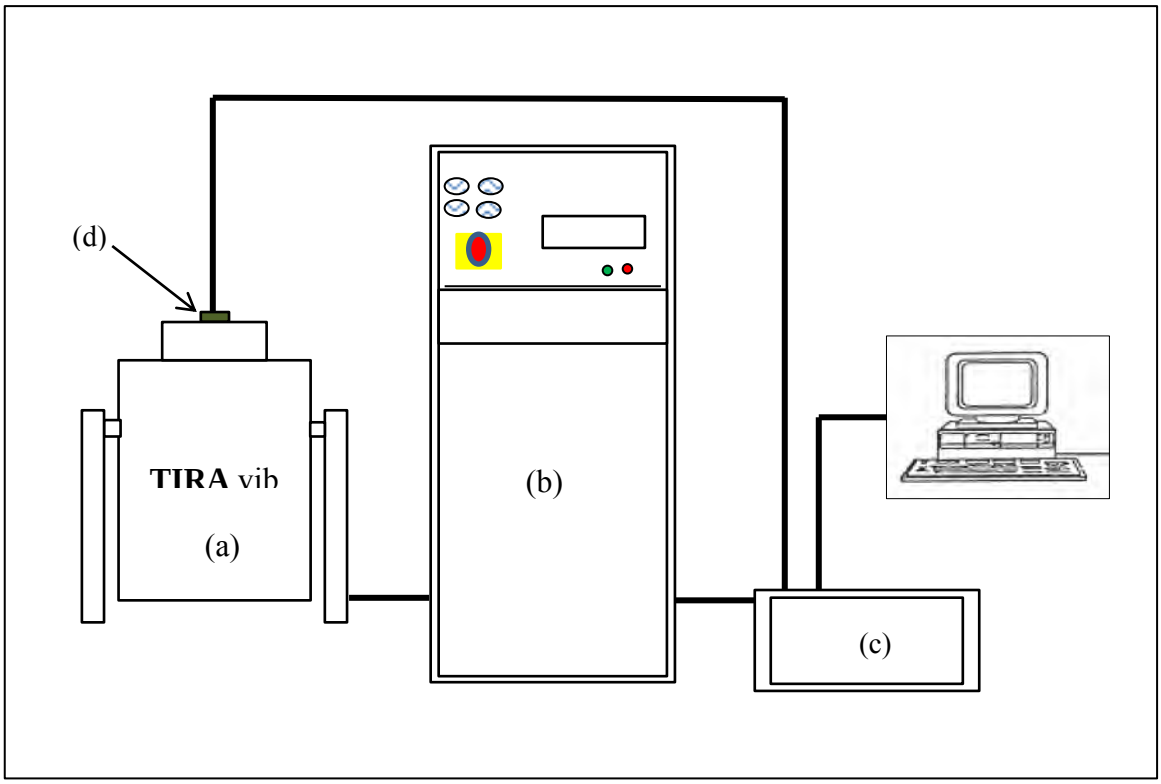

Figure 4.1: Components of the vibration test system on the shaker base. (a) Shaker. (b) Amplifier. (c) Controller. (d) Accelerometer.

4.1.1 Shaker, amplifier and controller

The production of vibration in the laboratory for this project has been made by using the electrodynamic shaker (Figure 4.2). The electrodynamic shaker used is a TIRA Model, Type TV 56263/LS and is pivoted to enable the excitation in a horizontal or vertical direction. In order to guarantee the performance of the system, the digital amplifier is used. In principal the electrodynamic shaker operates like a speaker where the armature movement is created by an electrical current in the coil. The coil produces a magnetic field which is opposite to the static magnetic field produced by the electromagnet in the shaker. Electrical power (voltage and current) is provided to the armature of the shaker through the amplifier. It also provides the necessary field power supply for the cooling fan, and auxiliary supplies. In addition to those functions, the role of the amplifier is to monitor the system interlock signals. It shuts down when any abnormality is observed in the vibration system which is a closed loop system. The controller role is to ensure that what has been programmed is the same as the output signal from the shaker base accelerometer.

Figure 4.2: Electrodynamic shaker at the Vibration Research and Testing Center.

4.1.2 Accelerometer

An accelerometer is a device which senses the motion of a component or object to which it is attached and produces a signal electrical voltage or current) which is proportional to the component or object motion. The object motion is characterized by some quantity of vibration which could be acceleration, velocity, or displacement. The signal produced by the accelerometer passes through typical steps which include amplification, attenuation, filtration, differentiation and integration. The accelerometer is a link between the vibrating object and the measurement equipment. In this project, piezoelectric accelerometers model Bruel & Kjaer type 4508-002 and 4507 B were used. The measurements were captured by PUMA Vibration Control and Analysis System software (Figure 4.3).

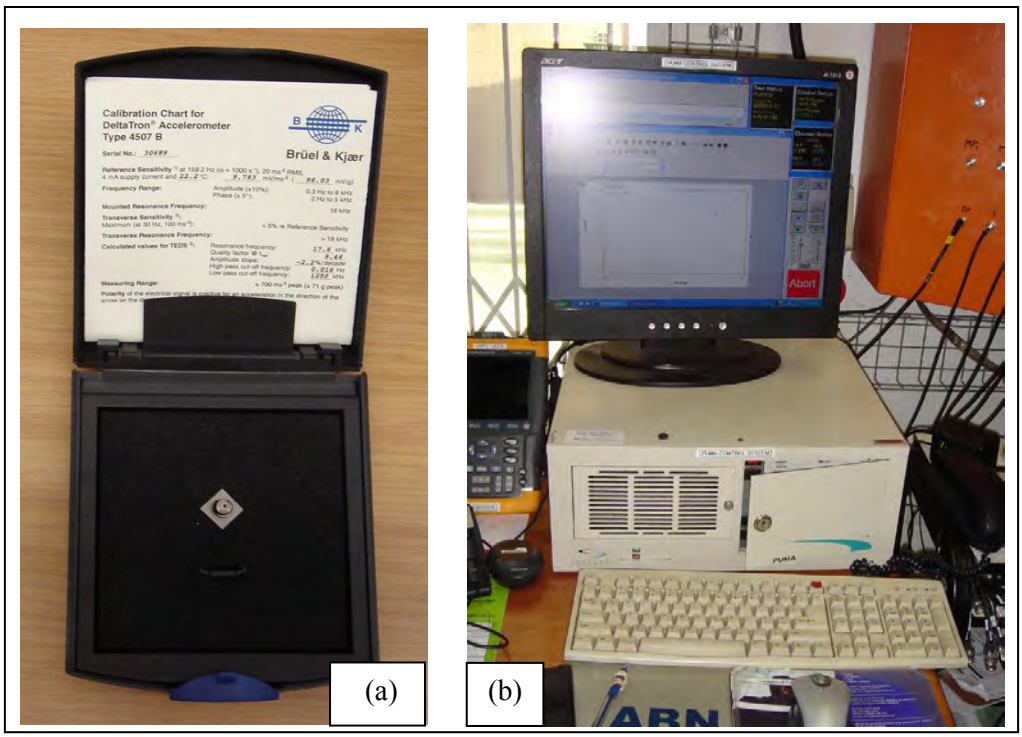

Figure 4.3: (a) Piezoelectric accelerometer model Bruel & Kjaer type 4507 B. (b) PUMA Vibration Control and Analysis System software.

Compared to other types of sensors piezoelectric accelerometers are widely used in vibration research because of their advantages. Some of the important advantages of piezoelectric accelerometers are:

- Wide frequency range of measurement;
- No moving parts therefore no wear or inertial problem;

- The accelerometer signal can be easily integrated to obtain velocity as well as displacement;
- High sensitivity.

4.1.3 Strain gauges

a. Introduction

A strain gauge is a sensor used to measure the strain on the object's surface during the experiment. The most widely used is the metallic strain gauges of which the main part is the very fine resistance wire. The resistance changes when the object is deformed and this change cannot be measured with an ordinary ohmmeter. Therefore the use of the Wheatstone bridge is necessary to measure the small changing of resistance.

The strength of material plays a very important part during engineering design. Strength is used to determine if the parts can carry their loads with or without deformation or failure. The ability to carry the load is characterized in terms of stress which can be calculated as:

$$\sigma = \frac{F}{A} \tag{4.1}$$

Where σ is the stress

F is the applied force

A is the area.

The loads applied can be also characterized in term of strain which is the amount of deformation per unit length. According to the strain definition, the following expression is used:

$$\varepsilon = \frac{\Delta L}{L} \tag{4.2}$$

Where ε, ΔL, and L are respectively the strain, the length change and the initial length.

The relation between strain and stress has been defined by Hooke's law as:

$$E = \frac{\sigma}{\varepsilon} \tag{4.3}$$

Where E is the Young's modulus, σ is the stress and ε is the strain.

b. Characteristics of strain gauges

A strain gauge is characterized by gauge dimensions, gauge factor, gauge resistance, gauge pattern, gauge series, range, temperature and self-temperature compensation. The points below provide a brief explanation of the different characteristics of the strain gauge.

- Gauge dimension: The length and the width of the grid determine respectively the length and the width of the strain gauge (Figure 4.4). These are the main dimensions of the strain gauge as they concern the main part dimensions. Figure 4.4 shows also the overall length and width, the matrix length and width and the gridlines dimensions.

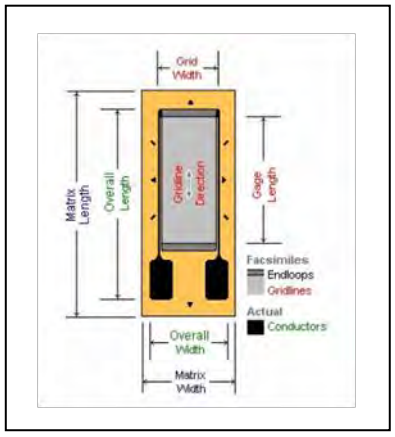

Figure 4.4: Dimensions of strain gauge.

- Gauge factor: Also called the gauge sensitivity k is the ratio between the relative change of resistance and the strain measured.

$$k = \frac{\Delta R / R}{\varepsilon} \tag{4.4}$$

Where k : Strain gauge factor

$\Delta R/R$: Relative changing of resistance;

ε : Strain.

- Gauge resistance: The resistance of a strain gauge is the resistance measured between the two metals used for the connection. The nominal resistance of strain gauges are: 120, 350, 600 and 700ohms. The strain gauge with a gauge resistance of 120 ohms is the most popular in terms of and the most produced is the one with 350ohms which is also used in transducers.

- Gauge pattern: This is the number of grids whether uniaxal or multiaxial. When only one direction of strain is investigated the uniaxal is selected and the multiaxial when many directions of strain are investigated. The multiaxial strain gauge is also called a rosette strain gauge.

- Gauge series: The gauge series are grouped according to the standard. The gauge series is usually selected after the gauge pattern and the gauge size.

- Range: The range of a strain gauge is defined as the maximum strain which the gauge can measure without resetting or replacing it. For each strain gauge, the range is related to the sensitivity of that gauge.

- Temperature: The strain gauge's proprieties as well as the material's proprieties to which the strain gauge is glued can be altered by the temperature. The contraction or expansion due to temperature variation can be source of errors which are difficult to correct.

- Self-Temperature expansion: This characteristic is related to the materials where the strain gauge will be used. It is given as the approximate thermal expansion coefficient of material.

c. Bridge circuit for stain gauges

The bridge circuit was invented by Charles Wheatstone. Called the Wheatstone bridge (Figure 4.5), this circuit can precisely measure small variations of resistance. Therefore, the Wheatstone bridge is used to measure small resistance variations in the strain gauge.

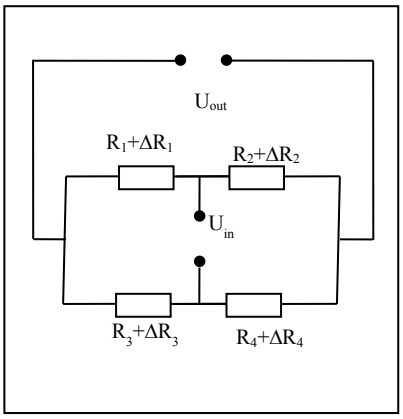

Figure 4.5: Wheatstone bridge circuit.

Applying Kirchhoff's laws to the Wheatstone bridge, the ratio between the input voltage and the output voltage is given by:

$$\frac{U_{out}}{U_{in}} = \frac{R_3 + \Delta R_3}{R_3 + \Delta R_3 + R_4 + \Delta R_4} - \frac{R_2 + \Delta R_2}{R_1 + \Delta R_1 + R_2 + \Delta R_2} \tag{4.5}$$

The Wheatstone bridge is balanced when Equation 4.5 is respected:

$$\frac{R_1}{R_2} = \frac{R_4}{R_3} \tag{4.6}$$

When only two resistances are used, you have the half bridge (Figure 4.6). In case of strain gauges, two strain gauges (identical strain gauges) are used and the two resistances are equal:

$$\Delta R_3 = \Delta R_4 = 0 \ , \ R_1 = R_2 \tag{4.7}$$

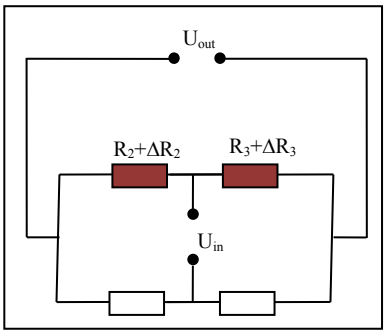

Figure 4.6: Wheatstone half bridge circuit.

Considering that the bridge is balanced, the ratio between the input voltage and the output voltage becomes:

$$\frac{U_{out}}{U_{in}} = \frac{1}{4}\frac{\Delta R_1 - \Delta R_2}{R} \tag{4.8}$$

During the experiment, an MP55 module was used to amplify the signal from strain gauges. Strain gauges with a resistance of 120 ohms were used. The strain gauges and the amplifier module for strain gauge used during the experiment are shown in Figure 4.7.

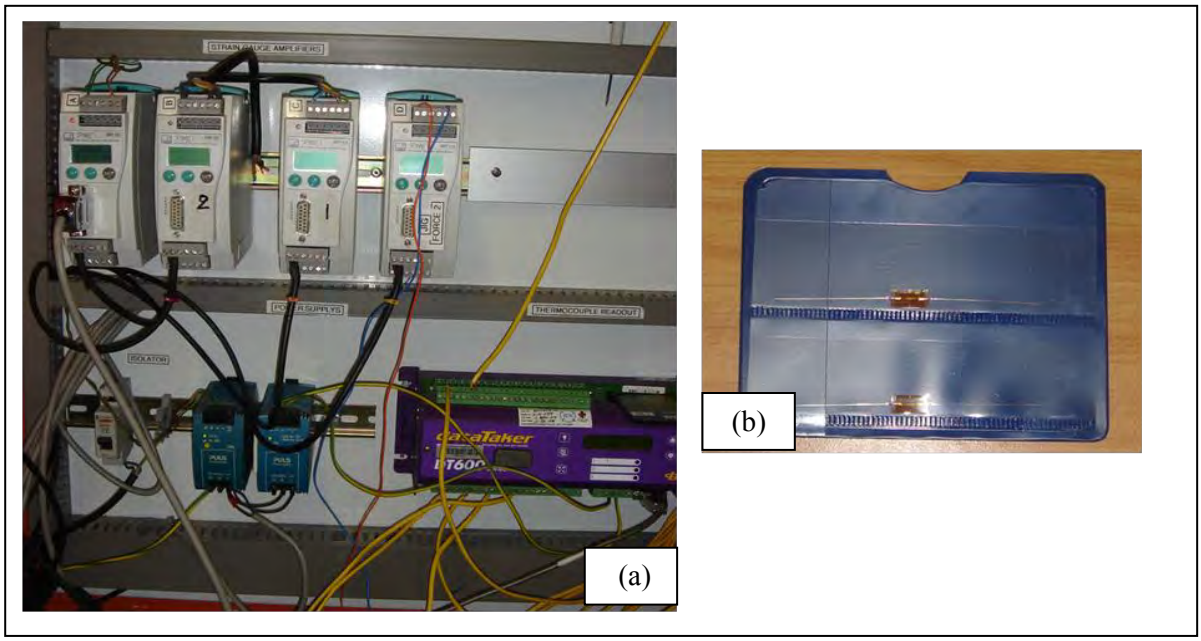

Figure 4.7: (a) The strain gauge module amplifier MP55. (b) The strain gauge used during the experiment.

4.2 Tests of Stockbridge damper and experimental set up

Testing is very important in the field of engineering research in order to reach the goal which is to make conclusions from results. Standard tests on Stockbridge dampers are briefly presented here. Previews of the fatigue tests on Stockbridge dampers conducted by Wagner et al. (1973) and Lara-Lopez and Colin-Venegas (2001) are presented. For each test, the parameters controlled during the test and the set up are emphasized. More details will be presented for the test where the Stockbridge damper is mounted directly on the shaker because this is the method used for this research study. Although that method does not exactly reflect the field reality, it has the advantage of being cheaper from a research budget point of view. However, the procedure for tests using a conductor span is briefly presented.

4.2.1 Standard tests of Stockbridge damper

Two forms of standard test are used currently:

- The IEEE 664 standard
- The IEC 61897standard

The IEEE 664 standard

a. Test method using the conductor span

The Institute of Electrical and Electronics Engineers standard 664 (IEEE 664 standard) (2007) is the laboratory manual which describes the methodologies, measurement accuracies, apparatus and procedures for testing Stockbridge dampers. The power dissipation characteristic is measured for vibration of Stockbridge dampers using this guide standard which is for indoor testing. Testing the damper mounted on the conductor (conductor test span) and mounted directly on the shaker are the two main methods and procedures used in IEEE 664 standard. Even though the second procedure does not refer to the reality in the field, it has the advantage of being cheaper to conduct than the first. More details will be presented for the IEEE 664 where the damper is mounted directly on the shaker.

The IEEE 664 standard (2007) layout procedure test using a conductor span for testing the Stockbridge damper is showed in the Figure 4.8. It is conducted at a constant antinode velocity (200 mm/s), although additional tests at 100 and 300mm/sec can be done. Three different tests method are presented:

- **ISWR method**: The Inverse Standing Wave Ratio is the test which determines the Stockbridge damper's power dissipation. The damper is mounted on the conductor which is vibrated by the shaker. During the experiment, the nodal and the antinodal amplitudes on the span are measured after which the power dissipation is determined. After the data acquisition, the calculation of the damper's power dissipation is undertaken by using the following equation:

$$P_d = \sqrt{Tm}\,\frac{V_a^2}{2}\left(\frac{a}{Y_o}\right) \tag{4.9}$$

Where:

P is the damper's power dissipation

T is the tension of the conductor

m is mass per unit length of the span

V_a is the velocity of the antinode

a is the amplitude of the node

Y_0 is the amplitude at the antinode

- **Power method**: Conducted in the same condition as the preview test. The power method test permits determination of the characteristic dissipation of dampers at each tunable harmonic of the span by collecting the velocity and the force during the test. After the data acquisition, the calculation of the damper's power dissipation is undertaken by using the following equation:

$$P_d = 0.5(F_d V_s)Cos\theta_v \tag{4.10}$$

Where:

P is the power dissipated by the damper

F_d is the dynamic force transmit by the shaker to the damper

V_s is the velocity of the shaker base

θ_v is the phase angle between the force and the velocity

- **Decay method**: The power dissipation of a damper is determined by measuring the decay of amplitude vibration conductor at each tunable harmonic of the span. After the data acquisition, the calculation of the damper's power dissipation is undertaken by using the following equation:

$$P = 0.5 f m V_a^2 L \delta \tag{4.11}$$

Where

P is the power dissipated by the damper

m is the mass per unit length of the span

V_a is a maximum loop velocity at the initial antinode amplitude

f is the driven frequency

δ is the logarithmic decrement

L is the length of the span

b. Forced response test

The second method of IEEE 664 standard where the damper is directly mounted on the shaker is the forced response method. The characteristic of a Stockbridge damper is determined by measuring the force transmitted by the shaker to the damper and the velocity of the shaker base.

A basic sketch layout of this test is shown in Figure 4.8. The damper is mounted directly on the shaker by using a device and force transducer. One accelerometer is put on the shaker base for control. Force transducers and the accelerometer on the base are for acquisition of force, velocity (displacement) and phase between force and velocity (displacement).

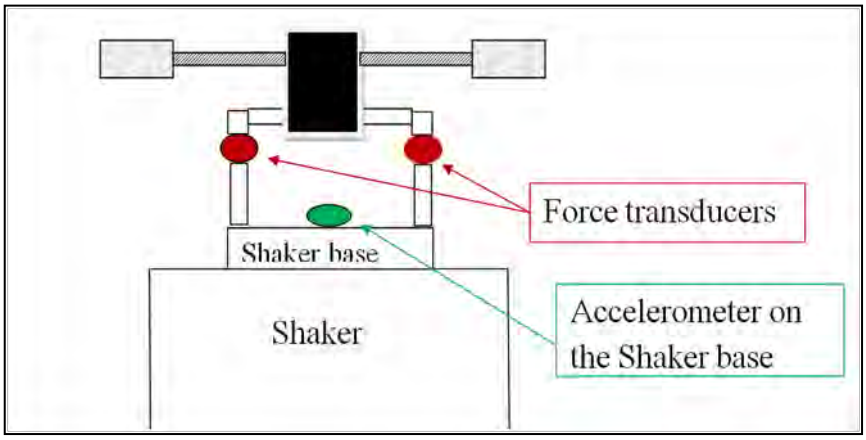

Figure 4.8: Sketch of experimental set up according to IEEE 664 standard.

The forced response test requires a shaker which must control the output velocity with the absolute error less or equal to 2% of the value selected. The velocity (displacement) and force signal should be measured within 2% of measurement value. The cosine of the measurement of the phase angle between the force and the velocity signals should be made

with sufficient accuracy to ensure that the cosine of the phase angle is within ±1% of the measure value. The damper is clamped to a rigid bar which has a diameter adapted for a Stockbridge damper. The damper and the device are mounted on the shaker (Figure 4.8).
The procedure used for the forced response test is as follows:

a. Calibrate apparatus using a fixed mass;
b. Mount the fixing device;
c. Install force transducers on the fixing device;
d. Put the damper on the device;
e. Stick the accelerometer on the shaker base for control;
f. Make a sweep in the frequency range of wind velocity (1 to 7 m/s) at constant velocity (0.1 m/s) for 30 minutes. Additional tests can be made at different velocities (0.2, 0.3 m/s). The lower and upper frequency limits are calculated by using the Strouhal formula.
g. Repeat the procedure on another Stockbridge damper.

After the data acquisition, the calculation of the damper's power dissipation is made by using the Equation 4.11.

The IEC 61897 standard

The test requirements for Stockbridge dampers are presented in International Electrotechnical Commission (IEC) standard 61897 (1998). A series of tests on Stockbridge damper and the methods for such tests are recommended by the IEC 61897. Tests related to the prediction of Stockbridge life are presented below. Only the characteristic and fatigue tests on Stockbridge dampers are developed at this point.

a. Damper characteristic test

The damper is mounted directly on the shaker via its clamp attached to the device. The shaker output signal must be sinusoidal oscillation with a variable amplitude and frequency which can be controlled. The damper is excited in the range of wind induced frequency. This range must accord with the range the damper is designed for. The automatic sweep rate is used during the test. The sweep rate of 0.2 decade per minute for the logarithmic sweep and 0.5 Hz/min for the linear sweep may be used. The displacement of the shaker base is controlled and must be equal to 100 mm/sec.

Force transducers are used to measure the dynamic force transmitted by the shaker to the damper. An accelerometer is put on the shaker base to control the constant velocity during the test. During the test the force is collected from the force transducer. The phase angle between the velocity and the force is collected also. The experiment set up of the characteristic test for the damper is shown below.

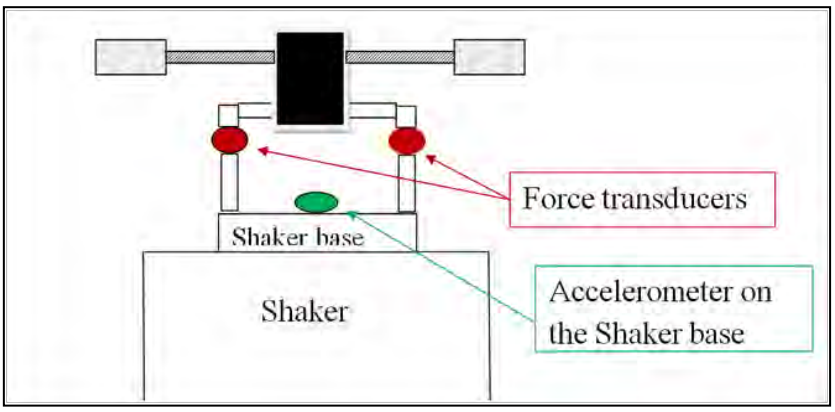

Figure 4.9: Sketch of experimental set up for characteristic test of Stockbridge damper according to IEC 61897 standard.

After the data acquisition, the damper impedance is calculated by using the equation:

$$Z_d = \frac{F_d}{V_s} \tag{4.12}$$

Where:

Z_d is the impedance of Stockbridge damper

F_d is the dynamic force transmitted by the shaker to the damper

V_s is the velocity of the shaker base

The phase angle between the force and the velocity of shaker base is determined as well as the power dissipation of the damper. The results from the test are graphs of the impedance, the phase and the power dissipation versus driving frequency.

b. Fatigue test of Stockbridge damper

The swept frequency and the resonant method are two methods presented by the IEC 61897 standard (1998). This test is performed with the damper directly mounted on the shaker. One accelerometer on the shaker base is used (Figure 4.10) during the test as the shaker control.

The swept method consists of doing the sweep in the range of wind frequency with an automatic rate. The velocity of the shaker base must be maintained constant during the test and equal to 100 mm/sec. This velocity corresponds to an antinodal amplitude (mm) of 67/f where f is the vibration frequency. This rate must be equal to 0.2 decade/min for logarithmic sweep and 0.5Hz/min for the linear sweep. The damper must accumulate 100 million cycles. With these parameters, one test may take 60 or 70 days.

The second method is the resonant frequency method. This method consists of exciting the damper at one of its resonance frequencies. The displacement may be 0.5mm and must be constant during the test. Instead of the constant displacement 0.5 mm, the velocity may also be used 100mm/sec. The IEC 61987 requires for the asymmetrical Stockbridge damper to be tested at its highest resonance frequency on each side. The damper must accumulate 10million cycles. The damper which has the highest resonance frequency (of around 30Hz) is suitable to be tested. With these parameters, the test can take 3 or 4 days.

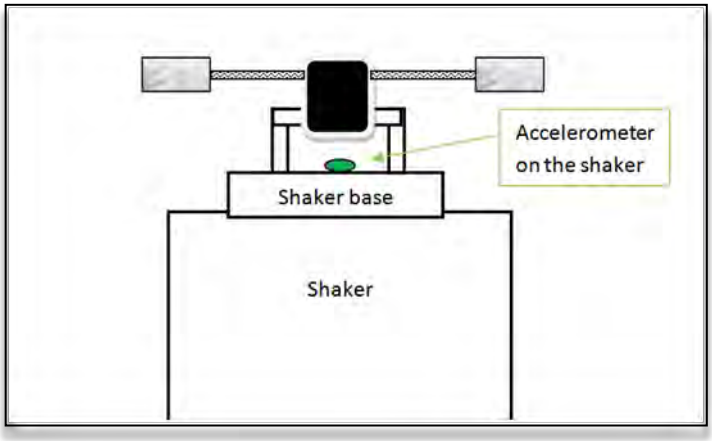

Figure 4.10: Experimental set up on a Stockbridge damper for a fatigue test according to the IEC 61897 standard.

The following acceptance criteria have been established by the IEC 61897 standard:

- Before and after the test the resonance frequency and the power dissipation of the damper should not be more than 20% of resonance frequency.

- After the test the strands of the messenger cable must unbroken.

The test procedure is as follows:

a. Calibrate the apparatus using a fixed mass;
b. Mount the fixing device;
c. Mount the damper on the device;
d. Stick the accelerometer on the shaker base for control;
e. Make a first sweep to find resonance frequencies in the range of wind induced vibration;
f. Fix the displacement (0.5mm) or the resonance frequency;
g. Fix the sweep rate;
h. Set the sweep method (100million cycles) or the resonant method (10million) cycles;
i. Compare the resonant frequency and the power dissipation before and after the test.

4.2.2 Fatigue test

The literature survey on the fatigue test of Stockbridge dampers is very limited. The procedure and the experimental test set up conducted by previous researchers are presented.

Wagner et al. (1973) conducted a fatigue test on a symmetrical Stockbridge damper (Figure 4.11). A load cell was designed and mounted on a shaker. One accelerometer was for shaker control. The test was stopped when the damper's mass become loose. During the test, the resonance frequency and the displacement peak to peak of shaker were controlled. The following procedure was used:

a. Place the built load cell in such a way as to get the dynamic force applied to the damper by the shaker;
b. Calibrate it;
c. Mount the damper on the load cell;
d. Stick the accelerometer on the shaker base;
e. Obtain the first resonance frequency;
f. Vibrate the damper at its second resonance frequency with a constant displacement peak to peak (2mm);

g. The test is stopped when the mass of damper becomes loose.

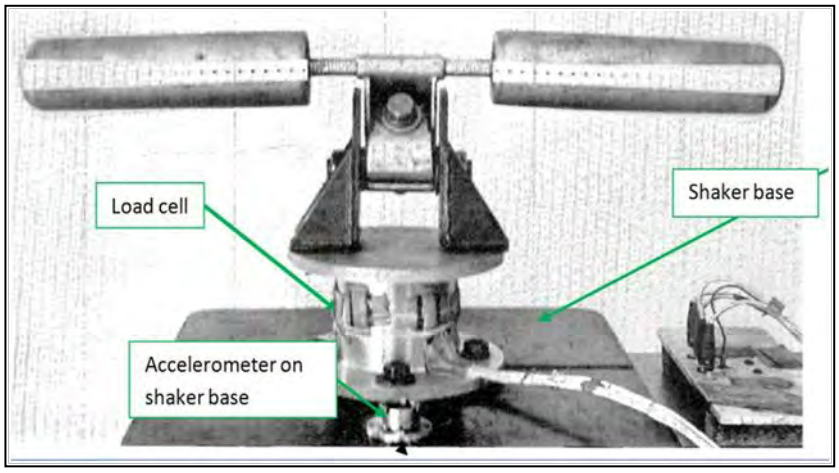

Figure 4.11: Experimental set up of a Stockbridge damper with a load cell and an accelerometer on the shaker base (Wagner et al., 1973).

Lara-Lopez and Colin-Venegas (2001) also conducted a fatigue test on the symmetrical Stockbridge damper. They controlled the second resonance frequency and the displacement of the shaker base. They used two accelerometers, one for shaker control and another on the center of damper's mass (Figure 4.12). The test procedure is the following:

a. Mount the damper on the shaker;
b. Put two accelerometers on each center mass of damper;
c. Put one accelerometer on the shaker base;
d. Find the first resonance frequency;
e. Vibrate the damper at its first resonance frequency at constant displacement peak to peak (1mm), until failure occurs (damper's mass become loose);
f. Record the time during the experiment;
g. Get the number of cycles by dividing the time by the test frequency.

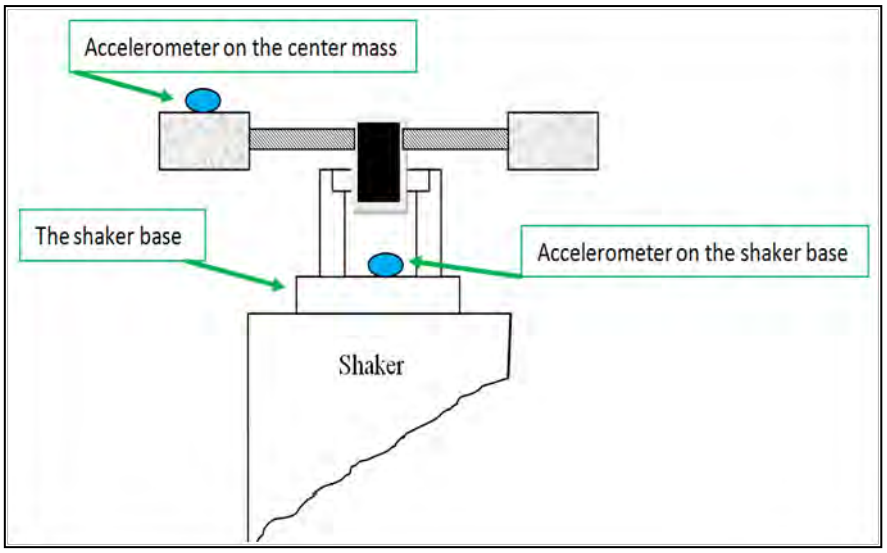

Figure 4.12: Sketch of experimental set up used by Lara-Lopez and Colin-Venegas with two accelerometers, one on the mass of a Stockbridge damper and another on the shaker control.

According to the standard test presented, the resonance frequency method has been used in this dissertation for fatigue test. This method allowed shortening the duration of the fatigue test. In addition, the forced response test has been used to get the resonance of the Stockbridge damper at each stage during the fatigue test. The frequency or the displacement will be controlled during the test has it is recommended by all standards.

CHAPTER 5

EXPERIMENTAL RESULTS AND DISCUSSION

In this study, free vibration as well as forced response vibration tests were conducted on a symmetrical and an asymmetrical Stockbridge damper. On the symmetrical damper, the forced vibration test was conducted and thereafter the Matlab model was computed. For the symmetrical damper the forced response test was conducted on a new and an old damper. In addition the fatigue test was conducted on a new symmetrical damper. The finite element simulation was conducted for the forced response and for the free vibration test. From the fatigue tests mathematical models have been established to predict the life of a Stockbridge damper referring to the used symmetrical damper.

5.1 Symmetrical damper

5.1.1 Experiment set up and methods

Figure 5.1 shows the experimental set up used in this work to measure the bending stress of messenger cable as a function of frequency. The Stockbridge damper was mounted on the electrodynamic shaker (TIRA, Type 56263LS). The damper was vibrated in the range of wind induced vibration (sweep) at constant displacement (1mm) peak to peak. The frequency ranged from 5 to 60Hz was determined by using Strouhal formula (Chan, 2006). The characteristics of the tested damper are given in Table 5.1.

Five accelerometers (Bruel & Kjaer, Delta Tron, Type 4508002) were necessary during the experiments to measure the resonance frequency and the displacement. Four accelerometers, two on each Stockbridge damper's weight, were used and one on the shaker base. Strain gauges (half-bridge circuits) (Hoffmann, 1987) were put on both sides of the messenger cable near the clamped end.

Table 5.1: Characteristics of damper

Designation	Symbol/ Unit	Value
Length of messenger cable	L [mm]	115
Length between B and G (Figure 5.3)	L_1 [mm]	65
Length between A and G	L_2 [mm]	50
Mass of weight	m [kg]	20533
Diameter of messenger cable	D [mm]	14
Moment of inertia about the center mass	J_G [kgm^2]	0.018
Logarithmic decrement	δ	0.169

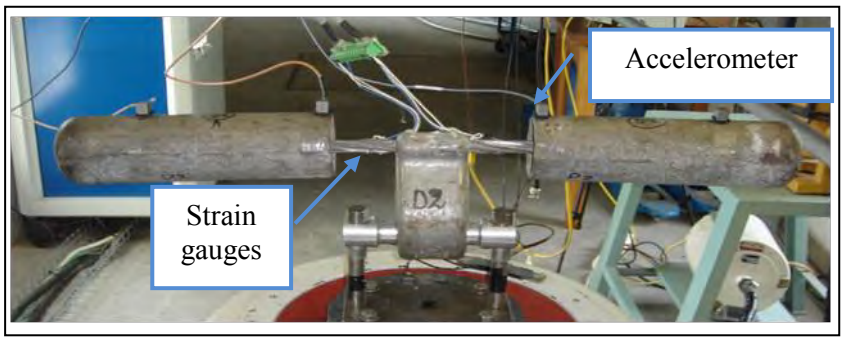

Figure 5.1: Symmetrical dampers experimental set up with four accelerometers and strain gauges on both sides of the messenger cable at the clamp point.

The fifth accelerometer was put on the shaker base to control the displacement (1 mm) during the experiment. The two accelerometers permitted the measurement of the two modes of vibration of the Stockbridge damper (the first and the second mode) during the sweep.

The strain data of the messenger cable were conditioned by a MP55 strain gauge amplifier and data from accelerometers was captured by PUMA control systems software.

All accelerometers were calibrated by means of a calibration exciter type 4294 (Bruel & Kjaer). A calibration unit, type K 3607 (HBM) was used to calibrate the strain gauges. Through instrument calibration, deviations were 0.05 g and ± 10 μm/m respectively for accelerometers and for strain gauges. The curve generated by the PUMA software was compared with the one from the mathematical model which was generated through Matlab code. (Appendix E) Basic characteristics of dampers tested are summarized in Table 5.1. The length of messenger cable was measured by using a ruler. L1, L2, m, J, and G were determined by constructing a model using the Solid Edge package. The messenger cable's Young modulus was determined by means of Solid Edge after determining the density of the messenger cable. The free vibration has been made by knocking the mass of the Stockbridge damper to determine the logarithmic constant decrement, δ by:

$$\delta = \frac{1}{n}\ln\left(\frac{x_0}{x_n}\right) = \frac{1}{5}\ln\left(\frac{0.0289063}{0.0124430}\right) = 0.1686 \qquad (5.1)$$

5.1.2 Model description

A Stockbridge damper is attached to a power line, therefore moves with it through the wind. Bending stress is developed on the messenger cable which vibrates. Two mathematical models for bending stress calculation have been presented in the literature (Lara-Lopez and Colin-Venegas, 2001; Richardson, 1995). In this dissertation, the model presented by Wagner et al. (1973) is used due to the availability of the required properties of the damper.

During the vibration of a Stockbridge damper, the movement of the damper's weight is characterized by two degrees of freedom: the alternative motion of translation, y, and the rotation, θ (Figure 5.2). The damper's equation of motion is (Bishop and Johnson, 1960):

$$m\ddot{x} + c\dot{x} + kx = c\dot{y} + ky \qquad (5.2)$$

m, c, k are respectively the mass, the damping, the stiffness matrix and y and x are the excitation of the damper clamp and displacement.

a. Calculation of the axial acceleration and the angular acceleration

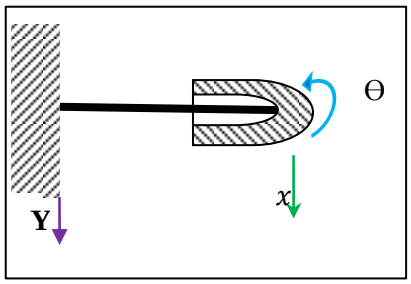

Figure 5.2: Two degrees of freedom for the Stockbridge damper.

The displacement of damper's weight is determined (Claren and Diana, 1969; Wagner et al., 1973) by vector q which is given by Equation 5.3.

$$q = \begin{bmatrix} x \\ \theta \end{bmatrix} \tag{5.3}$$

The component expressions of q are given by Equations 5.4 and 5.5 (Claren and Diana, 1969; Wagner et al., 1973). Figure 5.2 shows the half part of damper with x and θ which functions of driving frequency are

$$x = Xe^{(\omega t+\beta)i} = Y(1+i\mu)\frac{1+i\mu-S_1\eta^2}{(1+i\mu-\eta^2)(1+i\mu-\alpha\eta^2)} \tag{5.4}$$

$$\theta = \Theta e^{(\omega t+\varphi)i} = \frac{Y}{L_2}(1+i\mu)\frac{-\alpha\eta^2 S_2}{(1+i\mu-\eta^2)(1+i\mu-\alpha\eta^2)} \tag{5.5}$$

Where:

$\omega = 2\pi f$ is the angular frequency (5.6)

t is the time

β and φ are phase angles

Y is the constant displacement of the damper's clamp (peak-to-peak)

$$\mu = \frac{\delta}{\pi} \tag{5.7}$$

$$\eta = \frac{f}{f_1} \tag{5.8}$$

$$\alpha = \left(\frac{f_1}{f_2} \right)^2 \tag{5.9}$$

In the above three expressions, δ is the logarithmic decrement of the damper's messenger cable whereas, f, f_1, f_2 represent the driving frequency, the first resonant frequency and the second resonant frequency.

In the Equations 5.4 and 5.55.12, S_1 and S_2 are respectively the first and the second dimensionless stiffnesses. They are given by:

$$S_1 = \frac{\alpha(1+\rho)c_{11}}{m\rho L_2 f_1^2} \tag{5.10}$$

$$S_2 = \frac{c_{12} - L_2 c_{11}}{m\rho L_2 f_1^2} \tag{5.11}$$

Where:

$$\rho = \left(\frac{r}{L_2} \right)^2 \tag{5.12}$$

is the square ratio between the radius of gyration, r, and the distance between the center of gravity and the damper attachment point, L_2.

The elements of the stiffness matrix are:

$$c_{11} = 4\left(\frac{3EI}{L^3}\right) \tag{5.13}$$

$$c_{12} = c_{21} = 2L\left(\frac{3EI}{L^3}\right) \tag{5.14}$$

$$c_{22} = \frac{4L^2}{3}\left(\frac{3EI}{L^3}\right) \tag{5.15}$$

The axial acceleration $\ddot{x}$ and the angular acceleration $\ddot{\theta}$ are obtained respectively by second derivative of the axial and angular displacement

$$\ddot{x} = -\varpi^2 X e^{(\omega t+\beta)i} \tag{5.16}$$

Where the argument is given by :

$$\left|\ddot{x}\right| = \varpi^2 X \tag{5.17}$$

and

$$\ddot{\theta} = -\varpi^2 \Theta e^{(\varpi t+\varphi)i} \tag{5.18}$$

Where the argument is given by:

$$\left|\ddot{\theta}\right| = \varpi^2 \theta \tag{5.19}$$

b. Bending moment

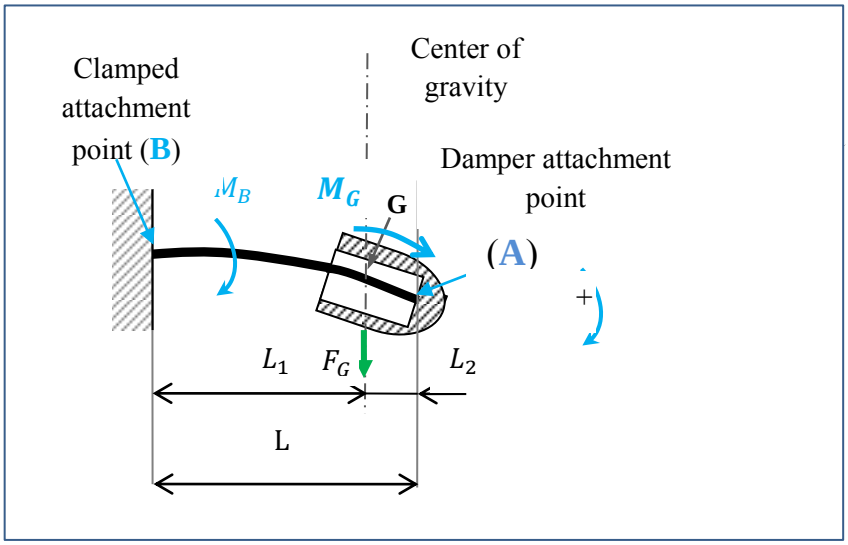

Figure 5.3: Moments and forces acting on the damper's messenger.

The bending moment of the messenger cable M_B at the clamp attachment point of the cable is calculated by using the sum of all torques at the attachment damper. Applying this principle to Figure 5.3, the expression of bending moment is:

$$M_B = M_G - L_1 F_G \tag{5.20}$$

M_G, L_1 and F_G are respectively the bending moment from the damper's mass acting at its center of gravity, the length between the clamp attachment point, B, and the center of gravity, G, of the damper's mass and the force at the clamp through the center of gravity.

With $\ddot{\theta}$ calculated in Equation 5.20 and J_G as a known, the moment M_G may be calculated by using the principal of moment of inertia. Its expression is:

$$M_G = J_G \left|\ddot{\theta}\right| \tag{5.21}$$

where:

J_G is the damper's mass moment of inertia

$\left|\ddot{\theta}\right|$ is the argument of the damper's mass angular acceleration

The force F_G may be determined by using the Newton law applies on the damper's mass. Referring to Figure 5.3, the expression of F_G is given by:

$$F_G = m\left(|\ddot{x}| + L_2|\ddot{\theta}|\right) \tag{5.22}$$

where:

m is the damper's mass.

$|\ddot{x}|$ is the argument of the damper's mass axial acceleration.

$|\ddot{\theta}|$ is the argument of the damper's mass angular acceleration.

c. The dynamic bending stress

The dynamic bending stress of the messenger cable at the attachment point B as function of frequency f is given by:

$$\sigma(f) = \frac{|M_B|}{W} \tag{5.23}$$

where:

M_B is the bending moment,

W is the modulus of the cross sectional area of the messenger cable.

As the messenger cable is the stranded cable, the modulus of the cross sectional area is W in the expression:

$$W = k\frac{\pi D^3}{32} \tag{5.24}$$

Where :

k is the factor which takes into account the fact that the messenger cable is not a circle but a stranded cable ($k = \frac{2}{3}$ for the messenger cable with 7 wires) (Wagner et al., 1973).

D is the overall diameter of the messenger cable.

5.1.2 Results and discussion

Resonance frequency and strain data were collected when the damper was vibrating in the frequency range of wind induced vibration. Table 5.2 shows the correlation of measurement from strain gauges and accelerometer, the average error is 0.6 % for the first resonance frequency and 1 % for the second resonance frequency. The comparison of curve from mathematical model and experiment is presented in Figure 5.4. These values can be used as data to determine the life expectancy of Stockbridge dampers on the basis of the relationship between resonance frequency changes and the fatigue history of the cable (Salawu, 1997; Wang and Shang, 2008).

Table 5.2: Measurement of resonance frequency from accelerometer and strain gauge.

Measurement From	1st Resonance frequency [Hz]	2nd Resonance frequency [Hz]
Accelerometer	8.63	27.9
Strain Guage	8.69	28.23

In this work, the experimental curve of stress as a function of frequency at constant peak to peak displacement has been generated using the PUMA control systems software. Figure 5.4 presents a comparison between experimental data at 1 mm peak to peak and predictions using the model derived by Wagner et al. (1973)

The graph shape obtained from the mathematical model is similar to that from experiment as they present two peaks each. Peaks correspond to the two resonance frequencies of the symmetrical damper. The first peak corresponds to the first resonance which is the

translation movement of the damper mass. The second frequency is corresponded to the second peaks. At the second resonance frequency, the mass of damper has an alternating rotational motion. The first and the second resonance frequency from the experiment are close to those from the mathematical model and the average error is below 1%. Stresses at the resonances frequency are also close in the frequency range from 5Hz to 14Hz. The mathematical model (Wagner et al., 1973) agrees with the experiment where the average error is equal to 5%. Therefore the messenger cable can be regarded as a tube as all wires vibrate at the same moment. In addition, the less slipping there is between wires, the smaller the gap there is between graphs, indicating in the same frequency range. From 14Hz to 27Hz, the gap between curves is created by the interactions of the two modes of damper vibration. Data from 14Hz up to 60Hz present a gap between the experiment and the model. However the curve from the experiment is the rotation of the curve from the model with the peak as the rotation centre. On the other hand, the strain gauges must be glued exactly at the clamp end of messenger in order to reduce the gap between both curves.

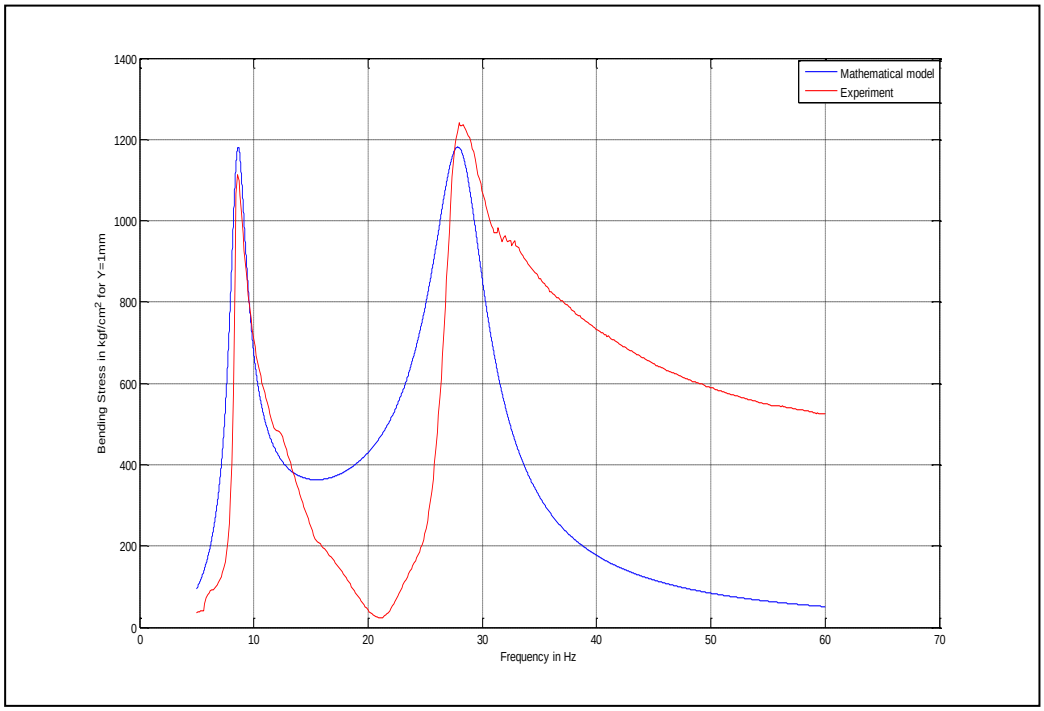

Figure 5.4: Bending stress of messenger cable versus frequency for constant displacement Y=1mm.

5.2 Asymmetrical damper

5.2.1 Temperature variation of messenger cable

The cyclic bending as well as the friction between messenger cable's wires which are caused by vibration leads to temperature evolution of the messenger cable. The change of temperature of the messenger cable during the Stockbridge test cannot be ignored as it can affect the behaviour of sensors such as strain gauges. Strain gauges have been used in this dissertation to measure of the strain of the messenger cable. Therefore knowing the temperature variation of messenger cable is quite important.

5.2.1.1 Experimental set up and method

The experiment was conducted on Stockbridge damper (type 855017-00 babcock) (Appendix B). The forced response method was used for this work by keeping the temperature constant around the tested damper. The damper was mounted on the electrodynamic shaker and vibrated in the frequency range corresponding to the wind induced vibration for 30 minutes (Chan, 2006). A constant velocity of 100mm/sec was used according to the conducted standard test procedure (IEEE 664 standard, 2007). The forced response test at constant displacement peak to peak (1mm) was also conducted (Chan, 2006). By using the Strouhal formula (Chan, 2006), the frequency range for the sweep was determined to be from 5 to 55Hz. Four thermocouples were used in each case to measure the temperature of the messenger cable during the forced response test. Thermocouples (Type K) were placed as follows: one at each side of the clamp on the messenger cable and one at each point where the messenger cable is attached to the mass (Figure 5.5). Care was taken to calibrate all the four thermocouples using a temperature standard. The accelerometer (Bruel & Kjaer, Delta Tron, Type 4508002) used to control the shaker base was calibrated by means of a calibration exciter type 4294 (Bruel & Kjaer). Estimated uncertainty in temperatures measurements is ± 0.7K which is the maximum absolute error among those from thermocouples. Experimental temperature data obtained from thermo couples were made available on a PC monitor via a DT 600 S3 data logger and Delogger Pro software.

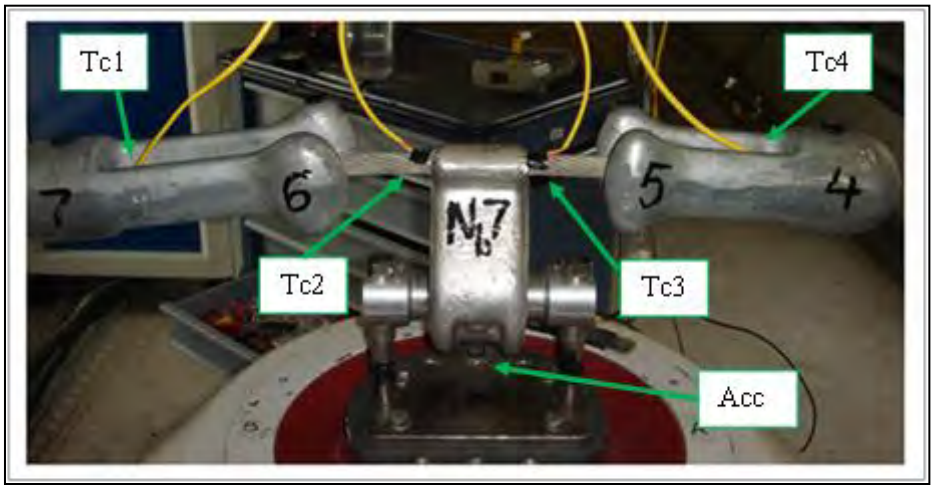

Figure 5.5: Experimental set up. Tc1, Tc2, Tc3, and Tc4 are thermocouples. Acc is the accelerometer.

5.2.1.2 Results and discussion

Messenger cable temperatures were recorded every 300 seconds while the damper was vibrating. In each case, three readings were made and thereafter the average was considered. The temperature variation was determined as the difference between the initial temperature and the final temperature of the messenger cable.

The temperature variation results for the vibration at 100 mm/sec peak to peak are presented in Table 5.3 as well as on the Figures 5.6, 5.7, 5.8, and 5.9. It was observed that during vibration at 100mm/sec, the highest temperature variation was almost 2.8K near the small mass attached point (Figure 5.9). The highest temperature variation was 2.5K, read using Tc2 (Figure 5.7), during the vibration of the damper at constant velocity. These temperature variations can be estimated around the second resonant frequency of the Stockbridge damper. The temperature variation read using Tc3 near the clamp at the side of the big mass of damper is shown in Figure 5.8. This variation temperature is linear in the frequency range of 5 to 13Hz and becomes almost constant around 1 K from 13 to 38 Hz. In the last interval of frequency (38 to 55Hz) the temperature variation decreases linearly up to 0.2K.

The temperature near the attached point of the big mass Tc1 presents the temperature variation with a peak around 2K. In the frequency range from 38 to 46Hz the temperature variation increase linearly up to 1.7 K. At the end the variation temperature passes through the highest value (2 K) before starting to decrease and reaches almost 1.5K at the end of the experiment (Figure 5.6). The temperature variation measured by Tc4 presents the highest

variation (almost 3K) around the highest resonant frequency of the Stockbridge damper (Figure 5.9).

Table 5.3: Temperature variation of the messenger cable at 100mm/sec peak to peak.

Frequency [Hz]	Variation Temperature ΔTc1[K]	Variation Temperature ΔTc2[K]	Variation Temperature Δ Tc3[K]	Variation Temperature Δ Tc4[K]
5	0	0	0	0
13.26	0.178	0.431	1.031	1.114
21.65	0.157	2.532	1.013	0.992
30	0.381	2.086	1.018	2.198
38.29	0.405	0.940	1.070	1.731
46.68	1.835	1.502	0.744	2.915
55	1.612	1.530	0.200	2.406

The polynomial regression has been applied as it is the most reliable and present a reality to the temperature variation of the messenger cable in the range of vibration frequency.

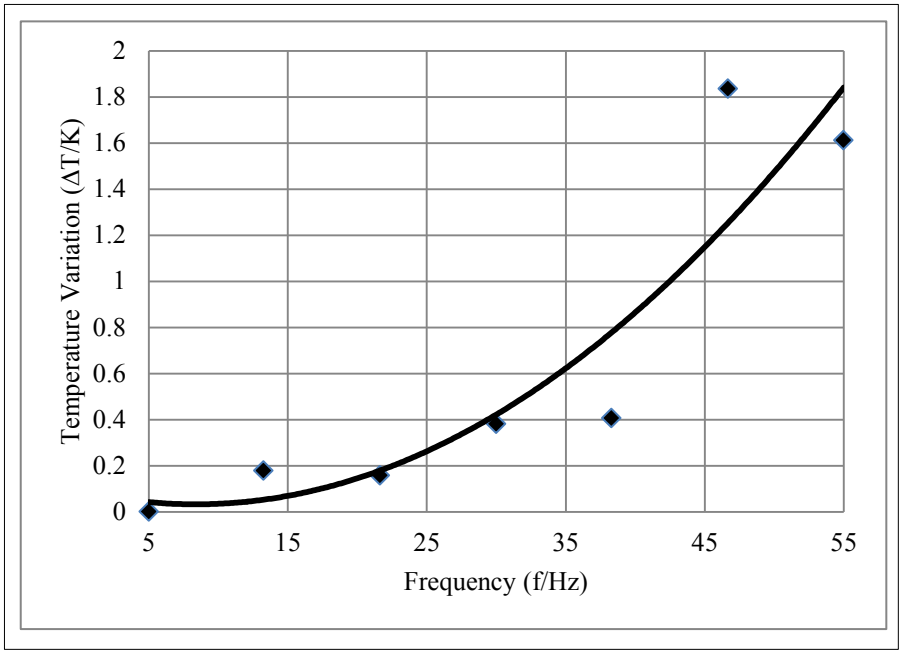

Figure 5.6: Temperature variation of the messenger cable's damper at the attached point of the big mass (Tc1) as a function of excitation frequency at constant velocity.

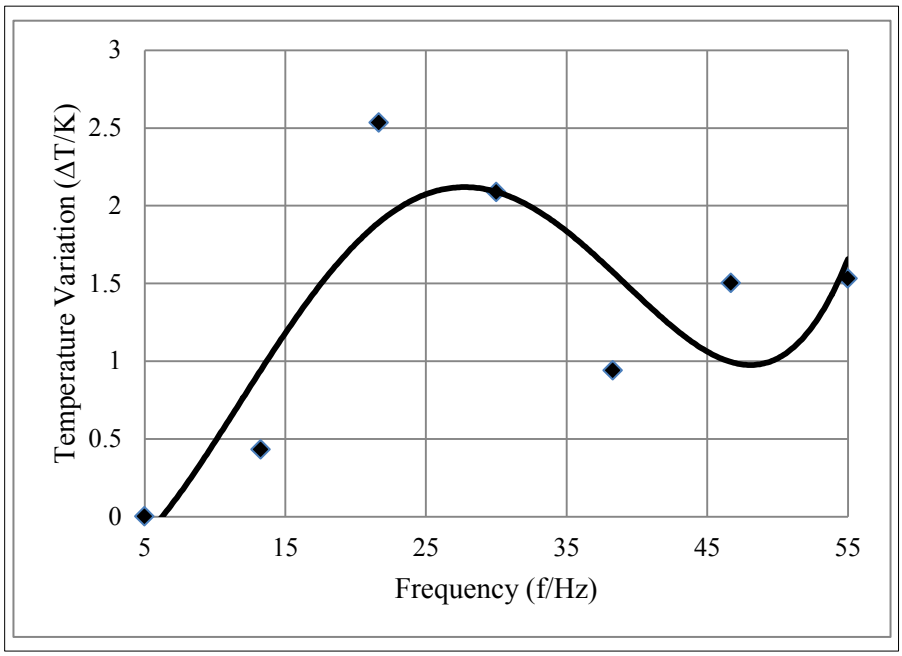

Figure 5.7: Temperature variation of messenger cable's damper at the clamp point on the big mass side (Tc2) as a function of excitation frequency at constant velocity.

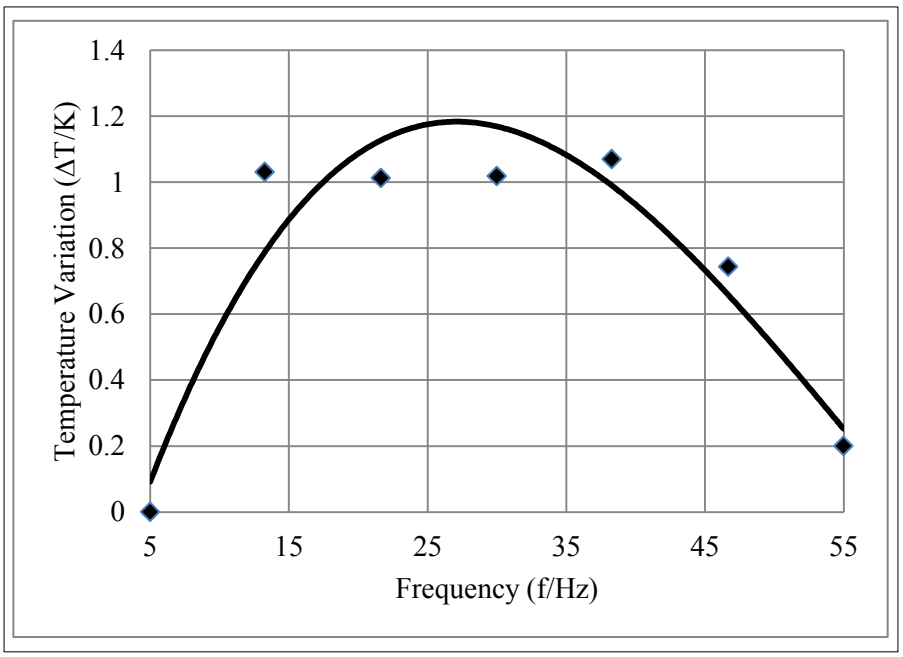

Figure 5.8: Temperature variation of messenger cable's damper at the clamp point of the small mass (Tc3) as a function of excitation frequency at constant velocity.

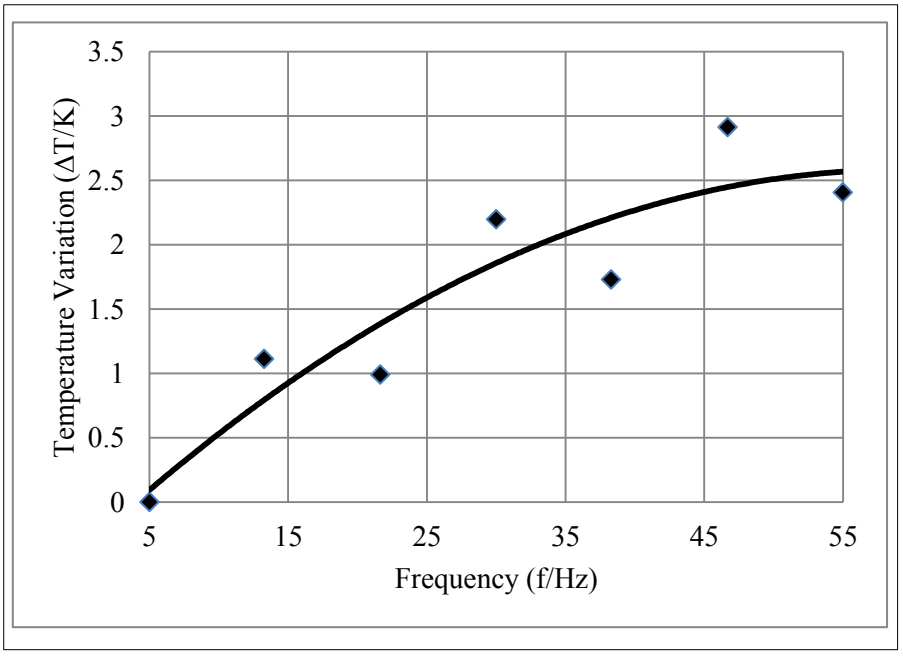

Figure 5.9: Temperature variation of messenger cable's damper at the attached point of the small mass (Tc4) as a function of excitation frequency at constant velocity.

Equations 5.25, 5.26, 5.27 and 5.28 represent the correlation data collect between the messenger cable variation temperature and the excitation frequency in Hz respectively for Tc1, Tc2, Tc3 and Tc4. The R-squared value regressions are respectively 0.8361, 0.7163, 0.8989 and 0.8553 for Equations 5.25, 5.26, 5.27 and 5.28.

$$\Delta Tc1 = 0.0008f^2 - 0.0139f + 0.0909 \quad (5.25)$$

$$\Delta Tc2 = 5E\text{-}06f^4 - 0.0006f^3 + 0.015f^2 - 0.0154f - 0.3612 \quad (5.26)$$

$$\Delta Tc3 = 2E\text{-}05f^3 - 0.0035f^2 + 0.1422f - 0.5352 \quad (5.27)$$

$$\Delta Tc4 = -0.0008f^2 + 0.1001f - 0.3863 \quad (5.28)$$

Where $\Delta Tc1$, $\Delta Tc2$, $\Delta Tc3$, $\Delta Tc4$ are temperature variation in Kelvin and t is the time in seconds.

At constant 1mm peak to peak displacement, it was observed that the highest temperature variation of the messenger cable is around 2.3K. This happened near the attached point on the big damper mass. The temperature variations of the messenger cable for 1mm peak to peak are presented in Table 5.4 as well as in Figures 5.10, 5.11, 5.12, and 5.13. The variation temperature (Tc1) reaches its maximum at 2.3K between 45 and 55Hz (Figure 5.10). This temperature variation (Tc1) looks constant in the range from 13 to 38Hz, and reaches the peak between 46 and 55Hz. The temperature variation (Tc2) has the form sinusoidal between 5 and 38Hz and becomes linear up to the end of the experiment where the value is almost 2K (Figure 5.11). Tc3 and Tc4 present similar graph form with different peak. However peaks are observed at different times, as suggested by Figures 5.12 and 5.13.

Table 5.4: Temperature variation of the messenger cable at 1mm peak to peak.

Time (second)	ΔTc1[K]	ΔTc2[K]	ΔTc3[K]	ΔTc4[K]
5	0	0	0	0
13.26	0.17	0.14	0.19	0.16
21.65	0.11	0.15	0.17	0.12
30	0.11	0.27	0.07	0.15
38.29	0.19	0.30	0.43	0.78
46.68	2.09	1.28	0.88	0.90
55	2.30	2.25	0.93	0.48

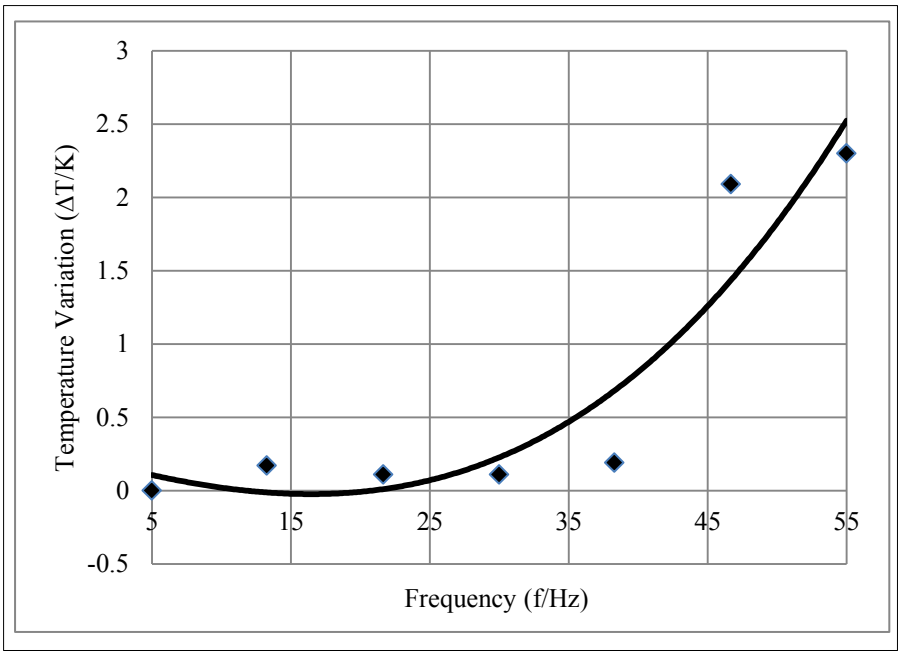

Figure 5.10: Temperature variation of the damper's messenger cable at the attached point of the big mass (Tc1) as a function of excitation frequency at constant displacement.

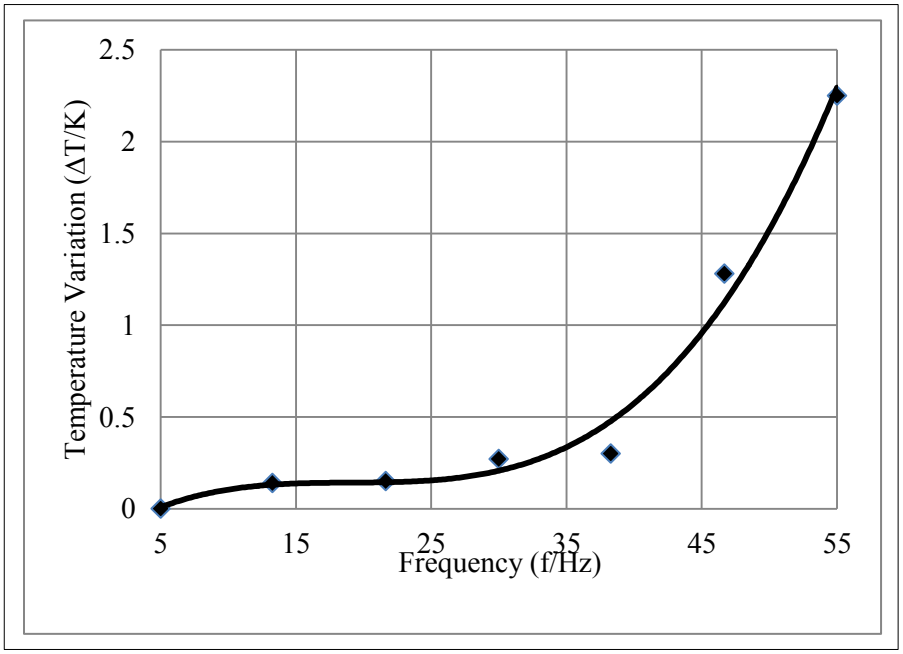

Figure 5.11: Temperature variation of the damper's messenger cable at the clamp point on the big mass side (Tc2) as a function of excitation frequency at constant displacement

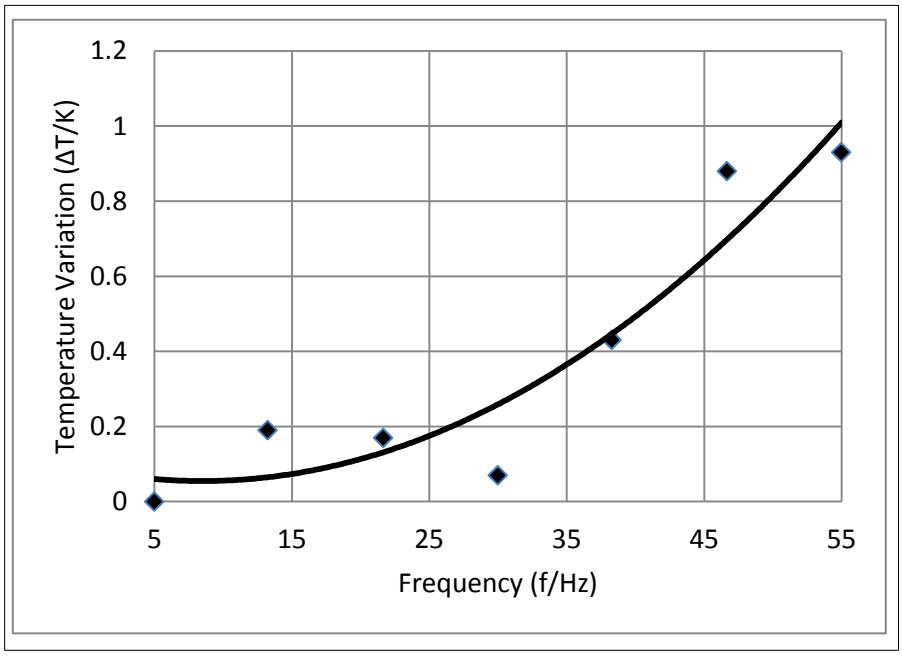

Figure 5.12: Temperature variation of the damper's messenger cable at the clamp point of the small mass (Tc3) as a function of excitation frequency at constant displacement.

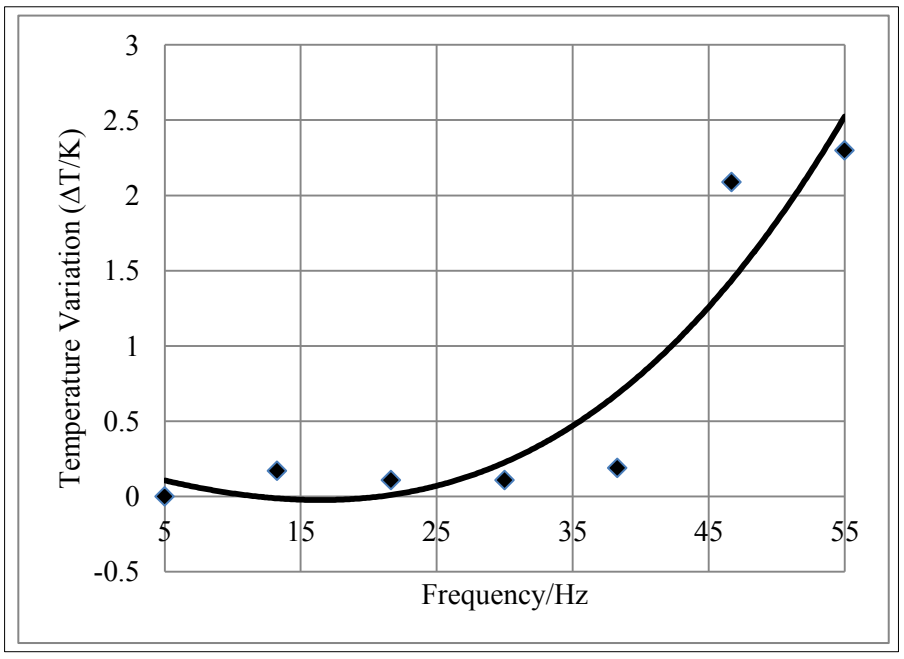

Figure 5.13: Temperature variation of the damper's messenger cable at the attached point of the small mass (Tc4) as function of excitation frequency at constant displacement.

The correlation between temperature variation and the excitation frequency at constant displacement are presented by the Equations 5.29 through 5.31 for Tc1, Tc2, Tc3 and Tc4. R-squared values regressions are respectively 0.8732, 0.9851, 0.8903 and 0.8732 respectively for Equations 5.29, 5.30, 5.31, and 5.32.

$$\Delta Tc1 = 1E\text{-}05f^3 + 0.0005f^2 - 0.0267f + 0.2267 \quad (5.29)$$

$$\Delta Tc2 = 5E\text{-}05f^3 - 0.0026f^2 + 0.0506f - 0.1841 \quad (5.30)$$

$$\Delta Tc3 = 0.0004f^2 - 0.0075f + 0.0865 \quad (5.31)$$

$$\Delta Tc4 = 1E\text{-}05f^3 + 0.0005f^2 - 0.0267f + 0.2267 \quad (5.32)$$

where ΔTc1, ΔTc2, ΔTc3 and ΔTc4 are temperature variation in Kelvin and t is the time in seconds.

Equations 5.25-5.32 describe the temperature evolution of the messenger cable for different forced response tests. As temperatures rises, the strain gauges glued on the messenger cable try to expand longitudinally and increase their resistance. This has as consequence to induce the apparent strain in the reading. It appears that the apparent strain associated with the strain gauges used in this work was close to 5, referring to the temperature rise (equation 5.25-5.32). This was obtained using the graphical method presented by Neubert (1961). Thus the apparent strain was negligible. For this reason, apparent strains were not taken in account during measurements. In addition, care was taken to make the Wheatstone bridge circuit for strain measurements in order to minimize uncertainties on reported values.

5.2.2 Free vibration test

5.2.2.1 Experimental set up

A free vibration test was conducted on a new and an old asymmetrical damper by using an impact hammer (Figure 5.14). The impact hummer used was the Bruel & Kjaer type, mode 8206 with a sensibility of 22.7 mV/N and a head extension of 40gr. The goal of this test on the Stockbridge damper was to analyze its natural response to some form of impact or displacement. The amplitude of vibration decays with time due to the Stockbridge damper damping.

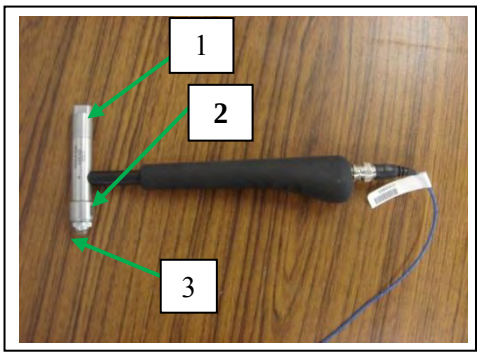

Figure 5.14: Impact hammer used during the free vibration test. (1) Head extension. (2) Force transducer. (3) Rubber.

Figure 5.15 shows the experimental set up used for the vibration test on the old Stockbridge damper. The same set up was used for the new Stockbridge damper. Four accelerometers were attached to the damper's mass to collect the displacement during the experiment.

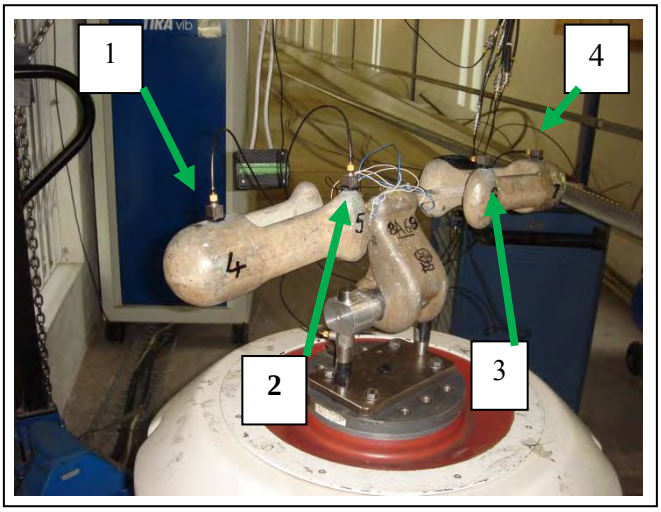

Figure 5.15: Experimental set up on the old Stockbridge damper for free vibration; (1), (2), (3) and (4) are accelerometers.

The impact on the Stockbridge damper was delivered by means of using an impact hammer which simulated the second and the fourth mode vibration of the Stockbridge damper. Figure 5.16 shows the location of the impact on the Stockbridge damper's mass. Four accelerometers (Acc 1, Acc 2, Acc 3, and Acc 4) were used during this experiment. Accelerometer 1 (Acc 1) and accelerometer 2 (Acc 2) were placed on the big mass of the damper and accelerometer 3 (Acc 3) and accelerometer 4 (Acc 4) on the small mass of the damper.

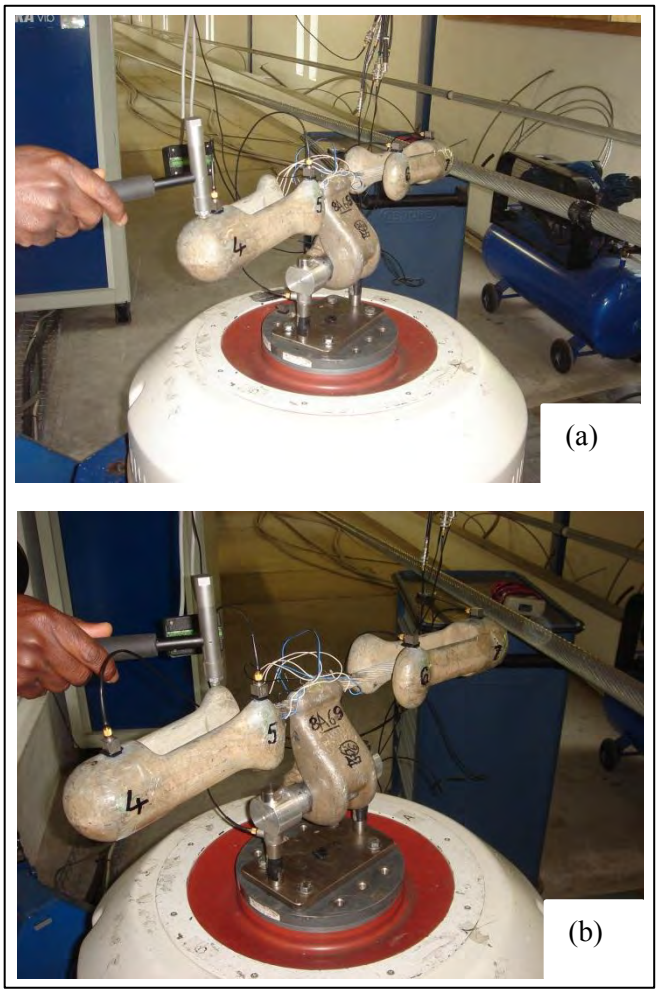

Figure 5.16: Free vibration test on Stockbridge damper. (a) The impact to simulate the second mode. (b) The impact to simulate the fourth mode.

5.2.2.2 Results and Discussion

Results from the free vibration test of the Stockbridge damper are presented in this section. Impacts of 25, 50, 75 and 100N were delivered to the Stockbridge damper on the damper's small mass. The displacement from acc 1 And acc 2 was collected as a function of time. The displacement from the accelerometer 3 and 4 did not give enough information as displacements were close to zero. Results are presented in two groups, the first group for the second and for the fourth mode of vibration damper. All dampers have the same design and are from the same company.

a. Impact to simulate the second vibration mode of Stockbridge damper

The old damper was knocked to simulate the second mode of vibration by hammer the damper (5.16 a) at the center of the small mass. Figure 5.17 presents the results from the free vibration test on the old damper, arising from simulation of the second mode vibration of Stockbridge damper with different knock forces.

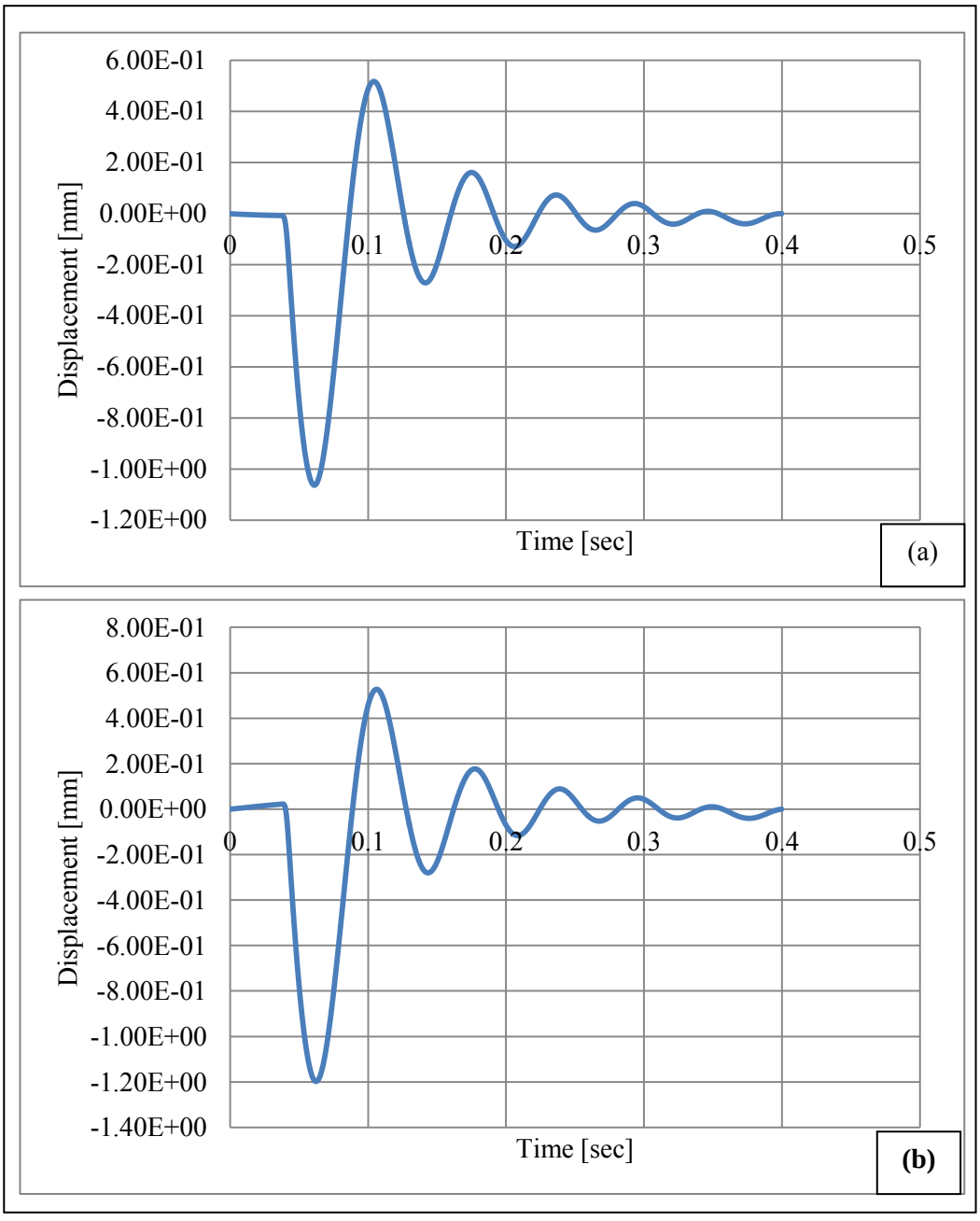

Figure 5.17: Free vibration of old Stockbridge damper by simulating the second mode of vibration. (a) The knocking force is 25N. (b) The knocking force is 50N.

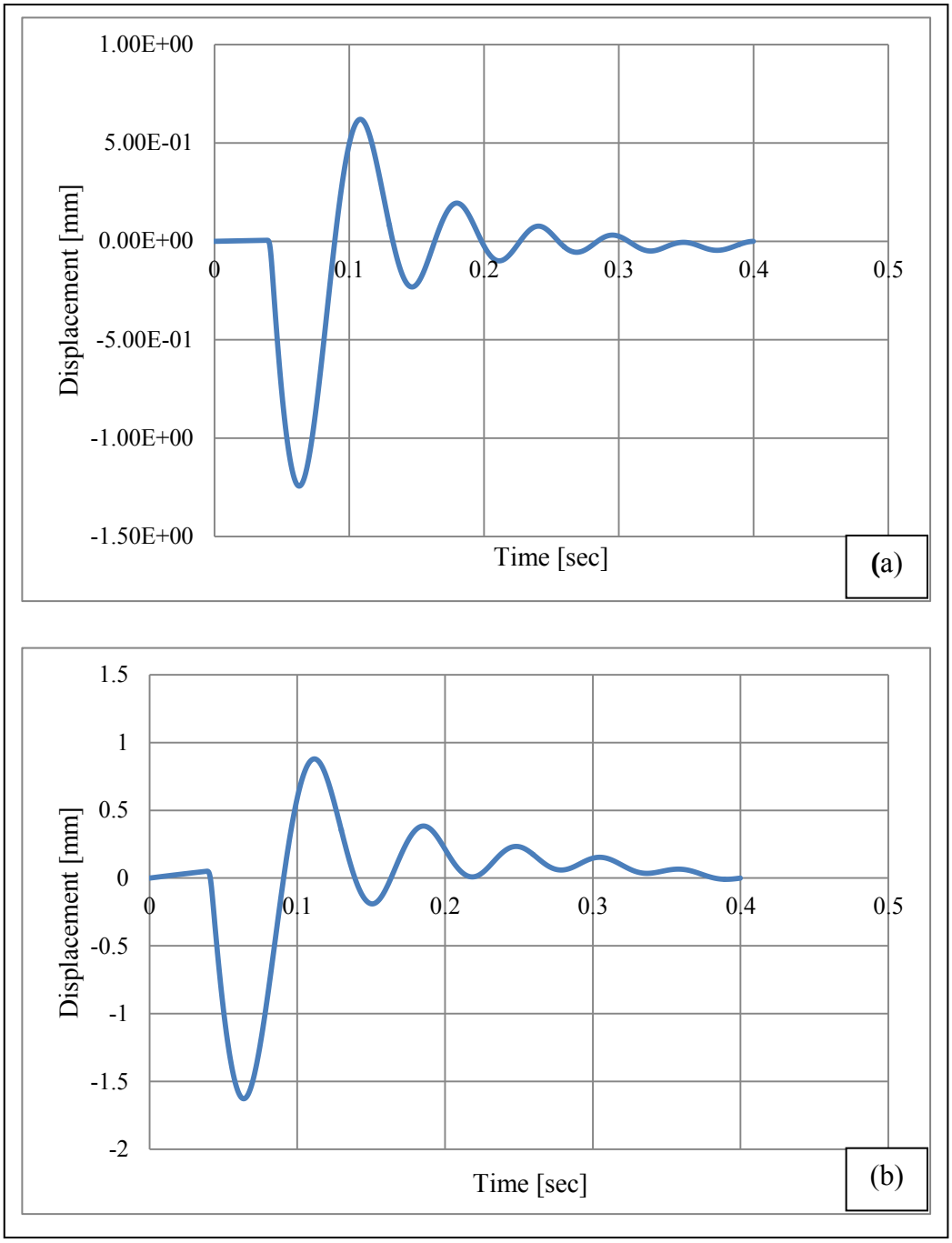

Figure 5.18: Free vibration of old Stockbridge damper by simulating the second mode of vibration. (a) The knocking force is 75N. (b) The knocking force is 100N.

Concerning the new damper, the same impacts were applied to it. The results from the free vibration tests are presented in the Figures 5.19 and 5.20 for the hammer impacts producing the second vibration mode.

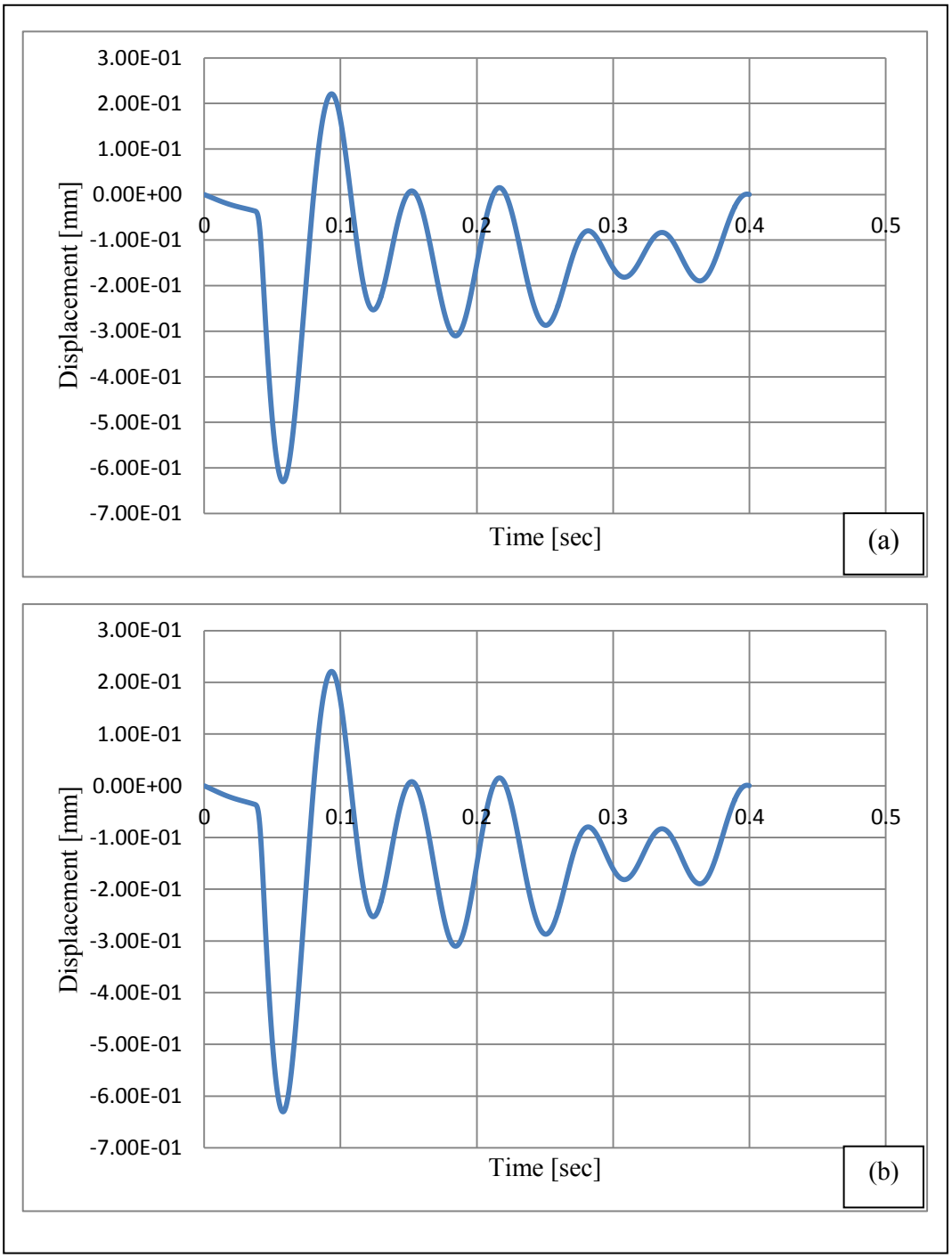

Figure 5.19: Free vibration of new Stockbridge damper by simulating the second mode of vibration (a) The knocking force is 25N (b) The knocking force is 50N.

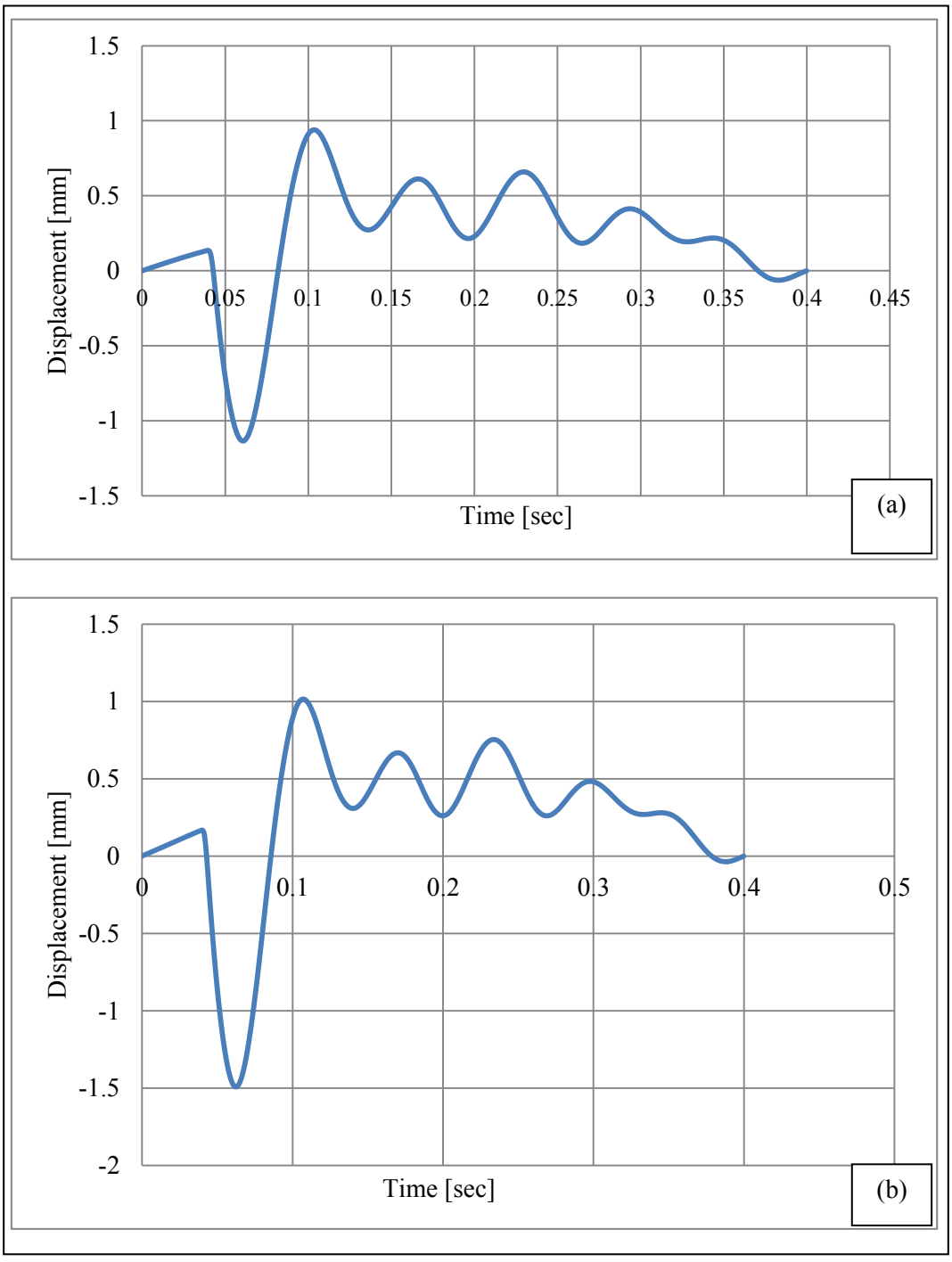

Figure 5.20: Free vibration of new Stockbridge damper by simulating the second mode of vibration. (a) The knocking force is 75N. (b) The knocking force is 100N.

Comparison between the old and the new damper for the second mode was made. Figures 5.21 and 5.22 show the comparison between data from the old damper and new damper for different knocks used during the free vibration test.

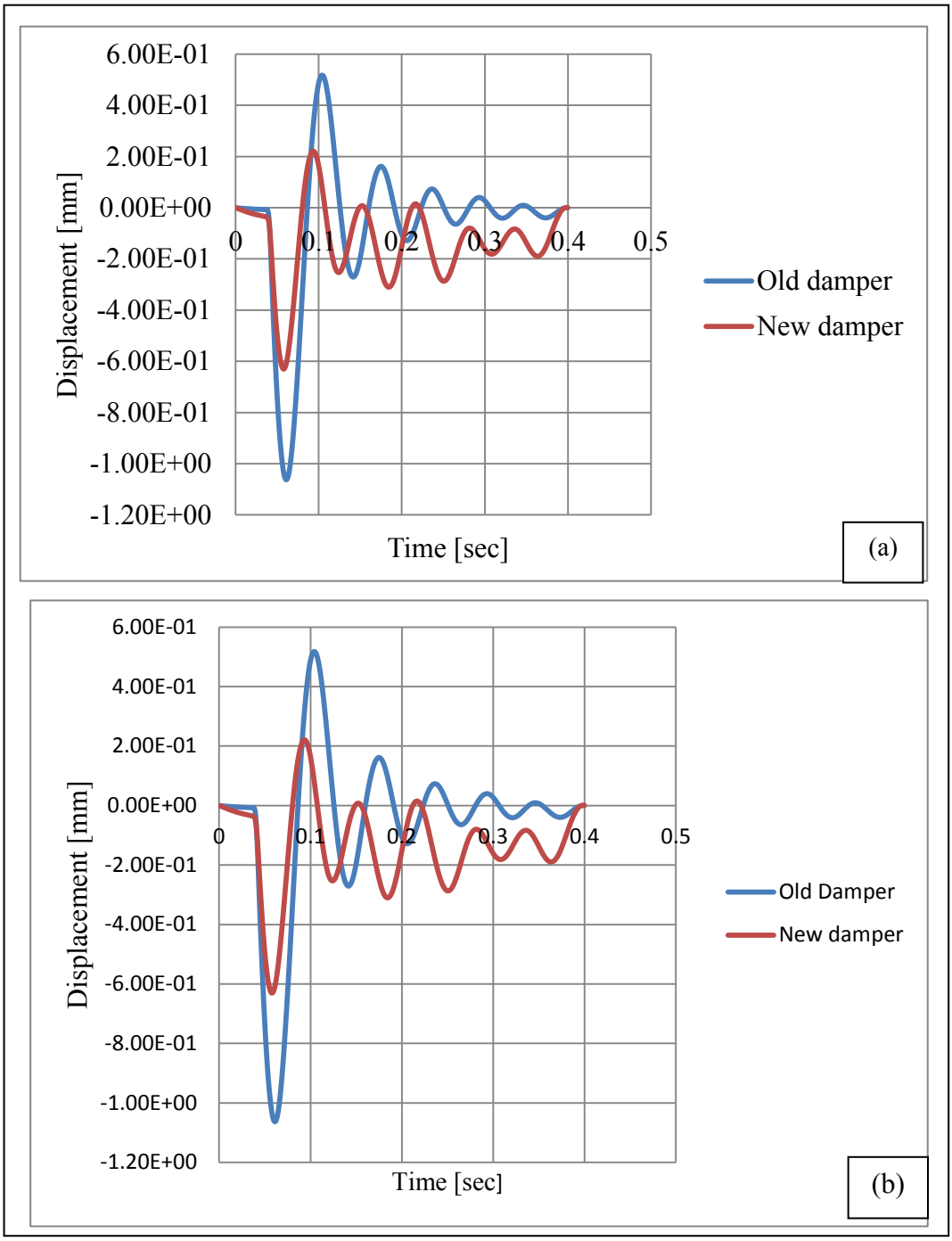

Figure 5.21: Comparison between the old and the new Stockbridge damper by simulating the second mode of vibration. (a) The knocking force is 25N. (b) The knocking force is 50N

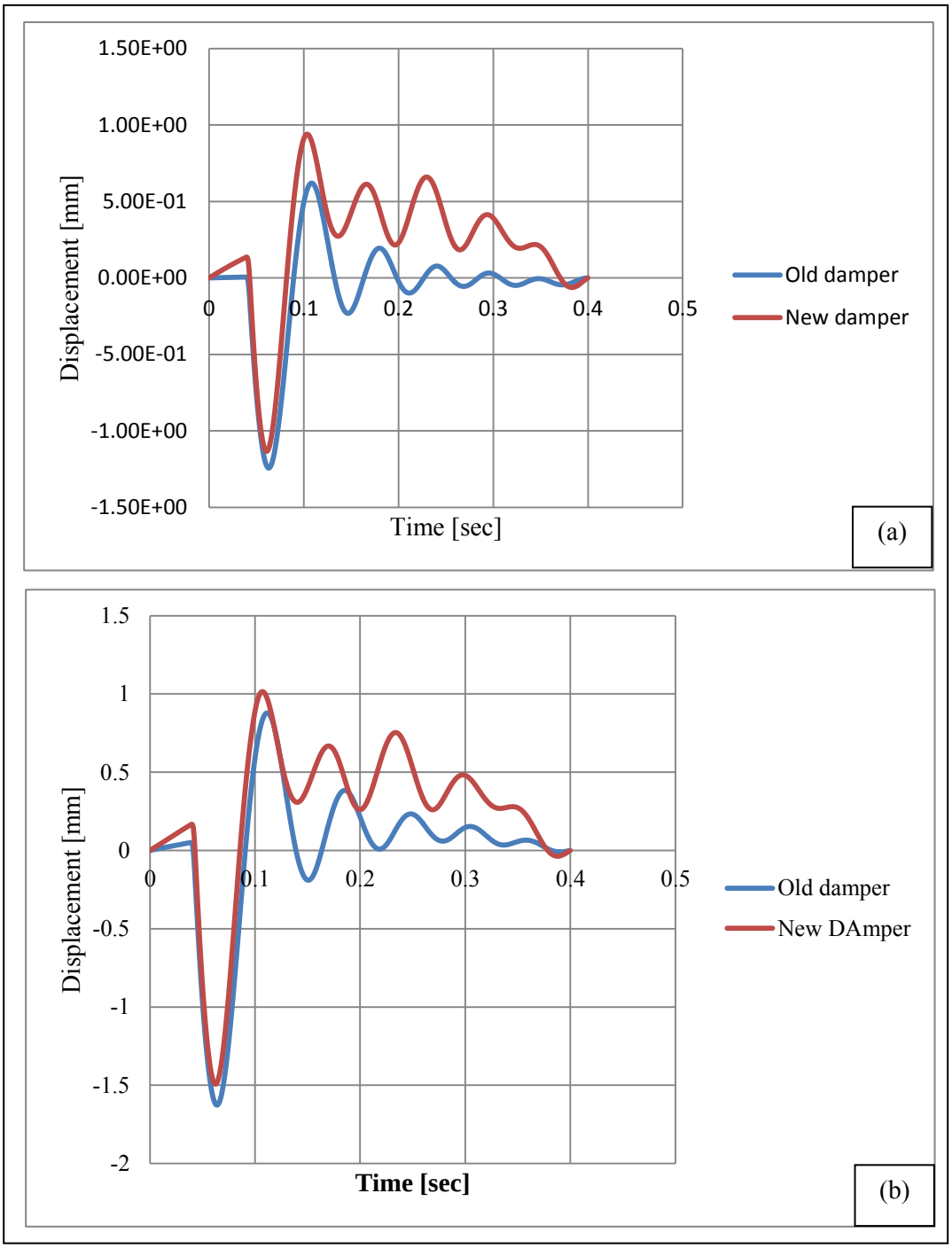

Figure 5.22: Comparison between the old and the new Stockbridge damper by simulating the second mode of vibration. (a) The knocking force is 75N. (b) The knocking force is 100N.

b. Impact to simulate the fourth vibration of Stockbridge damper

The fourth mode was simulated during the free vibration test by hammer the damper (5.16 b) at the end of the small mass. The result from the old damper is presented in Figures 5.23 and 5.24. It was observed that the vibration signal decays in time.

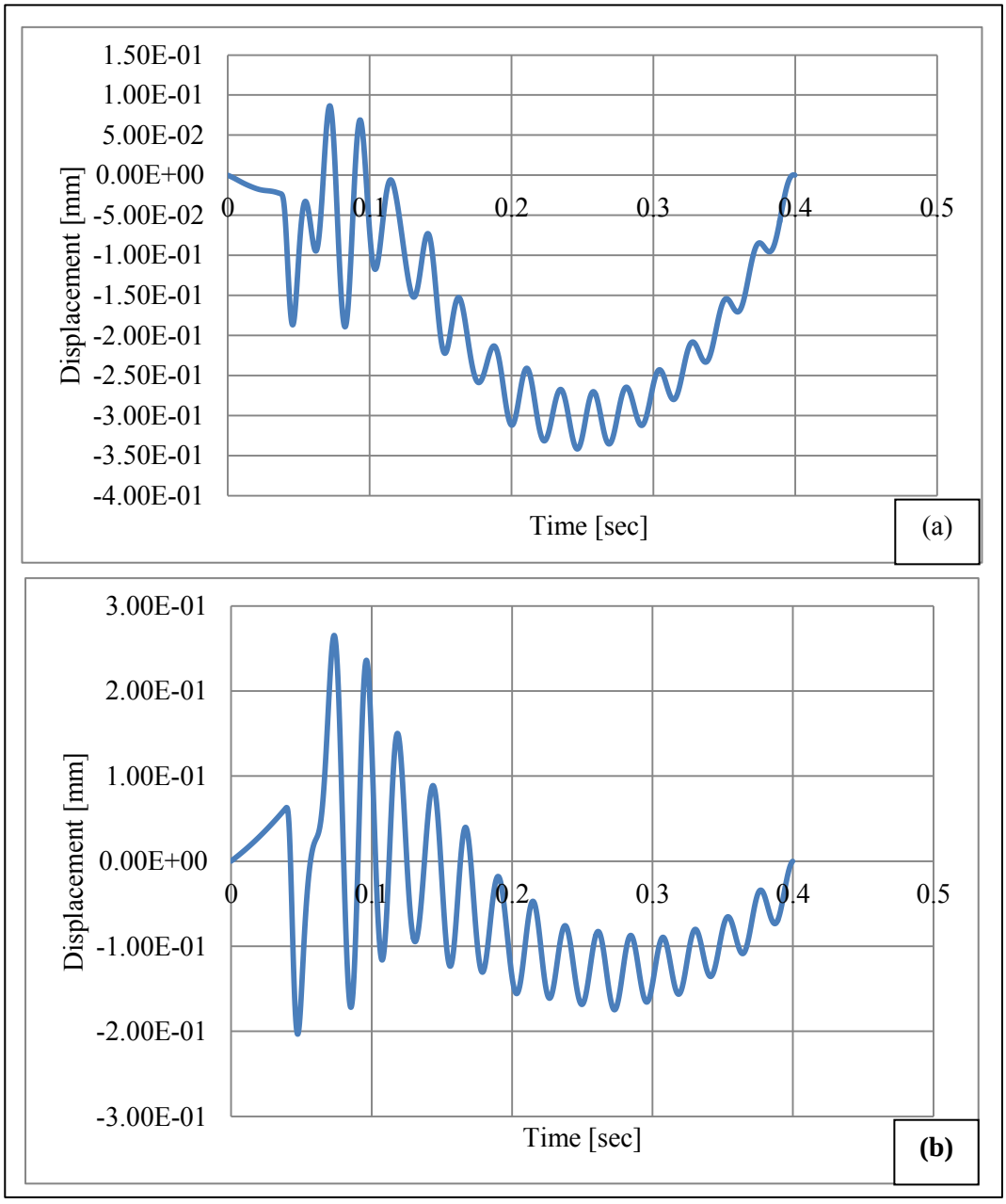

Figure 5.23: Free vibration of old Stockbridge damper by simulating the fourth mode of vibration. (a) The knocking force is 25N. (b) The knocking force is 50N.

Displacements have been collected by means of the acc 2 for each knocking. The 25N, 50N, 75N and 100N hammer knock has been applied.

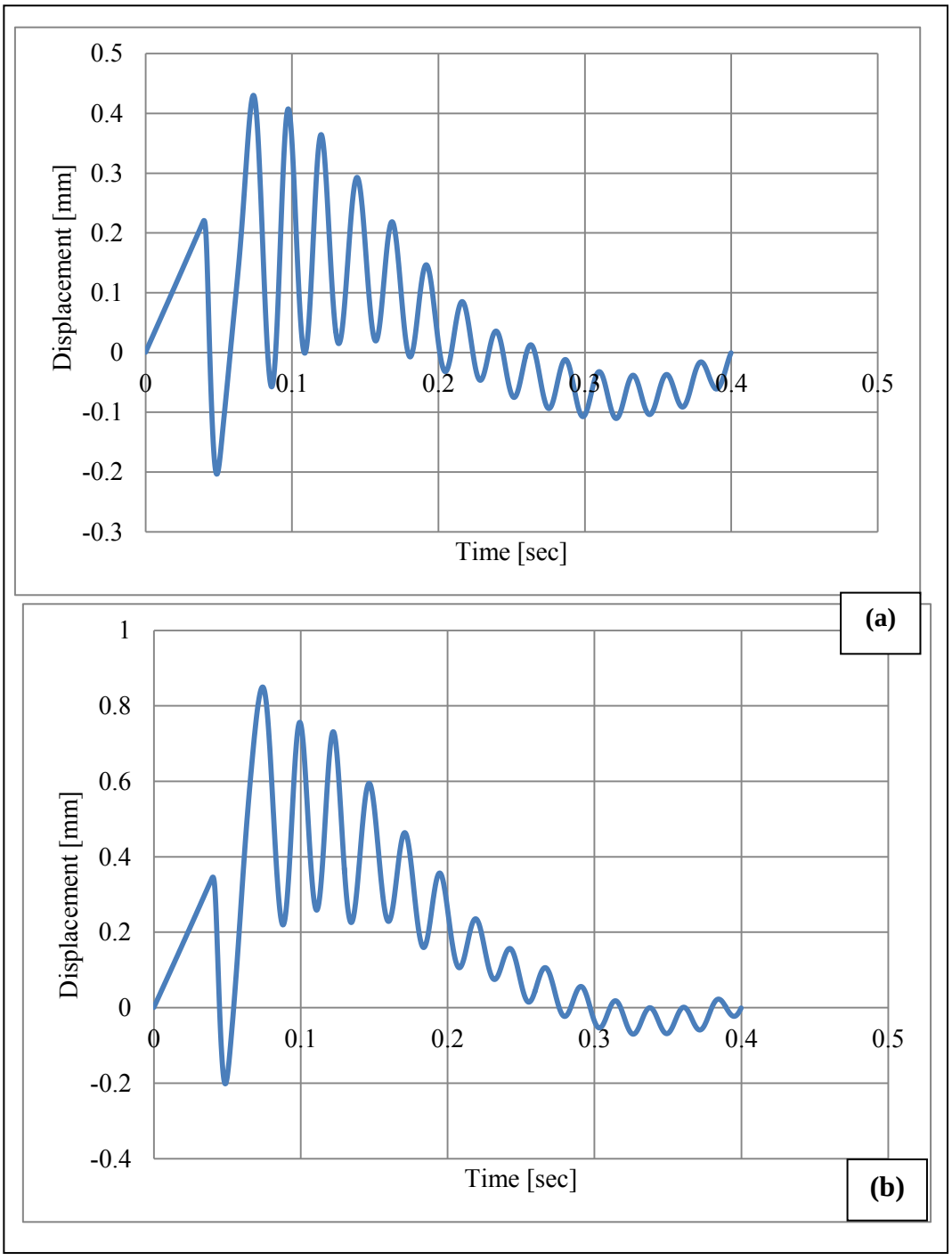

Figure 5.24: Free vibration of old Stockbridge damper by simulating the fourth mode of vibration. (a) The knocking force is 75N. (b) The knocking force is 100N.

Concerning the new damper, the same impacts were applied as for the old damper. The results from the free vibration tests are presented in Figures 5.25 and 5.26 for the hammer impacts producing the fourth vibration mode.

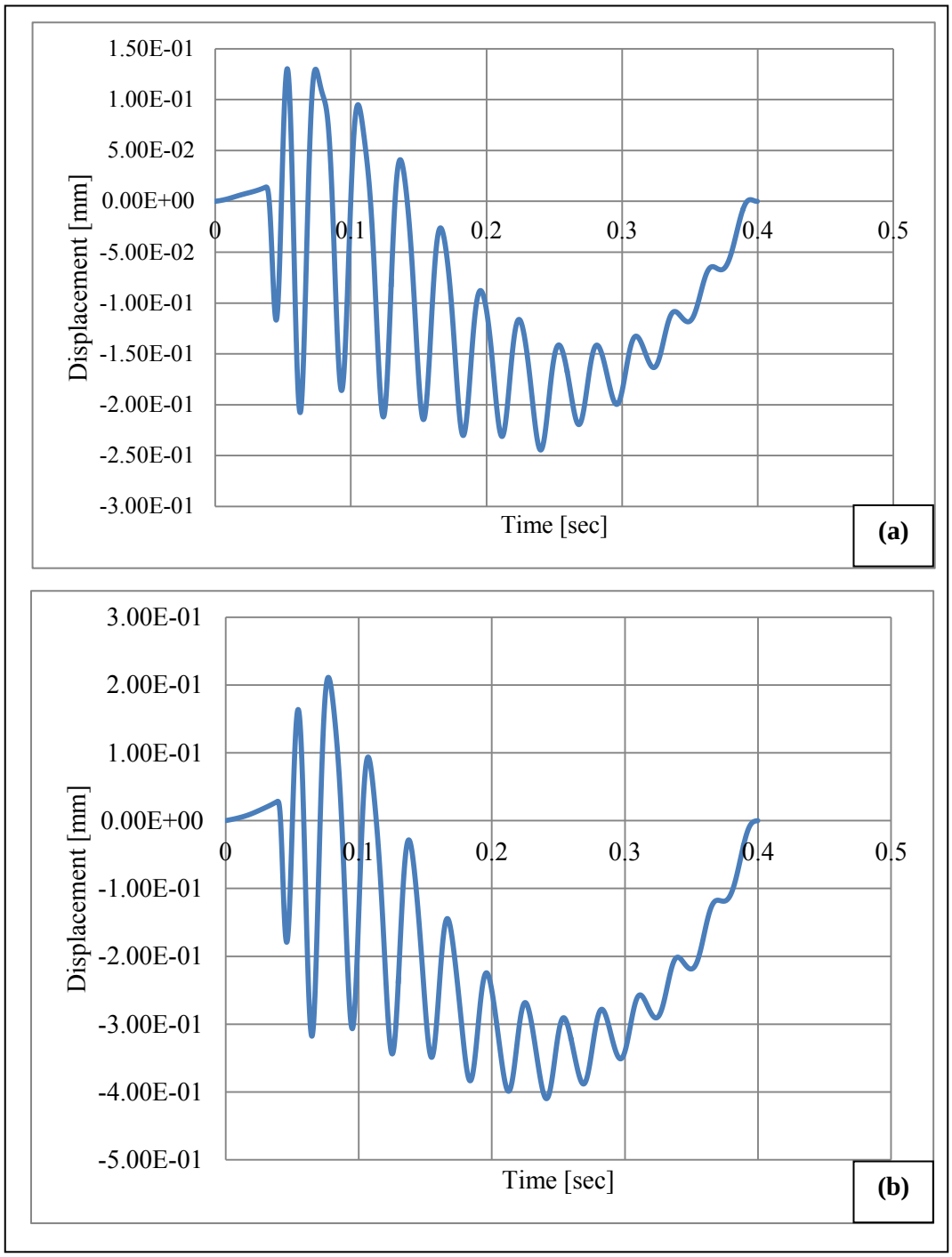

Figure 5.25: Free vibration of new Stockbridge damper by simulating the fourth mode of vibration. (a) The knocking force is 25N. (b) The knocking force is 50N.

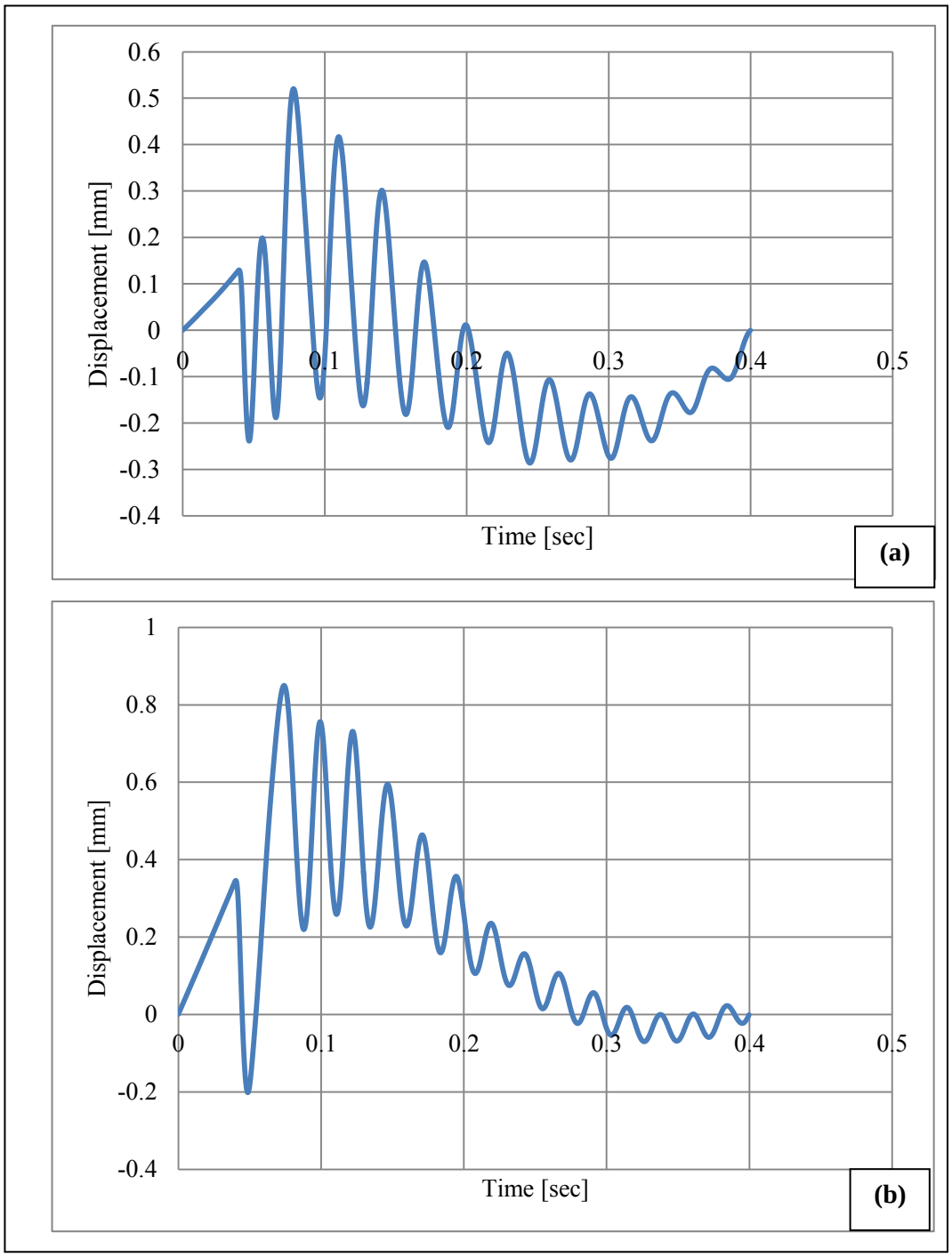

Figure 5.26: Free vibration of old Stockbridge damper by simulating the fourth mode of vibration. (a) The knocking force is 75N. (b) The knocking force is 100N.

Comparison between the old and the new damper for the fourth mode was made. Figures 5.27 and 5.28 show the comparison between data from the old damper and new damper for different knocks used during the free vibration test.

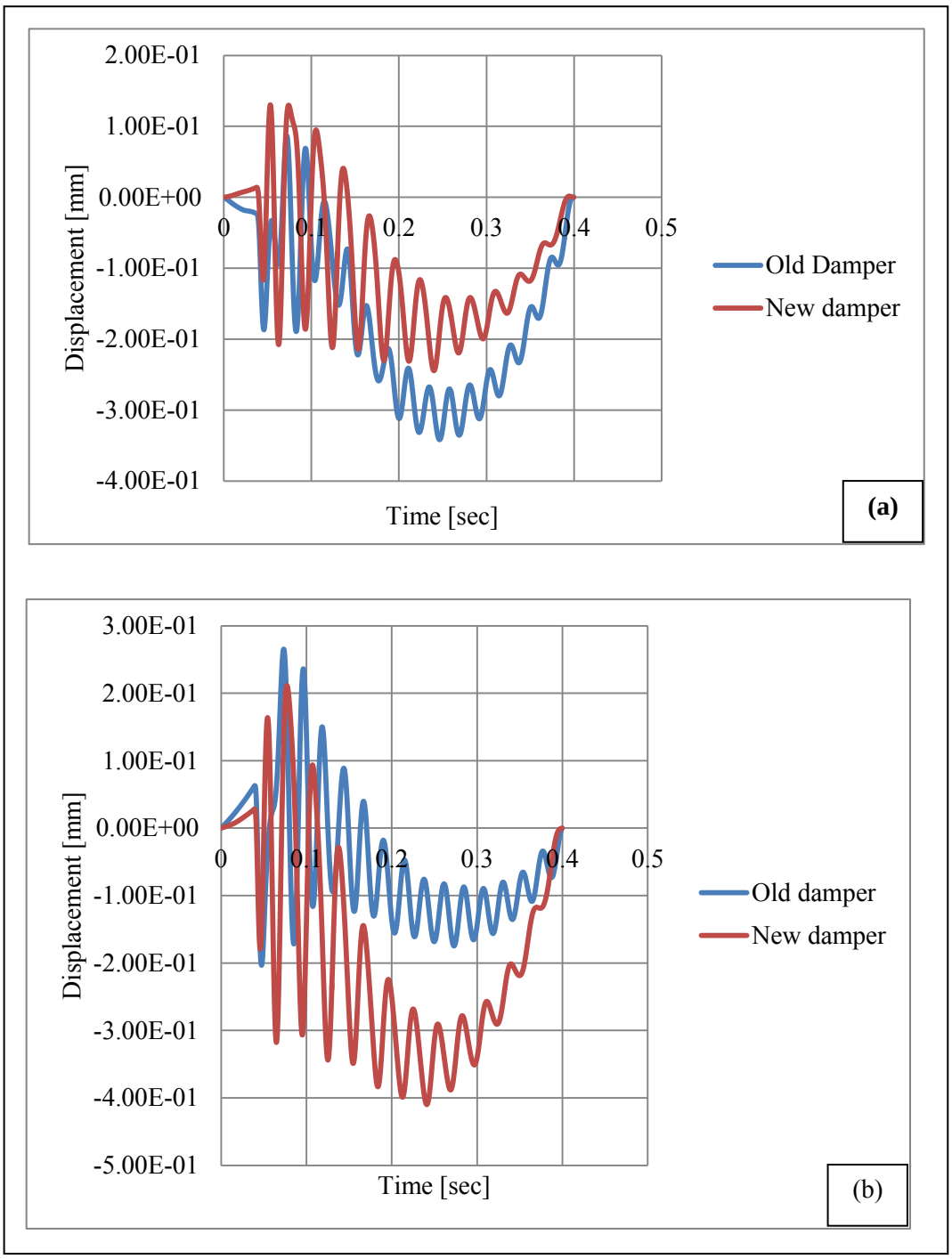

Figure 5.28: Comparison between the old and the new Stockbridge damper by simulating the fourth mode of vibration. (a) The knocking force is 75N. (b) The knocking force is 100N.

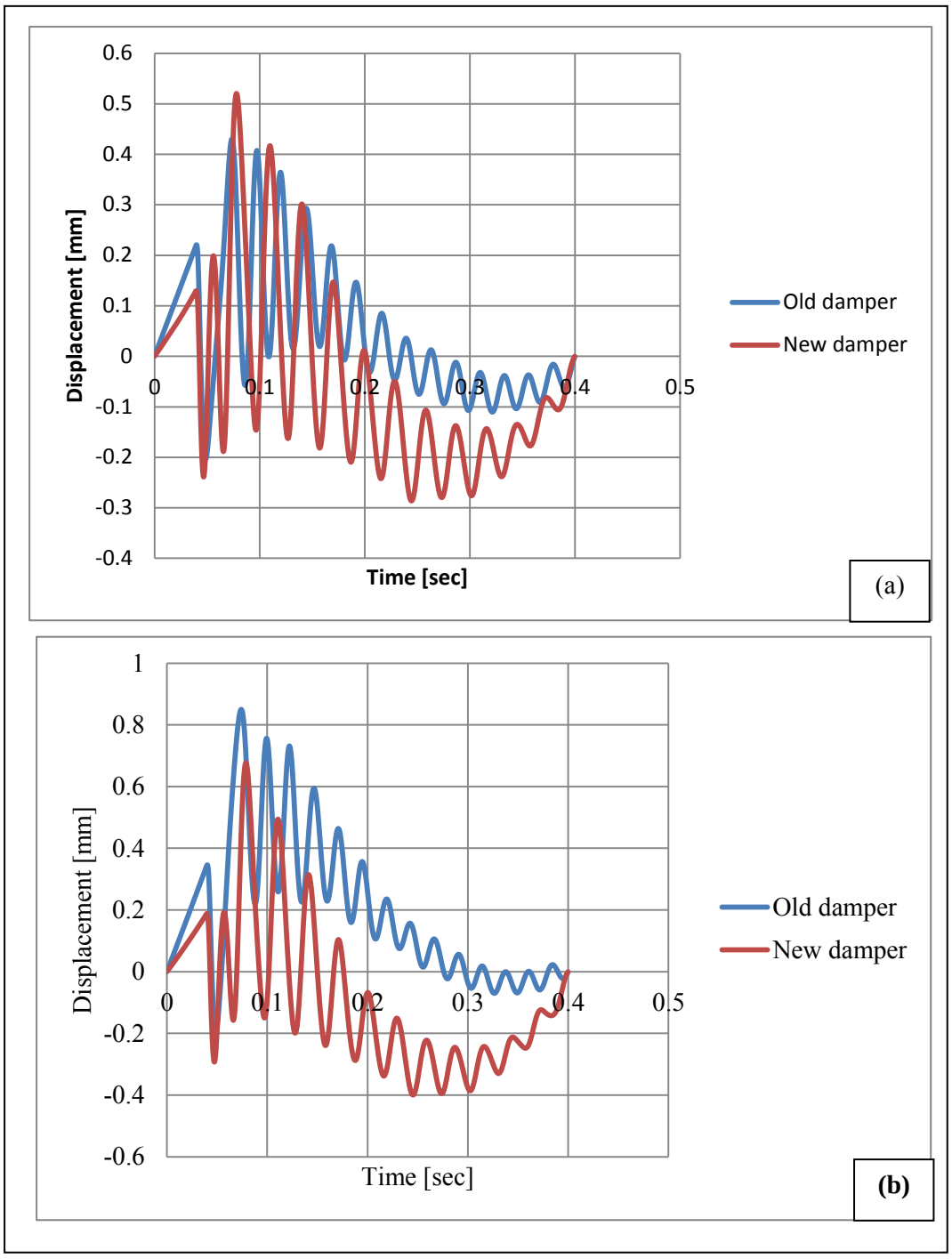

Figure 5.28: Comparison between the old and the new Stockbridge damper by simulating the fourth mode of vibration. (a) The knocking force is 75N. (b) The knocking force is 100N.

5.2.2 Forced response and fatigue test

5.2.2.1 Experiment set up

The forced response and fatigue tests were conducted on the Stockbridge damper to determine its life prediction as well as its remaining life. Figure 5.29 shows the experiment set up used in the present study.

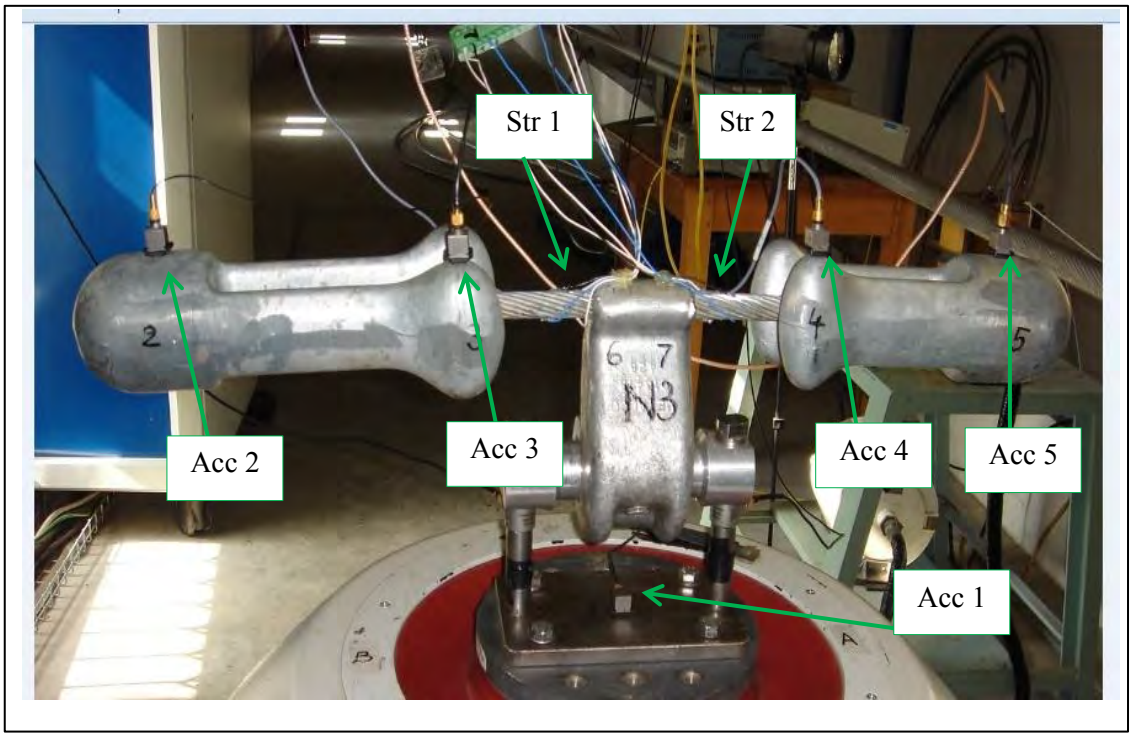

Figure 5.29: Experimental set up for forced response test and fatigue test with five accelerometers (Acc 1, 2, 3 ,4 and 5) and two strain gauges (Str 1 and 2).

The following sensors were used for the forced response test and the fatigue test:

- One accelerometer (Acc 1) on the shaker base for shaker control;
- Four accelerometers (Acc 2, 3, 4 and 5) on the damper masses, two on each mass to detect each vibration mode of the Stockbridge damper;
- Two strain gauges (Str 1 and 2) in half bridge were glued near the clamp of the messenger cable at each side, and one on the top and the other on the bottom. This Wheastone bridge has been adopted for temperature compensation.

5.2.2.2 Results and discussion

The new damper was running before testing in order to stabilize its mechanical proprieties. One sweep in the frequency range of wind induced vibration has been made as a running in (VIP 2.0, 2008). After the running in, the forced response test was conducted by making a sweep in the range of wind induced vibration. The frequency range was determined by using the Strouhal formula. Thereafter the damper was vibrated at constant displacement peak to peak for a certain number of cycles. The procedure was repeated until the damper failed. The loss of the small damper mass which is one of the commonest modes of failure was investigated. The procedure for the experiment was as follows:

a. Make a sweep in the range of wind induced vibration and detect the fourth resonance frequency of the Stockbridge damper, which is the point of excitation at which the damper loses its small mass (after a number of cycles). During the sweep the frequency range and the displacement peak to peak are controlled.
b. Vibrate the damper at its resonance frequency (highest) with 1mm of displacement peak to peak for a certain number of cycles.
c. Make another sweep in the same condition as in (a) to get the new fourth resonance frequency.
d. Repeat the procedure until the damper fails.
e. Failure is detected by noise on the graph from the sweep (Figure 5.32).

Data was collected during the sweep only and not when the damper was vibrated at a constant frequency. Using the principle of cumulative damage presented in the literature review, the number of cycles accumulated was collected and are presented in Table 5.4.

Table 5.5: Number of cycles elapsed and number of cycles accumulated by the Stockbridge damper

Number of cycles elapsed	Number of cycles accumulated
1068000	
100000	1168000
100000	1268000
100000	136000
100000	1468000
100000	1768000
100000	1868000
	1968000

At the highest resonance frequency, the change of vibration acceleration of the big mass was low. Figure 5.30 shows the acceleration of the big mass during the fatigue test from acc 2 and acc 3 at different numbers of accumulated cycles N.

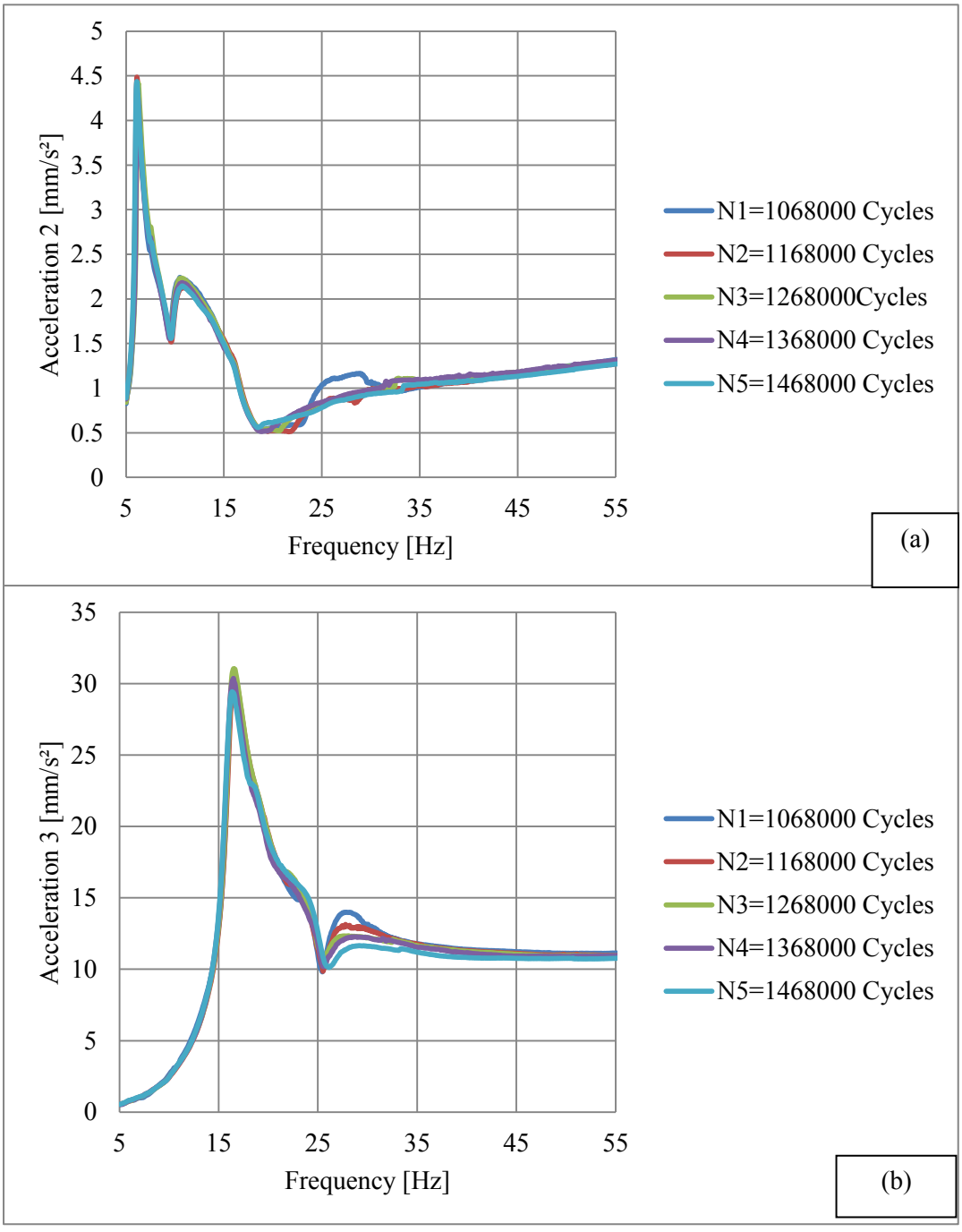

Figure 5.30: Acceleration vs frequency of the big mass of the Stockbridge damper at different number of cycles accumulated (a) acc 2 (b) acc 3.

The strain collected from strain gauges Str 1 near the clamp at the long side of the messenger cable did not change during the fatigue test. Figure 5.31 shows the strain from Str 1 during the fatigue test. The observation that there was no change from Str 1 makes sense as the amplitude of the vibration of the long side of the Stockbridge damper was small during the fatigue test.

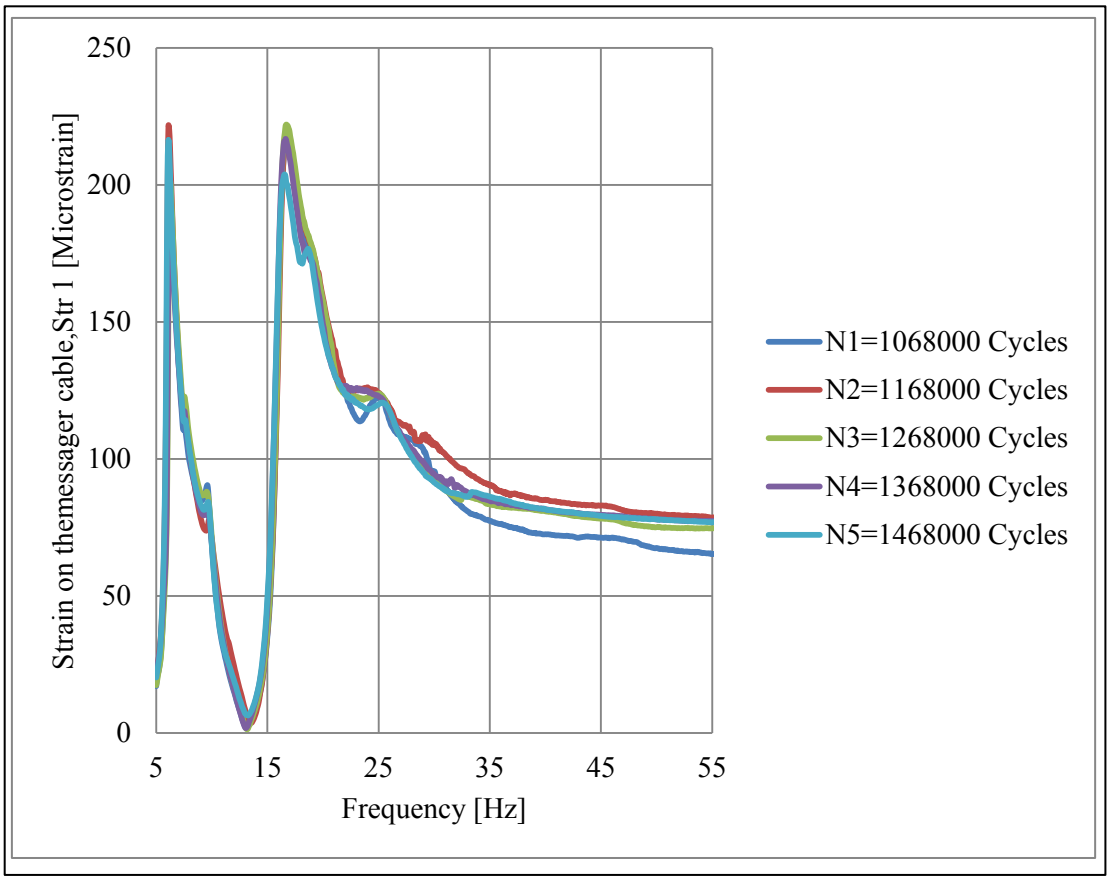

Figure 5.31: Strain of the messenger cable from Str1 during the Stockbridge damper test as a function of frequency at different number of cycles accumulated.

The change of resonance frequency has been used by many researchers to investigate the damage of engineering structures. This was reviewed in Chapter 3 of this dissertation. The change of Stockbridge damper resonance frequency is a function of the degree of damage of the Stockbridge damper. The change of the highest resonance frequency is presented in Figure 5.32 by using the acceleration from acc 4 and at different levels of the cycles accumulated. The location of acceleration 4 allowed for the collecting of data related to the fourth vibration mode which is the one which creates the loss of the small mass. The resonance frequency is observed by the peak on the graph from the sweep. The failure criterion is the presence of the noise in the sweep graph (Figure 5.32).

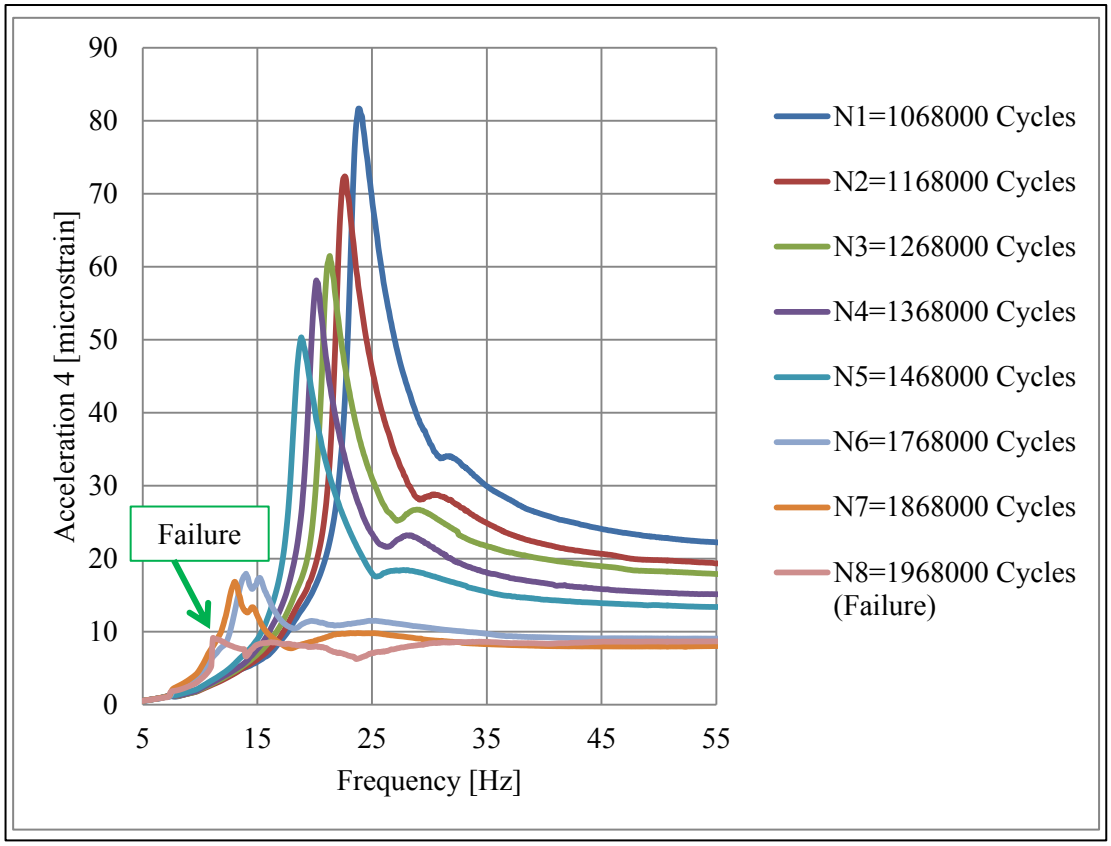

Figure 5.32: Acceleration (acc 4) vs frequency at different level of accumulated number of cycles.

Figure 5.32 presents the resonnance frequencies which correspond to the peaks of the graph. Resonance frequencies at different number of accumulated cycles are presented in Table 5.5.

Table 5.6: Change of the fourth resonance frequency of damper function of the acceleration from accelerometer 4.

Resonance frequency [Hz]	74.27	81.66	72.37	61.47	58.12	50.32	17.94	15.55	9.15
Acceleration Acc4[mm/sec^2]	26.61	23.86	22.62	21.31	20.14	18.83	14.01	12.71	11.12

5.2.2.3 Life prediction

The life prediction of Stockbridge damper was established by using the change of resonance frequency. Data from accelerometer 4 (acc 4) (Table 5.5) and from strain gauge 2 (Figure 5.29) (Str 2) was utilised. A correlation was established which describes the relation between resonance frequency and the acceleration of the small mass. Figure 5.33 shows the correlation between resonance frequency and the acceleration of the damper's small mass. The new, running in and failure state of the damper are shown respectively in Figure 5.33 by means of black, green and red dots.

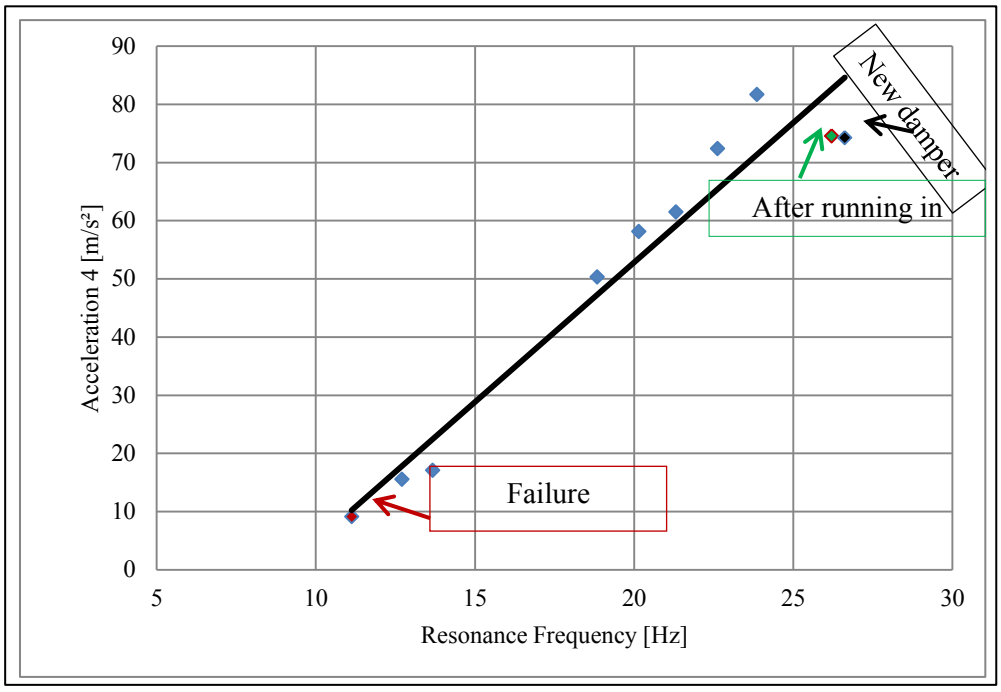

Figure 5.33: Correlation between the acceleration (acc4) and the fourth resonance frequency for Stockbridge damper.

The mathematical model of the relationship between the fourth resonance frequency f_{res} [Hz] and acceleration $Acc4$ [m/s^2] established through the correlation is presented in Equation5.33 with 0.94 as the square correlation coefficient.

$$Acc4 = 4.82 f_{res} - 43.21 \tag{5.33}$$

Where $Acc4$ and f_{res} are acceleration and the fourth resonance frequency.

Taking into account the number of accumulated cycles as a function of the resonance frequency a correlation was made to predict the life of a Stockbridge damper. Figure 5.34 shows the linear correlation between the numbers of accumulated cycles and the resonance frequency.

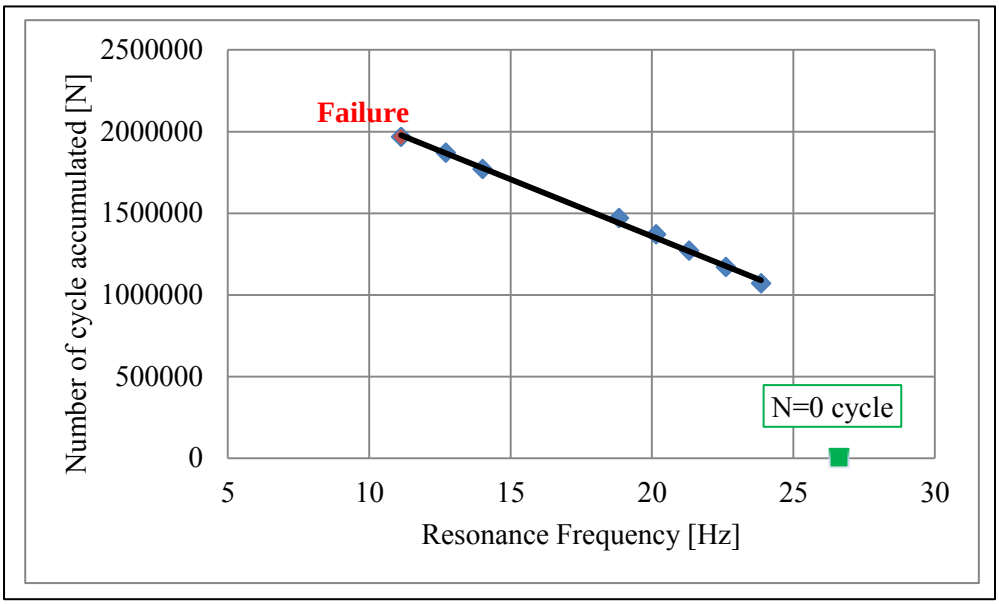

Figure 5.34: Linear correlation between the number of cycles accumulated and the fourth resonance frequency of Stockbridge damper.

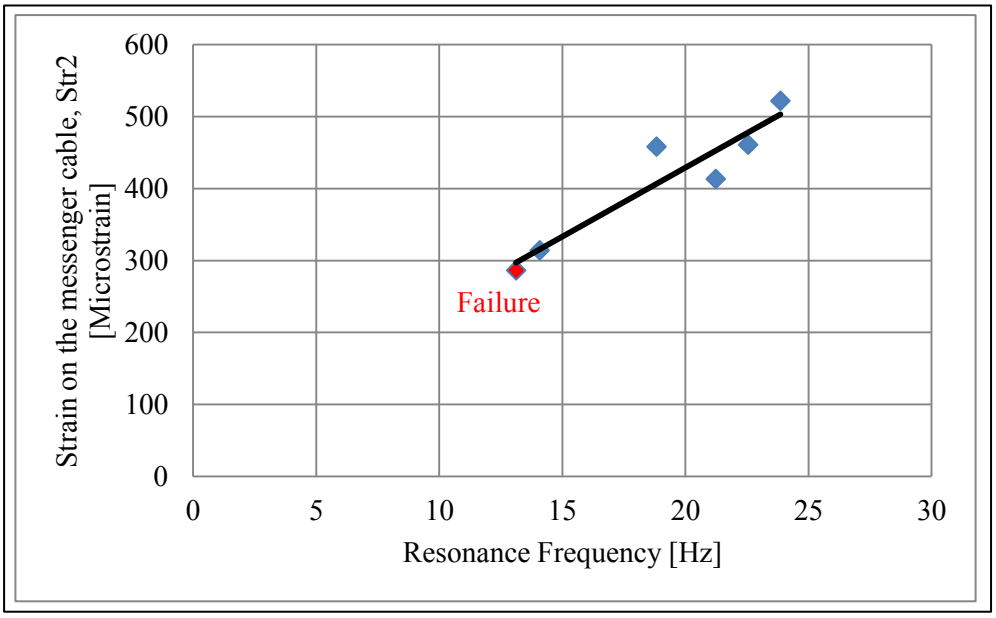

Figure 5.35: Correlation between the strain on the messenger cable near the clamp at the short side (Str 2) and the fourth resonance frequency.

Equation 5.34 presents the regression model between the accumulated number of cycles N and the fourth resonance frequency of the Stockbridge damper f_{res} established from data Figure 5.35. The linear correlation was made with 0.997 as the square correlation coefficient.

$$N = -6974 f_{res} + 3 * 10^6 \tag{5.34}$$

The correlation between the strain on the messenger cable near the clamps at the short side of the Stockbridge damper and the resonance frequency is given by Equation 5.35.

$$\varepsilon = 19.19 f_{res} + 44.99 \tag{5.35}$$

where: ε is the strain on the messenger cable near the clamp at the short side of the Stockbridge damper. This linear correlation presents the square factor of correlation equal to 0.881.

In addition to the mathematical model which was established between the strain near the clamp (Str 2) and the number of cycles accumulated (Figure 5.36).

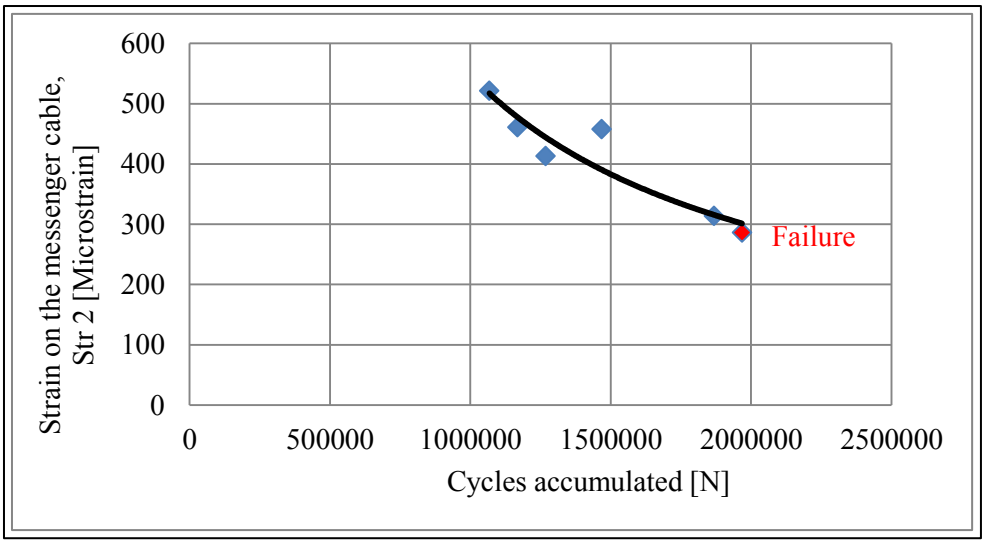

Figure 5.36: Correlation between the strain on the messenger cable near the clamp at the short side (Str 2) and the number of accumulated cycles.

The correlation between the strain and the number of cycles accumulated for the Stockbridge damper and the strain is given by Equation 5.36 with the square coefficient of correlation equal to 0.876.

$$\varepsilon = 10^{8} N^{-0.883} \tag{5.36}$$

Where ε and N represent respectively the strain on the messenger cable near the clamp at the point where the small mass is located and the number of cycles accumulated.

5.2.2.3 Different life prediction models established for Stockbridge damper

Based on the data presented in the preview point as well as on the previews, also referring to previous publications on the damage model, the damage model of Stockbridge damper has been established. This model is based on the change of the fourth resonance frequency ratio λ (Equation 5.37).

$$\lambda = \frac{f_{res,0} - f_{res}}{f_{res,0}} \tag{5.37}$$

where $f_{res,0}$ and f_{res} are respectively the resonance frequency of the new damper (N=0 cycle) and the resonance frequency of the used damper.

The relation between the acceleration of the damper's small mass during the fatigue test and λ for the Stockbridge damper is shown in the Figure 5.37.

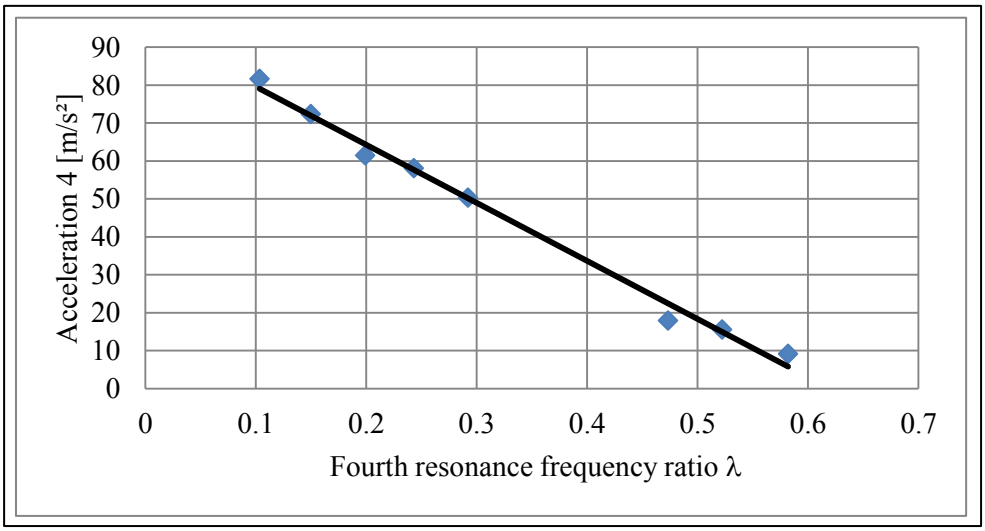

Figure 5.37: Correlation between the acceleration 4 and λ.

The relationship which links the acceleration of the damper's small mass at its fourth mode, $Acc4$, and λ has been established. The mathematical model for this relationship is given by Equation 5.38 and the square coefficient of correlation is equal to 0.99.

$$Acc4 = -151.11\lambda + 94.93 \tag{5.38}$$

The correlation between the change of the fourth resonance frequency permit and the life ration $\frac{N}{N_F}$ in term of number of cycle accumulated has been made. The life ratio characterizes the degree of damage Δ for the Stockbridge damper as it was reviewed in Chapter 3. Figure 5.38 shows the polynomial correlation between the change of the fourth resonance frequency and the damage for Stockbridge damper.

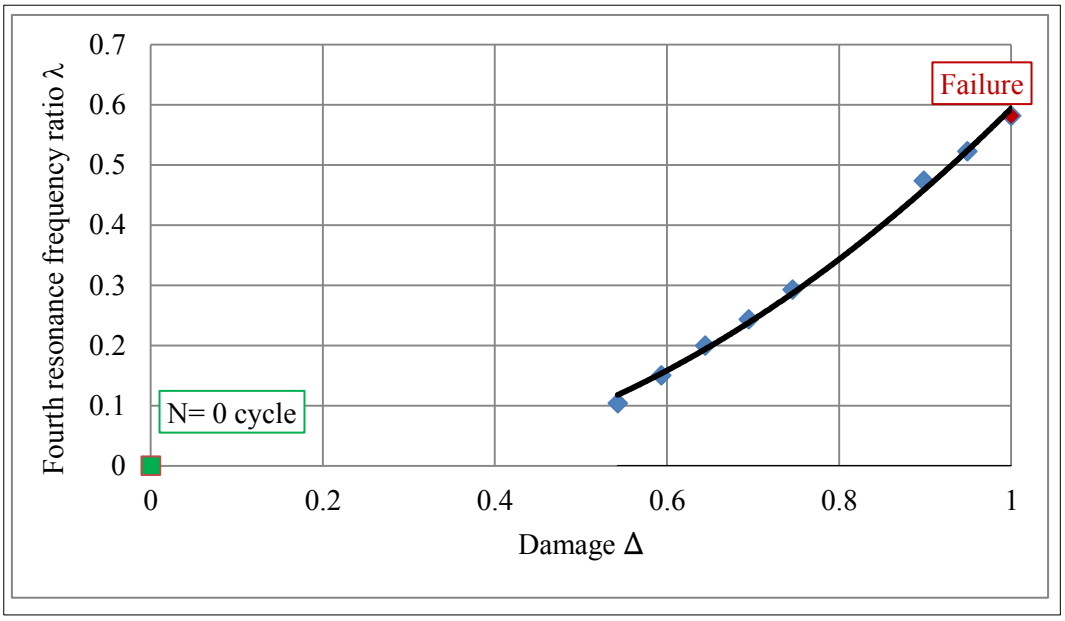

Figure 5.38: Correlation between the fourth resonance frequency ratio and damage of the Stockbridge damper.

Equation 5.40 gives the correlation between the change of the fourth resonance frequency ratio λ and the damage Δ. Referring to the literature review presented in Chapter 3, the mathematical model has been established based on the principal which attributes the value of zero ($\Delta = 0$) for the new sample and 1 for the failure damaged sample. Based on this, the mathematical model of damage must be the second degree which this expression is given by Equation 5.39.

$$\Delta = a\lambda^2 + b\lambda \tag{5.39}$$

Coefficients a and b have been determined by doing a correlation of data from Figure 5.38. The square coefficient of correlation is equal to 0.93. Equation 5.39 becomes:

$$\Delta = -3.34\lambda^2 - 4.052\lambda \tag{5.40}$$

5.2.2.4 Remaining life of Stockbridge damper

The procedure to determine the remaining life of Stockbridge damper is given in this point. This paragraph answers the following question: Can the remaining life of the used Stockbridge damper be determined by investigating the loss of its small mass as the mode of failure?

Having the used Stockbridge is fourth resonance frequency can be determined by sweep? With the fourth resonance frequency f_{res}, the ratio change of resonance frequency λ can be determined by using the Equation 5.37. The determination of the damage of the Stockbridge is established by using Equation 5.40.

The number of cycles elapsed for the damper will be determined by using Equation 5.41:

$$N = \Delta * N_F \tag{5.41}$$

Finally, the remaining life N_R of the Stockbridge damper will be given by the difference between the numbers of cycles until the damper fails and the elapsed number of cycles accumulated (Equation 5.42).

$$N_R = N_F - N \tag{5.42}$$

CHAPTER 6

CONCLUSION AND RECOMMENDATIONS

6.1 Conclusion

The main objective of the current study was the development of an approach to determining the life prediction and the remaining life of power line dampers. This approach integrates data collection such as acceleration, resonance frequency and strain measurement for life prediction and remaining life of the Stockbridge damper. The common mode of failure was analysed to determine the life prediction and the remaining life of Stockbridge damper.

Regarding the strain measurement, the bending stress of messenger cable near the clamped end point was investigated and a Matlab model was developed using the mechanical proprieties of a Stockbridge damper as input.

The symmetrical Stockbridge damper tests presented theoretically two vibration modes. Data from experiments corresponded with those from the theory for resonance frequencies and the related bending stress. The Matlab model and data from experiments confirmed that the symmetrical damper has two degrees of freedom as two peaks on the graphs were revealed; these peaks represent the two resonance frequencies.

A mathematical model was established using the Matlab program. In this particular case, the Matlab model agreed with the mathematical model of the symmetrical damper from the literature at all resonance frequencies. Unfortunately, the friction between wires, and the lack of homogeneity of Stockbridge damper messenger cable were the main reasons for the gap between the two graphs at certain points of the model.

The same experimental and mathematical procedure may be used to determine the bending stress of the messenger cable at other locations, such as those near the weight point. The change in resonance frequencies as well as the related bending stresses and strain of messenger cable can be used to determine the life assessment of Stockbridge dampers.

It was observed that temperature evolution was one of the causes of error during the strain measurement using the strain gauges. Therefore, knowing the temperature range of the sample at the points where the strain gauges will be glued it is very important to avoid this kind of error. Due to friction between wires of the messenger cable, variation of temperature was observed on the damper's messenger cable during the damper's operation and test. Also, the temperature of the messenger cable during the test was investigated in the frequencies range of wind induced vibrations of the symmetrical damper. The forced response test was made on the Stockbridge damper at constant velocity and constant peak to peak displacement. As a result, the highest temperature variation (2.8K) was observed at constant velocity peak to peak near the attached point of the big mass on the messenger cable. To predict the messenger cables temperature during the test, experimental data were successfully correlated using the polynomial function. Model parameters depend on the location of the thermocouple on the messenger cable.

This study presented an approach to determining the life of a Stockbridge damper. The most common mode of failure, which is the loss of the damper's small mass, was investigated. This mode of failure depends on the excitation parameters which are the resonance frequency and the displacement. Thus, mechanical proprieties of Stockbridge damper were investigated, especially those that are linked to this mode of failure and can change with the number of cycles elapsed. It was observed that the fourth resonance frequency of the Stockbridge damper changed with the number of cycles elapsed, as did the acceleration of the small mass including the strain on the messenger cable near the clamp.

By correlation, a mathematical model was established taking into account the resonance frequencies, the acceleration of the damper's small mass, and the stresses on the messenger cable near the clamp at the side of the small mass of the Stockbridge damper. The damage model of the Stockbridge damper was established based on the fourth resonance frequency change ratio. It was discovered that the main reason for loss of the small mass was the friction between wires at the junction between the messenger cable and the mass. These causes of failure started with the appearance of cracks on the wire of the messenger cable. Failure was constituted with the rupture of wires one by one, which reduces the power of vibration transmission from the clamp to the small mass through the Stockbridge damper's messenger cable. In the failure process, the stiffness and the damping capacity of the Stockbridge damper decays and therefore the resonance frequencies decay also. The approach to determine the remaining life is presented by using a regression after getting the fourth resonance frequency of the Stockbridge damper.

6.2 Recommendations

From the conclusions drawn during this study, the following additional studies to be completed by future researchers may be recommended:

- Investigation of the stiffness variations of the Stockbridge damper as a function of the number of cycles elapsed. This will involve the determination of life expectancy of Stockbridge damper as a function of the stiffness.

- Investigation of the temperature variation of the messenger cable. This will include the temperature distribution on the messenger cable while the Stockbridge damper is working under different conditions.

- Investigation of the life prediction of the Stockbridge damper in real time and condition by using in situ data.

- Extend the procedure presented in this study to all types of Stockbridge damper which can lead to the development of one mathematical model covering all types.

REFERENCES

Adams, R. D., Cawley, P., Pye, C. J. and Stone, B. J. 1978. A vibration technique for non-destructively assessing the integrity of structures. *Journal of Mechanical Engineering Science*, 20 (2):93-100.

Bennett, J. A. 1946. A study of the damaging effect of fatigue stressing on X4130 steel. Proceedings, *American Society for Testing and Materials*, 46:693-714.

Bishop, R. E. D. and Johnson, D. C. 1960. *The mechanics of vibration*. Cambridge: Cambridge University Press.

Bo, W. and Wei, H. 2009. A new method based on matrix perturbation and improved residual force vector for structural damage detection", IEEE *Computer Science and Information Technology*, 2:61-64.

Bui-Quoc, T., Dubuc, J., Bazergui, A. and Biron, A. 1971.Cumulative fatigue damage under stress-controlled conditions. *Journal of basic engineering,* 93:691-698.

Caetano, E. 2007. Structural engineering document, cable vibrations in cable-stayed bridge. SED9, Zurich.

Chan, J. 2006. EPRI transmission line reference book: Wind-Induced conductor motion. *Electric Power Research Institute, Palo Alto, California.*

Claren, R. and Diana, G. 1969. Mathematical analysis of transmission line vibration. *IEEE Transactions on Power Apparatus and Systems*, 88(12):1741-1771.

Diana, G., Manenti, A., Pirotta, C. and Zuin, A. 2003. Stockbridge-type damper effectiveness evaluation, Part II: the influence of the impedance matrix terms on the energy dissipated. *IEEE Transactions on Power Delivery*, 18(4):1470-1477.

Doucy et al, E. S. 1979. Wind induced conductor motion, transmission line reference book. *Electrical Power Research Institute.*

Elkin, S. 2010. Parametric study into the effectiveness of Stockbridge dampers on structural cables. MSc dissertation, UCL, Lodon, United Kingdom.

Fatemi, A. and Yang, L. 1998. Cumulative fatigue damage and life prediction theories: a survey of the state of the art for homogeneous materials. *International Journal of Fatigue*, 20(1):9-34.

Fitzgerald, B., Arrigan, J. and Basu, B. 2010. Damage detection in wind turbine blades using time-frequency analysis of vibration signals. *The 2010 International Joint Conference on Neural Networks (IJCNN).*

Gašperin, M., Juricic, D., Baškoski, P. and Jožef, V. 2011. Model-based prognostics of gear health using stochastic dynamic models. *Mechanical Systems and Signal Processing*, 25:537–548.

Gatts, R. R. 1961.Application of a cumulative damage concept to fatigue. *ASME Journal of Basic Engineering*, 83:529-534.

Gillen, K. T. and Celina, M. 2001. The wear-out approach for predicting the remaining lifetime of materials. *Polymer Degradation and Stability,* 71:15-30.

Guo, H. and Li, Z. 2008. Bayesian fusion theory and its application to the identification of structural damages. *Fourth International Conference on Natural Computation ICNC '08*, 4, 110-114.

Havard, D. G., Bissada, M. K., Fajardo, C.G., Horrocks, D. J., Meale, J. R., Motlis, J. Y., Tabatabai, M. and Yoshiki-Gravelsins, K. S. 1992. Aged ACSR conductors, Part II: prediction of remaining life. *IEEE Transactions on Power Delivery*, 7(2):588-595.

Henry, D. L. 1955. A theory of fatigue damage accumulation in steel. *Transactions of the ASME*, 77:913-918.

Herman, K. P. N. 1967. Strain Gauges- Kinds and uses. Mac millan, St. Martin Press

Hoffmann, K. 1987. An introduction to measurements using strain gages. *Hottinger Baldwin Messtechnik GmbH, Darmstadt, HBM.*

Hussey, M. 1983. Fundamentals of mechanical vibration. *London: The MacMillan Press.*

Huynh, D., He, J. and Tran, D. 2005. Damage location vector: a non-destructive structural damage detection technique. *Computers and Structures*, 83(28-30):2353-2367.

Hwang, H. Y. and Kim, C. 2004. Damage detection in structures using a few frequency response measurements. *Journal of Sound and Vibration,* 270:1-14.

IEC 61897 standard. 1998. *International Electrotechnical Commission*.

IEEE 664 standard. 2007. *Institute of Electrical and Electronics Engineers*.

Inman, D. J. 1996. *Engineering vibration*. Upper Saddle River, NJ: Prentice Hall.

Jardine, A. K. S., Joseph, T. and Banjevic, D. 1999. Optimizing condition-based maintenance decisions for equipment subject to vibration monitoring. *Journal of Quality in Maintenance Engineering,* 5:192-202.

Jiqun, C. and Shoutai, W. 2000. Method of estimating the remaining life of the l0 kV XLPE cable operated 10 years. *Proceedings of the 6th International Conference on Properties and Applications of Dielectric Materials,* 1(1):204-208.

Ju, F. D. and Mimovich, M. E. 1988. Experimental diagnosis of fracture damage in structures by the modal frequency method. Journal of Vibration Acoustics, 110(4): 456.

Kommers, J. B. 1945. The effect of overstress in fatigue on the endurance life of steel. *Proceeding, American Society for Testing and Materials*, 45:532-541.

Lara-Lopez, A. and Colin-Venegas, J. 2001. Endurance of dampers for electric conductors. *International Journal of Fatigue*, 23(1):21-28.

Li, S., Yu, S., Zeng, H., Li, J. and Liang, R. 2009. Predicting corrosion remaining life of underground pipelines with a mechanically-based probabilistic model. *Journal of Petroleum Science and Engineering*, 65, 162-166.

Li, Y. G. and Nilkitsaranant, P. 2009. Gas turbine performance prognostic for condition-based maintenance. *Applied Energy*, 86, 2152-2161.

Liu, T., Shang, D., Ren, C. and Nan, J. 2011. Dynamic characteristics of tower structure based on finite element analysis. *International Conference on Mechatronics and Automation (ICMA),* 1379-1383.

Marco, S. M. and Starkey, W. L. 1954. A concept of fatigue damage. *Transactions of the ASME*, 76:627-632.

Markiewicz, M. 1995. Optimum dynamic characteristics of Stockbridge dampers for dead-end spans. *Journal of Sound and Vibration,* 188:243-256.

Mazhar, M. I., Kara, S. and Kaebernick, H. 2007. Remaining life estimation of used components in consumer products : Life cycle data analysis by Weibull and artificial neural networks. *Journal of Operations Management*, 25:1184-1193.

Medda, A. and Debrunner, V. 2009. A localized vibration response technique for damage detection. IEEE *Acoustics, Speech and Signal Processing*, 1337-1340.

Meeker, W. Q. and Escobar, L.A. 1998. *Statistical methods for reliability data*. New York: John Wiley & Sons

Mukhopadhyay, N. K., Ghosh Chowdhury, S., Sinha, R. K. and Chaudhuri, S. 1999. Remaining life estimation of a service exposed economiser tube. *Engineering Failure Analysis*, 6:233-243.

Navarro Canales, C., Lara López, A., Colin Venegas, J. , Razo-García, J. and Aguilera-Cortés, L. A. 2008. Optimal design of Stockbridge dampers. *Ingenieria Mecanica Tecnologia y Desarrollo*, 2, 193-199.

Newmark, N. M. 1950. A review of cumulative damage in fatigue. Technical report, Department of civil engineering, University of Illinois, Urbana.

Ngargueudedjim, K. 2003. Contribution a l etude des lois d endommengement en fatigue. PhD thesis, L' institute National des sciences appliqués de Lyon, France.

Qiu, H., Lee, J., Lin, J. and Yu, G. 2006. Wavelet filter-based weak signature detection method and its application on rolling element bearing prognostics. *Journal of Sound and Vibration*, 289, 1006-1090.

Ray, A. K., Tiwari, Y. N., Roy, P. K., Chaudhuri, S., Bose, S. C., Ghosh, R. N. and Whittenberger, J. D. 2007. Creep rupture analysis and remaining life assessment of 2.25Cr – 1Mo steel tubes from a thermal power plant. *Materials Science and Engineering A*, 455:679-684.

Richardson, S. 1996. Performance requirements for vibration damper. *Electric Power Systems Research*, 36, 21-28.

Salawu, O. S. 1997. Detection of structural damage through changes in frequency: a review. *Engineering Structures*, 19(9):718-723.

Sauter, D. and Hagedorn, P. 2002. On the hysteresis of wire cables in Stockbridge dampers. *International Journal of Non-Linear Mechanics*, 37:1453 – 1459.

Si, X-S., Wang, W., Hu, C-H. and Zhou, D-H. 2011. Remaining useful life estimation - A review on the statistical data driven approaches. *European Journal of Operational Research*, 213:1-14.

Rao, S. S. 1990. *Mechanical vibration. Addison-Wesley series in mechanical engineering*. 2nd edition. Essex: Addison-Wesley.

Siriwardane, S., Ohga, M., Dissanayake, R. and Taniwaki, K. 2008. Application of new damage indicator-based sequential law for remaining fatigue life estimation of railway bridges. *Journal of Constructional Steel Research*, 64, 228-237.

Sivapragash, M., Lakshminarayanan, P. R., Karthikeyan, R., Raghukandan K. and Hanumantha, M. 2008. Fatigue life prediction of ZE41A magnesium alloy using Weibull distribution. *Materials and Design*, 29(8):1549-1553.

Tompkins, J. S., Merrill, L. L. and Jones, B. L. 1956. Quantitative relationships in conductor vibration damping. *IEEE Transactions on Power and Apparatus Systems*, 75:879-896.

Tse, S. F., Morse, E. I. and Hinkle, T. R. 1979. *Mechanical vibrations: Theory and application*. 2nd edition. Boston: Allyn and Bacon.

Tseng, S.T., Tang, J. and Ku, L.H. 2003. Determination of optimal burn-in parameters and residual life for highly reliable products. *Naval Research Logistics*, 50, 1-14.

Vecchiarelli, J. V., Currie, I. G. and Havard, D. G. 2000. Computational analysis of Aeolian conductor vibration with a Stockbridge-type damper. *Journal of Fluids and Structures*, 14:489-509.

VIP 2.0. Vibration Interactive program. 2008. Manuel of damper test

Wagner, H., Ramamurti, R. V. R. and Hartmann, K. 1973. Dynamics of Stockbridge dampers. *Journal of Sound and Vibration*, 30(2):207-220. Wang, R-J. and Shang, D-G. 2009. Fatigue life based on natural frequency changes for welds under random loading. *International Journal of Fatigue*, 31(2):361-366.

Wang, R-J., Shang, D-G, Li, L. and Li, C. 2008. Fatigue damage model based on the natural frequency changes for spot-welded joints. *International Journal of Fatigue*, 30(6):1047-1055.

Wang, W. and Christer, A. H. 2000. Towards a general condition based maintenance model for a stochastic dynamic system. *Journal of the Operational Research Society*, 51(2):145-155.

White, C., Li, H. C. H., Whittingham, B., Herszberg, I. and Mouritz, A. P. 2009. Damage detection in repairs using frequency response techniques. *Composite Structures*, 87:175-181.

Yan, J. and Guo, C. 2009. A FCM-weighted markov model for remaining life. *IEEE International Conference on Automation and Logistics, ICAL '09*. 493-497.

Yan, Y. J., Cheng, L., Wu, Z. Y. and Yam, L. H. 2007. Development in vibration-based structural damage detection technique. *Mechanical Systems and Signal Processing*, 21(5):2198-2211

Yeo, I., Suh, Y. and Mun, S. 2008. Development of a remaining fatigue life model for asphalt black base through accelerated pavement testing. *Construction and Building Materials*, 22(8):1881-1886.

Yong, X.and Hao, H. 2003. Statistical damage identification of structures with frequency changes. *Journal of Sound and Vibration*, 263: 853-870.

Zhang, W. Jiang, T. and Li, X. 2009. Life-Prediction of the CSADT Based on BP Algorithm of ANN. Annual Reliability and Maintainability Symposium, 2009. RAMS 2009.

Zhao, J., Han, S.-qi, Gao, H.-bo and Wang, L. 2004. Remaining life assessment of a CrMoV steel using the Z-parameter method. *International Journal of Pressure Vessel and Pipe*, 81:757-760.

Zishou, S., Kui, Z. and Husheng, L. 2010. Damage identification based on wavelet packets and frequency response function". International Conference on Computer Application and System Modeling (ICCASM). 458-460.

APPENDIX A

CALIBRATION DATA

Thermocouples were calibrated by using the circulator controller and the data are presented below.

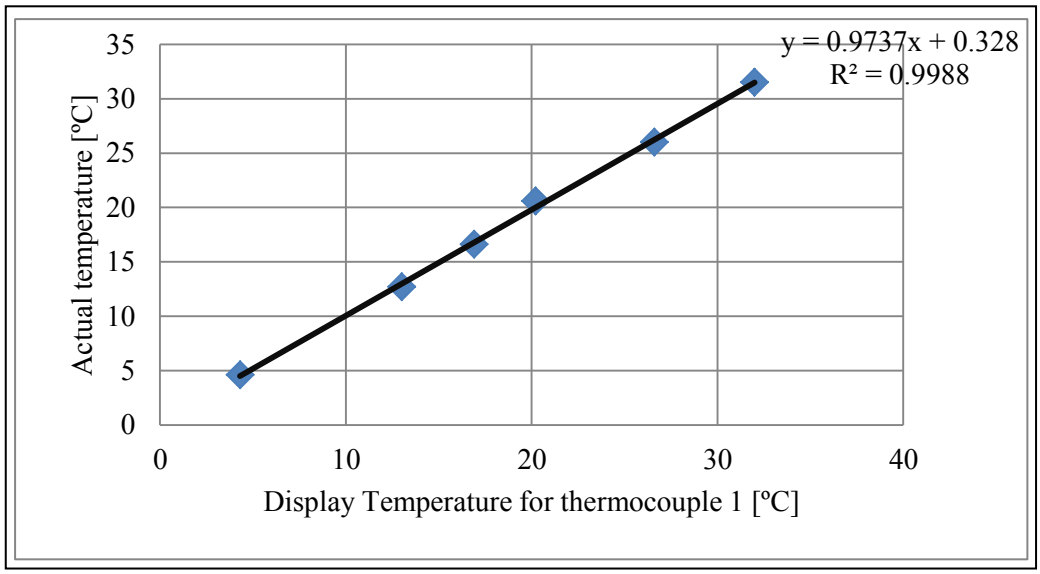

Figure A.1: Temperature calibration curve for the thermocouple ΔTc1.

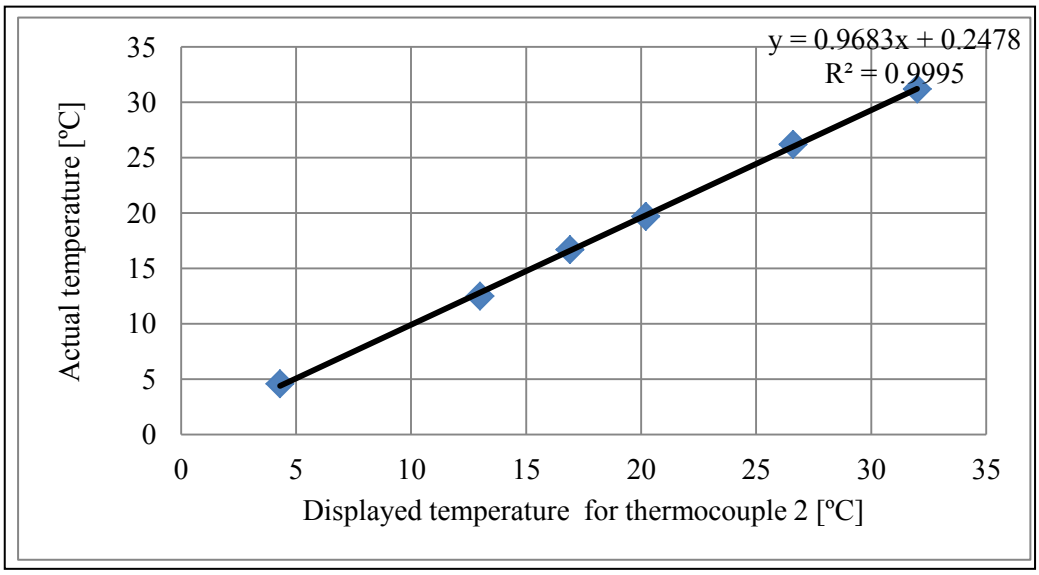

Figure A.2: Temperature calibration curve for the thermocouple ΔTc2.

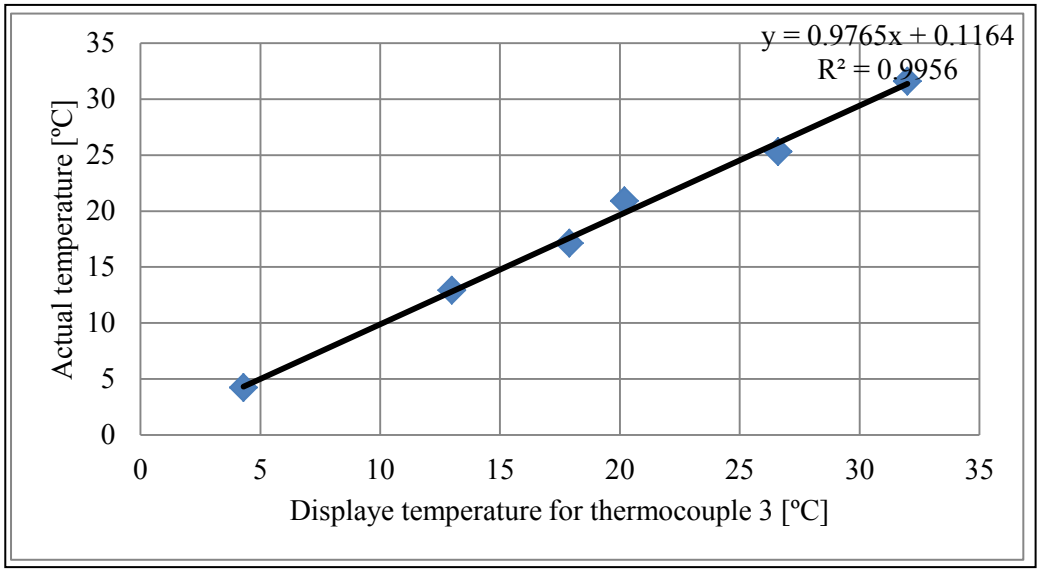

Figure A.3: Temperature calibration curve for the thermocouple ΔTc3.

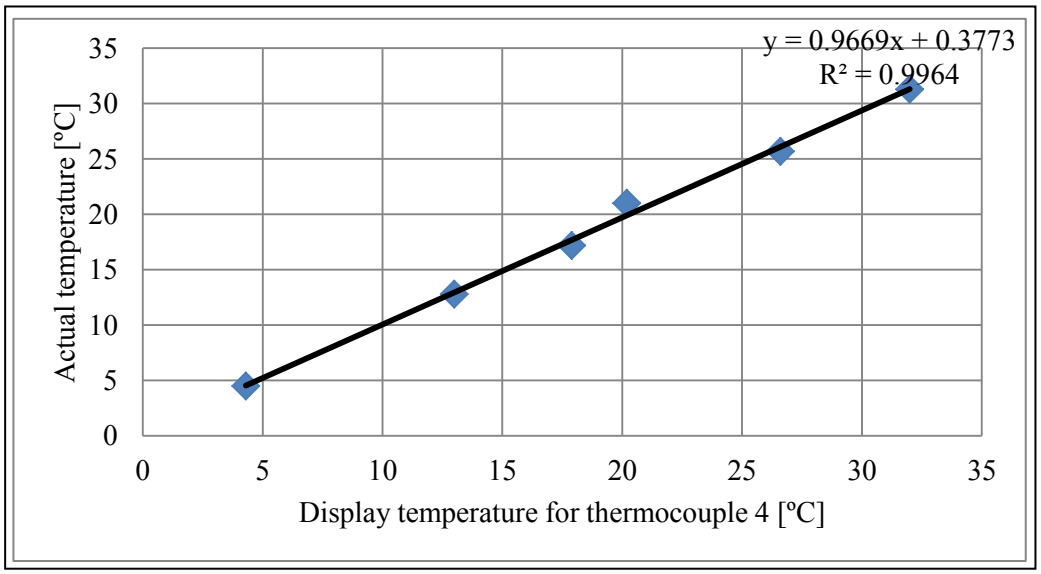

Figure A.4: Temperature calibration curve for the thermocouple ΔTc4.

A calibration unit, type K 3607 (HBM) was used to calibrate the strain gauges. Figure A.5 shows the calibration data for strain gauges.

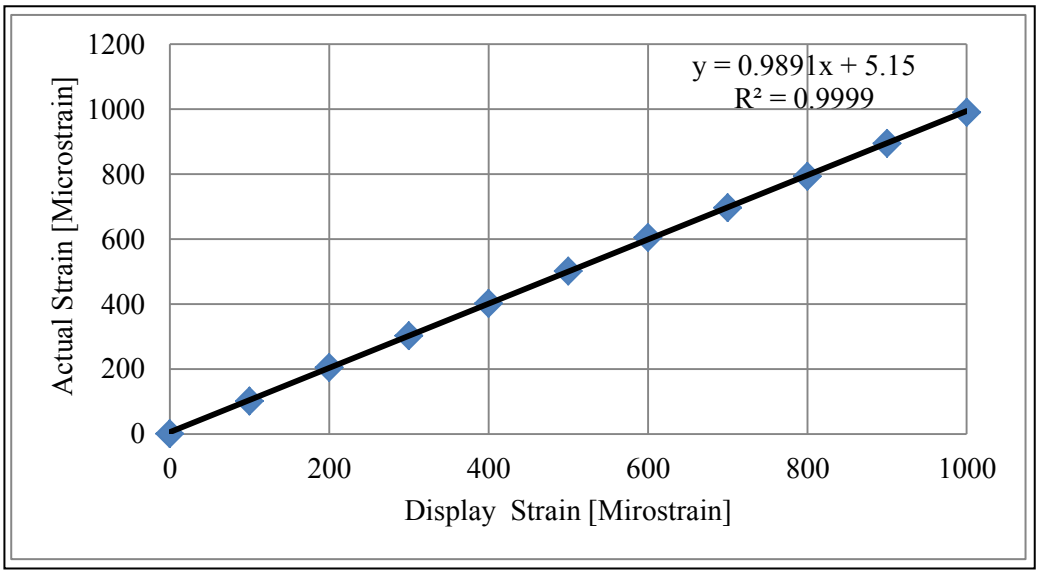

Figure A.5: Strain calibration curve.

APPENDIX B

DIMENSIONS OF ASYMMETRICAL STOCKBRIDGE DAMPER

The following dimensions are used to characterize the asymmetrical damper. The Figure below shows different dimensions and Table B.1 provides the different values. The asymmetrical damper is geometrically characterized by dimension, weight, diameter conductor range in mm, as well as the dimensions A and B in mm.

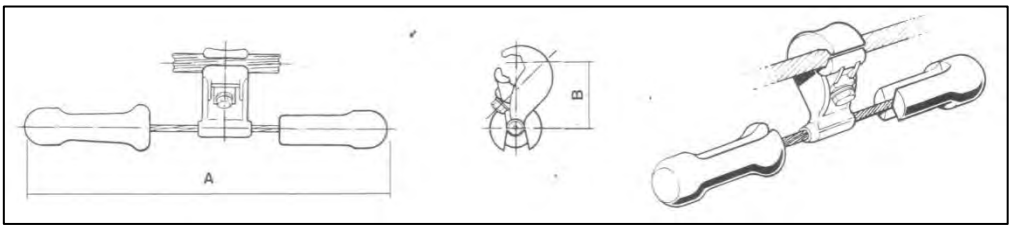

Figure B.1: Different dimensions of asymmetrical damper.

Three damper models are presented in the Table B.1. The 855017-00 model damper was used for this dissertation.

Table B.1: Geometrical characteristics of the asymmetrical Stockbridge damper.

Catalogue Number	Dimensions		Weight [kg]	Conductor Diameter [mm]	
	A [mm]	B [mm]		Min	Max
855009-00	411	78	2.06	11	19.42
855011-00	510	92	4.07	19.42	24.6
855017-00	566	100	6.99	19.42	38.5

APPENDIX C

CALCULATION OF THE WIND FREQUENCY RANGE

The calculation of the wind frequency range for the Stockbridge damper used for this dissertation (Catalogue number 855017-00) is shown by using the Strouhal formula (Equation 2.2).

The wind velocity is considered to be between 1 and 7 m/s (Chan, 2006).

Using Equation 2.2, and the conductor diameter range from Table B.1 ($D_{c,\min} = 24.60$ and $D_{c,\max} = 38.50$), the following frequencies have been found:

$$f_1 = 0.185\frac{1}{0.02460} = 41Hz$$

$$f_2 = 0.185\frac{1}{0.03850} = 5Hz$$

$$f_3 = 0.185\frac{7}{0.02460} = 53Hz$$

$$f_4 = 0.185\frac{7}{0.03850} = 34Hz$$

Considering the four frequencies, the frequency range will be between the minimal and the maximal frequency. Therefore, the frequency range will be from 5Hz to 55Hz.

APPENDIX D

TEMPERATURE DATA

The temperature variation of the messenger cable has been measured during the forced response test at constant displacement and velocity. Each experiment has been conducted three times and data collected. Thereafter, the average has been calculated. Data are presented below:

- At constant velocity

Table D.1: Temperature variation of the messenger cable's damper at the attached point of the big mass (Tc1) as a function of excitation frequency at constant velocity.

Frequency [Hz]	Reading 1 [K]	Reading 2 [K]	Reading 3 [K]	Average [K]
5	0.000	0.000	0.000	0.000
13.26	0.068	0.087	0.378	0.178
21.65	0.113	0.302	0.057	0.157
30	0.246	0.693	0.205	0.381
38.29	0.343	0.635	0.236	0.405
46.68	1.974	1.898	1.633	1.835
55	1.795	1.718	1.322	1.612

Table D2: Temperature variation of the messenger cable's damper at the attached point of the big mass (Tc2) as a function of excitation frequency at constant velocity.

Frequency [Hz]	Reading 1 [K]	Reading 2 [K]	Reading 3 [K]	Average [K]
5	0.000	0.000	0.000	0.000
13.26	0.635	0.211	0.446	0.431
21.65	2.621	2.377	2.597	2.532
30	2.401	2.160	1.696	2.086
38.29	1.140	0.855	0.824	0.940
46.68	1.570	1.676	1.273	1.506
55	1.920	1.288	1.378	1.529

Table D3: Temperature variation of the messenger cable's damper at the attached point of the big mass (Tc3) as a function of excitation frequency at constant velocity.

Frequency [Hz]	Reading 1 [K]	Reading 2 [K]	Reading 3 [K]	Average [K]
5	0.000	0.000	0.000	0.000
13.26	1.089	0.970	1.035	1.031
21.65	1.048	0.928	1.062	1.013
30	0.876	0.942	1.235	1.018
38.29	1.073	0.996	1.142	1.070
46.68	0.800	0.672	0.759	0.744
55	0.184	0.262	0.155	0.200

Table D4: Temperature variation of the messenger cable's damper at the attached point of the big mass (Tc4) as a function of excitation frequency at constant velocity.

Frequency [Hz]	Reading 1 [K]	Reading 2 [K]	Reading 3 [K]	Average [K]
5	0.000	0.000	0.000	0.000
13.26	1.123	1.154	1.064	1.114
21.65	0.682	0.823	1.470	0.992
30	1.928	2.046	2.620	2.198
38.29	1.500	1.688	2.004	1.731
46.68	2.764	2.937	3.043	2.915
55	2.758	2.10	2.450	2.406

- Constant displacement

Table D5: Temperature variation of the damper's messenger cable at the attached point of the big mass (Tc1) as a function of excitation frequency at constant displacement.

Frequency [Hz]	Reading 1 [K]	Reading 2 [K]	Reading 3 [K]	Average [K]
5	0.000	0.000	0.000	0.000
13.26	0.350	0.061	0.086	0.166
21.65	0.192	0.095	0.028	0.105
30	0.093	0.089	0.153	0.112
38.29	0.171	0.236	0.152	0.186
46.68	1.961	2.067	2.229	2.086
55	2.117	2.274	2.506	2.299

Table D6: Temperature variation of the damper's messenger cable at the attached point of the big mass (Tc2) as a function of excitation frequency at constant displacement.

Frequency [Hz]	Reading 1 [K]	Reading 2 [K]	Reading 3 [K]	Average [K]
5	0.000	0.000	0.000	0.00
13.26	0.184	0.080	0.146	0.137
21.65	0.159	0.032	0.267	0.153
30	0.420	0.068	0.322	0.270
38.29	0.093	0.220	0.573	0.295
46.68	1.165	1.490	1.179	1.278
55	2.063	2.347	2.346	2.252

Table D7: Temperature variation of the damper's messenger cable at the attached point of the big mass (Tc3) as a function of excitation frequency at constant displacement.

Frequency [Hz]	Reading 1 [K]	Reading 2 [K]	Reading 3 [K]	Average [K]
5	0.000	0.000	0.000	0.000
13.26	0.212	0.246	0.099	0.186
21.65	0.153	0.306	0.042	0.167
30	0.077	0.079	0.057	0.071
38.29	0.449	0.380	0.456	0.428
46.68	0.878	0.765	0.983	0.875
55	0.831	0.806	1.135	0.924

Table D8: Temperature variation of the damper's messenger cable at the attached point of the big mass (Tc4) as a function of excitation frequency at constant displacement.

Frequency [Hz]	Reading 1 [K]	Reading 2 [K]	Reading 3 [K]	Average [K]
5	0.000	0.000	0.000	0.000
13.26	0.267	0.080	0.142	0.163
21.65	0.100	0.049	0.214	0.121
30	0.184	0.180	0.078	0.147
38.29	0.703	0.823	0.817	0.781
46.68	0.822	0.878	1.012	0.904
55	0.582	0.459	0.389	0.477

APPENDIX E

MATLAB CODE

```
% Calculate the dynamic bending stress function of frequency (f)
%
% 1. Definition of the input variables (scalars).
%
m = 2.74            % mass of damper weight in kg
Jg = 0.001714       % moment of inertia in kgm^2
L = 0.23            %length of messengerr cable in meter
L2 = 0.048          %distance between attachment point and center of gravity in meter
rho = 2.44          %ratio between (r/L2)^2 with r radius of giration of the damper mass
c11 = 0.00314         % element of stifness matrix in kilogramme per meter, c11=4c
mu = 0.16           % damping onstant
f1 = 8.9            % first resonance frequency in radian per second
f2 = 23             % second resonance frequency in radian per second
Y = 0.001           % displacement of shaker in m
D = 0.009           % diameter of messenger cable in m
%
% 2. Calculation of calculation of alpha and c12 (scalars)
%
alpha = (f1/f2)^2;
c12 = c11*L/2;
%
```

```
% 3. Calculation of the dimensionless stiffnesses SX and Stheta (scalars)

%

S1 =(alpha*(1+rho)*c11)/(m*rho*L2*(f1^2));    % first stiffness

S2 = (c12-(L2*c11))/(m*rho*L2*(f2^2));        % second stiffness

%

% 4. Calculation of real amplitudes X and theta (vectors)

%

f = 0:0.001:40;    % range of driving frequency in Hz

omega = 2*pi.*f;    % vecteur

eta = f./f1;

X = (Y*(1+(i*mu)).*(1+(i*mu)-(S1.*(eta.^2)))./((1+(i*mu)-(eta.^2)).*(1+(i*mu)-(alpha.*(eta.^2))));          %Complex number

theta = ((Y/L2)*(1+(i*mu)).*(-alpha.*(eta.^2).*S2))./((1+(i*mu)-(eta.^2)).*(1+(i*mu)-(alpha.*(eta.^2))));    %Complex number

%

% 5. Calculation of Xdotdot and thetadotdot (vectors)

%

absX = abs(X);

abstheta = abs(theta);

Xdotdot = (-1).*absX.*(omega.^2);

thetadotdot = (-1).*abstheta.*(omega.^2);

%

% 6. Calculation of Force FG (vector)

%

FG = (m).*(Xdotdot+(L2.*thetadotdot));       % complex number
```

```
%

% 7. Calculation of Moment MB (vector)

%

L1 = L-L2;                          %lenght in meter

Mg = Jg.*thetadotdot;

MB = Mg-(L1.*FG);



%

% 8. Calculation of modulus of the cross-section Wa (scalar)

%

Wa = ((2/3)*pi*(D^3))/32;                %2/3 is the factor k which takes into account the fact that the messenger cable is not the circle but a stranded cable

%

% 9. Calculation of bending stress (vector)

%

bendingstress = (MB./(100000*Wa))/2;          %bending stress in kgf per cm^2

%

% 10. Plot the graph Bendingstress vs frequency

%

plot(f,bendingstress)

grid on

xlabel 'Frequency in Hz'

ylabel 'Bending Stress in kgf/cm^2 for Y=1mm'
```